62-3-1

491800

REPORT NO. 3642-11

FINAL REPORT FIBERGLASS MOTOR CASE STUDY POLARIS SECOND STAGE END CLOSURE

CONTRACT NO. NOw 61-0497-C(FBM)

MARCH 23, 1962

PRESENTED BY
Walter Kidde & Company, Inc.
KIDDE AERO SPACE DIVISION
BELLEVILLE 9, N. J.

Date March 23, 1962

REPORT NO. 3642-11

Acct. or Ct. No. A 65126

KIDDE AERO-SPACE DIVISION
Walter Kidde & Company, Inc.
Belleville, New Jersey

FINAL REPORT

TITLE FIBERGLASS MOTOR CASE MOTOR

POLARIS SECOND STAGE END CLOSURE

NOw-61-0497-C(FBM)

Tests Conducted by

Report Prepared by

T. Siuta
Project Engineer

Approved by

F. Wolff, Project Leader

J. McEnilly, Asst. Technical Director

FOREWORD

This report was prepared by Walter Kidde & Co., Inc. Aero-Space Division, Belleville, New Jersey under Navy Contract No. NOw61-0497-C (FBM) entitled Fiberglass Motor Case Study - Polaris Second Stage. The work was administered under the direction of the Naval Research Laboratory with Mr. J. Kies and Dr. I. Wolock acting as technical advisers.

This report covers the work conducted from April 1, 1961 to February 15, 1962 and was written by Mr. T. Siuta of the Walter Kidde & Co., Inc., Belleville, N.J. The writer is especially grateful to Mr. F. Wolff, Mr. T. Hadeler and Mr. H. Dalalian for their assistance in conducting the program and constructive criticism in the preparation of this report.

ABSTRACT

The main objective of this program was to review the Polaris second stage end closure configurations and to improve the existing design through experimental and analytical techniques. This was accomplished by refining the end contour so that bending and points of inflection in the pressurized dome structure were minimized.

A zero shear or geodesic contour was developed using an analog technique in which the fibers are stressed only in tension. Following subsequent hydrostatic tests which demonstrated the improved structural efficiency of this contour another modification was made in which the contour was made to conform with established deflection tendencies. An empirical equation for predicting deflections on other scale models was developed.

Zero shear contour deflections were shown to be essentially linear. Test results showed that upon pressurization an initial change in shape took place under very little loading and that following this reorientation deflections progressed in a linear fashion. Strain gage results indicated strains were distributed uniformly throughout the dome structure with very little bending evident.

Insight was gained into the mechanics governing dome deflections and effective methods were established for the determination of more efficient dome closures. With these techniques filament wound dome closure contours can be made mutually compatible with such parameters as winding angle, pattern, and various reinforcement and fabrication techniques.

TABLE OF CONTENTS

SECTION				PAGE NO
1.0			Introduction	1
2.0			Summary	3
3.0			Discussion	6
	3.1.0		Phase I - Parameter Studies Affecting Dome Closure Contours	6
		3.1.1	Theoretical Contour Concepts - Minimum Hoop Stress	6
		3.1.2	Isotensoid Concepts	11
		3.1.3	Determination of Optimum Contour	11
		3.1.4	Winding Angle Effects on Zero Shear Contour	13
		3.1.5	Effect of Multiple Winding Angles and Girth Reinforcement on Zero Shear Contours	18
		3.1.6	Dome Closure Model Tests	21
		3.1.7	Zero Shear Contour Determination	37
		3.1.8	Summary and Conclusions For Phase I	38
	3.20		Phase II - Rocket Chamber Scale Model Design and Study	43
		3.2.1	Design of 1/4 Scale Model	43
		3.2.2	Specimen Fabrication	48
		3.2.3	Instrumentation and Test Procedures	49
		3.2.4	1/4 Scale Model Test Results	55
		3.2.5	Strains Gage Results	70
		3.2.6	Empirical Equation For Dome Closure Deflections	75
		3.2.7	Full Scale Test Data and Results	77

SECTION			PAGE NO
	3.2.8	Comparison of Model Tests with Full Scale Chamber Test Results	83
	3.2.9	Summary and Conclusions For Phase II	89
3.3.0		Phase III - Modified Dome Design	90
	3.3.1	Dome Contour Selection	91
	3.3.2	Determination of Modified Zero Shear Contour	91
	3.3.3	Winding Angles	96
	3.3.4	Length of Cylindrical Section of Motor Case	96
	3.3.5	Glass Filament Requirements	98
	3.3.6	Design of Non-Polar Port Reinforcements	99
	3.3.7	Sizing Non-Polar Port Reinforcements Based On Load Requirements	102
	3.3.8	Sizing Non-Polar Port Reinforcements Based On Strain Requirements	104
	3.3.9	Summary and Conclusions For Phase III	109
3.4.0		Recommendations and Conclusions	110
		References	112
Appendix I		Specimen KB-9 Ovaloid Stress and Load Calculations	113
Appendix II		Specimen KB-15 Ovaloid Stress and Load Calculations	117
Appendix III		Equations For Calculating Bending Strains	119
Appendix IV		Simulation of Aluminum Skirt Thickness	120
Appendix V		Design Equations for a Cylindrical Container Wound with Two or more Winding Angles	121
Appendix VI		Design of Polaris X-250 Rocket Motor Case	126
Appendix VII		Fiberglass Reinforcement for Circular Ports	129

LIST OF FIGURES

FIGURE NO.		PAGE NO
1	Ellipsoidal and Zero Hoop Stress Contours	8
2	Zero Hoop Stress Contours	9
3	Winding Set-Up For Determining Zero Shear Contour	14
4	Empirical Contours	15
5	Empirical Contours	16
6	Empirical Dome Contours - Wind Ratio Effects	19
7	Empirical Dome Contours - Wind Ratio & Girth Reinforcement Effects	20
8	Typical Ovaloid Test Set-Up & KB-9 Failure	23
9	Ovaloid Specimen KB-9 Deflections	24
10	Ovaloid Specimen KB-10 Deflections	25
11	Ovaloid Specimen KB-15	28
12	Photograph of Specimen KB-15	30
13	Dome Closure Specimen KB-15 Deflections	31
14	Dome Closure Specimen KB-16 Deflections	32
15	Zero Shear Contour	40
16	Theoretical vs Actual Polaris Contours	42
17	SK134943 Scale Model Polaris Case	46
18	Typical Strain Gage Locations	50
19	Typical Instrumentation to Measure Deflections	51
20	Schematic Diagram of Test Set-up	53
21	Hydrostatic Test Set-up	54
22	Strain Gage Instrumentation	54

FIGURE NO		PAGE NO
23	Hydrostatic Pressure Test Failure	57
24	QP-1 Aft Dome Deflections	59
25	QP-3 Aft Dome Deflections	60
26	QP-3 Forward Dome Deflections	61
27	QP-3 Forward Dome Deflections (Retest)	62
28	QP-3 Aft Dome Deflections (Retest)	63
29	QP-3 Normalized Forward Dome Deflections	71
30	QP-3 Normalized Aft Dome Deflections	72
31	QP-3 Normalized Forward and Aft Dome Deflections	76
32	SK1344441 Polaris A-3 Full Scale Aft Head Deflections	80
33	SK1344446 Polaris A-3 Full Scale Aft Head Deflections	81
34	Polaris A-3 Full Scale Aft and Forward Head Deflections	82
35	QP-3 Zero Pressure Deflection	93
36	Modified Contour and Coordinates	94
37	Comparison of Original and Modified Zero Shear Contours	95
38	Sketch of A-3 Configuration	97

LIST OF TABLES

TABLE NO		PAGE NO
1	Coordinates For Zero Hoop Stress And Ellipsoid Contours	10
2	Specimen KB-15 and KB-16 Strain Gage Results	34
3	Equivalent Specimen KB-15 Deflections	36
4	Average Deflections For X-250 Cases	36
5	Comparison of Ideal Geodesic and Zero Shear Contours	41
6	QP-3 Aft Dome Deflections	64
7	QP-3 Forward Dome Deflections	65
8	QP-3 Cylinder Deflections	67
9	Comparison of Chamber Deflections	69
10	QP-1 Aft Dome Strain Gage Results	73
11	QP-3 Aft Dome Strain Gage Results	74
12	Comparison of Deflections between 1/4 Scale Model and Full Scale Chambers	84
13	Summary of Strain Gage Results on X-260 Cases	87
14	Comparison of Physical Properties	88

1.0 INTRODUCTION

The analysis and design of filament wound rocket chambers and dome closures is difficult due to the inherent laminate unidirectional properties encountered in this type of construction. Although the light weight-high strength characteristic of filament wound composites has increased the efficiency of rocket chambers, present day design and fabrication methods are still considered an art. Sound design techniques must still be evolved to supplement present day development methods.

In the past many theories were applied in the design of filament wound pressure vessel end closure contours, but in practice inconsistent results were achieved. This is partly due to the fact that the glass fibers, which are the main load carrying element, could not always be placed in the direction of the load being supported. A further complication is the disruption of filament continuity by inserts, reinforcements and off-center ports. Structural efficiency is also adversely affected by differences in the natural flexibility of the head and cylinder sections which cause the two parts to attempt to deform radially and angularly at different rates.

One of the primary purposes of this program was to take an objective look at the Polaris second stage forward and aft dome closure configurations and to refine the end contours so that the glass reinforced laminate is utilized to its maximum efficiency. This was successfully accomplished by obtaining a contour which is mutually compatible with the winding angle and pattern and which conforms with established deflection tendencies. Tests have shown this contour to be highly efficient.

An empirical technique was evolved for developing the optimum contour. In this technique the direction of the fibers is made to coincide with the direction of the applied load which resists the internal pressure forces. This results in a structure which produces zero or minimum shear stresses.

The work in this program was divided into the following categories:

1. Preliminary tests to determine the effect of winding angle and other factors on dome contours.
2. Selection of an optimum contour and winding pattern.
3. Tests on oblate spheroid specimens to determine deflection characteristics.
4. Design of a 1/4 scale model rocket case with polar ports.
5. Hydrostatic tests on several 1/4 scale model rocket cases.
6. Determination of an empirical equation governing the deflection tendencies.
7. Study of available deflection data on full scale cases.
8. Comparison of model and full scale chamber data and results.
9. Determination of a modified end closure configuration based on deflection tendencies.
10. Investigation of non-polar port reinforcements.
11. Evaluation of results and recommendations for the redesign of second stage dome configurations.

2.0 SUMMARY

The end contours of the second stage Polaris case were refined to eliminate or minimize bending and points of inflection in the pressurized dome structure. Tests on a polar ported scale model rocket chamber were conducted to demonstrate the successful achievement of this objective. The zero-shear contour developed in this program is compatible with winding angle and pattern requirements, produces uniform strain distribution throughout the dome structure and conforms to the established deflection characteristics. This empirically determined contour was shown to be in complete agreement with the theoretical geodesic contour. The use of this contour results in the attainment of a highly efficient structure in which the longitudinal and circumferential glass filaments are stressed equally. The fact that an excess of longitudinals was not required, as in the full scale chambers, permitted the attainment of a strength to weight ratio of 1.68×10^6 inches.

Of equal importance, an empirical method was developed in this program which permits the determination of an optimum zero shear contour for different winding angles, patterns and design configurations. Results are shown to agree with analytical calculations. Furthermore this method permits a much more expedient method for developing contours compatible with multiple winding angle systems. Hydrostatic pressure deflection tests were performed on a polar ported scale model simulating the X-250 configuration and indicated that dome deflections were proportional to pressure following an initial shape change which took place

at low pressures. Based on these deflection tests an empirical equation was established governing the scale model deflection characteristics. With this equation, deflections may be computed for larger sized chambers, provided design and fabrication techniques are identical.

The development effort under this contract was divided into three general phases entitled: 1. Parameter Studies Affecting Dome Closure Contours, 2. Scale Model Chamber Design and Study, and 3. Determination of a Modified Dome Design.

During the initial phase of this program a number of oblate spheroid test specimens were wound incorporating many variables such as winding angles and pattern. The purpose of these tests was to determine the effect of these variables on the shape of a natural contour and to study dome deflection characteristics as affected by the shape and winding geometry. A girth reinforcement simulating skirt effects was also studied. Results showed the winding angle and pattern did influence the natural contour requirements. In multiple winding angle systems it was found that the larger helix winding angle was more dominant in affecting the natural contour and that the ratio of the major to minor axis became smaller as the winding angle increased.

A comparison of deflections on the zero shear contour scale model and X-260 full scale chambers shows that the actual equivalent values were larger with the zero shear contour. This is due to the reduced amount of glass which was required in the longitudinal direction. No significant bending strains were detected in the dome section, although deflection

characteristics indicate bending and discontinuities at the point of skirt reinforcement.

Analytical studies of the port reinforcement problem indicate the most promising configuration is one which is based on matching the laminate stiffness and strain properties. Reinforcements based on loading alone may produce severe discontinuities. A simplified analysis was made to establish design parameters for determining the amount of reinforcement required around the non-polar ports. Results indicate that the actual reinforcement design should be coordinated with tests to insure that deflection compatibility is achieved between the reinforcement and dome configuration.

A review of test results obtained on full scale chambers showed a wide variation in dome deflection and strain characteristics existed between different chambers. Scalloping and negative bending strains were noted around the non-polar ports. This shows present reinforcing methods should be refined to increase local flexibility.

3.0 DISCUSSION

3.1 Phase 1 - Parameter Studies Affecting Dome Closure Contours

In this initial phase of the program, effort was expended in the review of existing theories concerning pressure vessel dome closure contours and a study was made to determine the most important parameters which affect these contours. A study of existing theory governing the "zero" minimum hoop stress contour showed that although its underlying concept was based on sound engineering principles its use was limited in actual practice.

3.1.1 Theoretical Contour Concepts

Minimum Hoop Stress

A thorough presentation of the zero hoop stress theory is found in references 1 and 2. Reference 1 develops a contour for minimum hoop stress based on a zero degree winding angle while reference 2 presents contours for winding angles other than zero. Theoretically the outstanding advantage of this contour is that hoop stresses in the "knuckle area" adjacent to the cylindrical section are kept low. This contour, however, has the disadvantage that it develops high meridional stresses at the peak of the dome. Therefore in actual practice the contour is used in combination with a spherical cap. The spherical cap is blended with the zero hoop stress contour so that meridional stresses near the peak of the dome are maintained at the cylinder hoop stress level. Figure 1 presents the zero hoop stress-spherical cap configura-

tion for winding angles less than five degrees. Two ellipsoidal configurations are also shown for comparison purposes. The 1.612:1 ellipse has the same a/b ratio as the zero hoop stress contour. This figure shows that the zero hoop stress contour provides a larger dome volume for a particular envelope. Calculations show the maximum hoop stress in the 1.612:1 ellipse which occurs at the longitudinal center line is 61% higher than that of the low winding angle zero hoop stress contour with the spherical cap. Figure 2 shows the zero hoop stress contours for winding angles of 0, 4, 20, and 35 degrees. The contours shown in this figure do not include spherical caps so that meridional stresses in the dome crown area become infinite. A comparison of the various zero hoop stress contours shows that their a/b ratio decreases with an increase in the winding angle. The non-dimensionalized coordinates for the contours depicted in Figures 1 and 2 are presented in Tables 1. A comparison shows that almost no difference exists in the coordinates for the zero and four degree winding angles. This implies that the use of a small diameter opening (polar fitting) might be possible with this contour with only a small drop in structural efficiency.

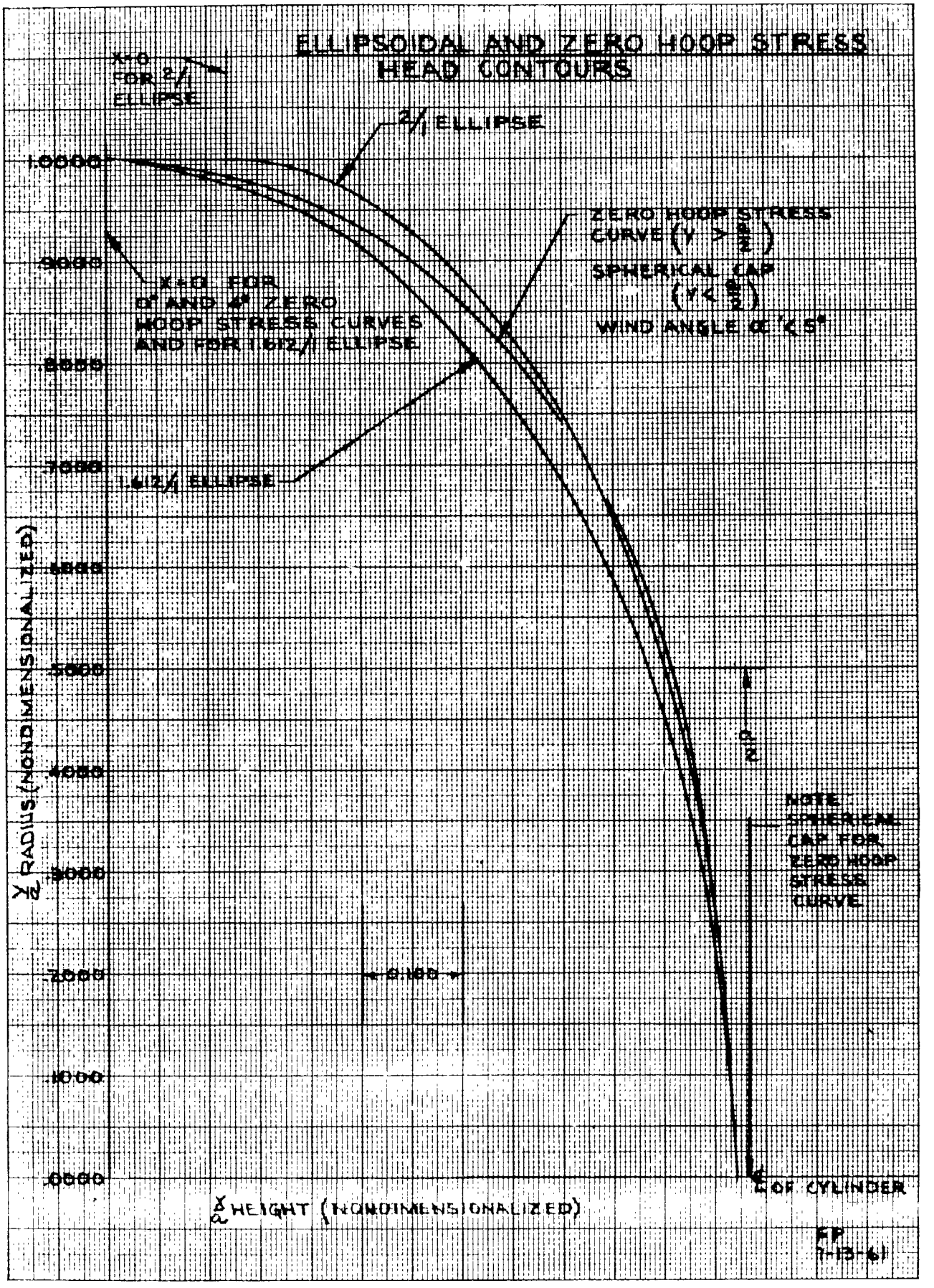
ELLIPSOIDAL AND ZERO HOOP STRESS HEAD CONTOURS
X=0 FOR 2/1 ELLIPSE
2/1 ELLIPSE
1.00000
.90000
.80000
.70000
1.612/1 ELLIPSE
X=0 FOR 0° AND 4° ZERO HOOP STRESS CURVES AND FOR 1.612/1 ELLIPSE
ZERO HOOP STRESS CURVE (Y > D/2)
SPHERICAL CAP (Y < D/2)
WIND ANGLE α = 4.5°
.50000
.40000
.30000
.20000
.10000
.00000
Y/a RADIUS (NONDIMENSIONALIZED)
0.100
D/2
NOTE SPHERICAL CAP FOR ZERO HOOP STRESS CURVE
℄ OF CYLINDER
X/a HEIGHT (NONDIMENSIONALIZED)
FP 7-13-61

FIGURE 1

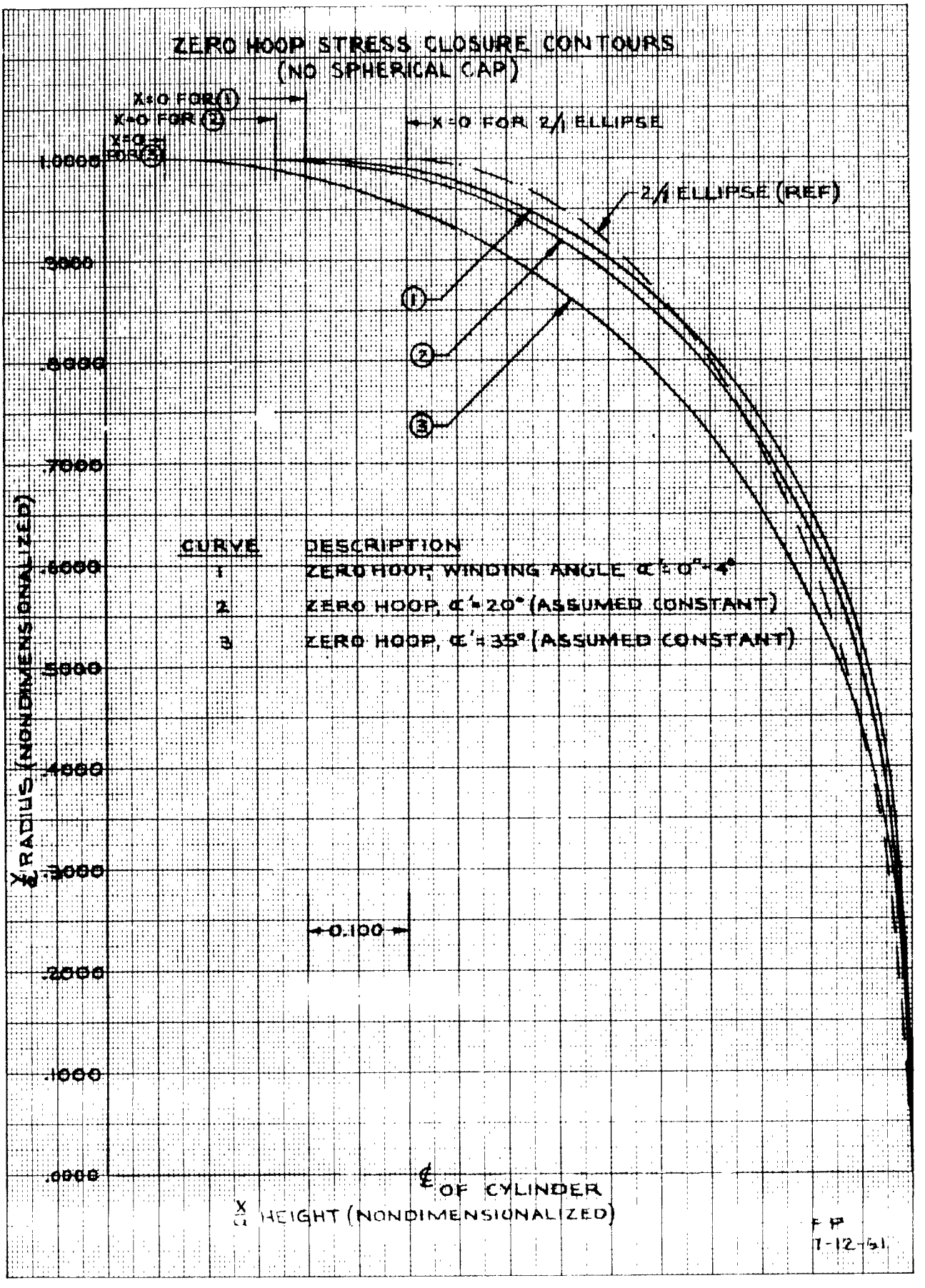
ZERO HOOP STRESS CLOSURE CONTOURS
(NO SPHERICAL CAP)
X=0 FOR (1)
X=0 FOR (2)
X=0 FOR (3)
X=0 FOR 2/1 ELLIPSE
2/1 ELLIPSE (REF)
1.0000
.9000
.8000
.7000
.6000
.5000
.4000
.3000
.2000
.1000
.0000
1
2
3
CURVE DESCRIPTION
1 ZERO HOOP WINDING ANGLE α' = 0°-4°
2 ZERO HOOP, α' = 20° (ASSUMED CONSTANT)
3 ZERO HOOP, α' = 35° (ASSUMED CONSTANT)
r/a RADIUS (NONDIMENSIONALIZED)
0.100
℄ OF CYLINDER
X/a HEIGHT (NONDIMENSIONALIZED)
F P
7-12-61

FIGURE 2

TABLE 1

COORDINATES FOR VARIOUS ZERO HOOP STRESS CONTOURS

	ZERO HOOP $\alpha = 0°$		ZERO HOOP $\alpha = 4°$		ZERO HOOP $\alpha = 20°$		ZERO HOOP $\alpha = 35°$		ELLIPSE 1.612/1	
	x/a	y/a	x/a	y/a	x/a	y/a	x/a	y/a	x/a	y/a
0	.0000	1.0000	.0000	1.0000	.0000	1.0000	0	1.0000	.0000	1.0000
5.00	.0436	.9980	.0437	.9981	.0467	.9979	.0578	.9975	.0541	.9962
10	.0871	.9924	.0873	.9924	.0932	.9918	.1152	.9899	.1078	.9848
15	.1302	.9828	.1305	.9828	.1393	.9816	.1721	.9773	.1606	.9659
20	.1728	.9694	.1732	.9693	.1849	.9672	.2281	.9596	.2122	.9397
25	.2147	.9520	.2152	.9519	.2297	.9500	.2830	.9369	.2623	.9063
28.75	.2456	.9363	.2462	.9362	.2617	.9320	.3232	.9165	.2985	.8767
32.50	.2760	.9184	.2766	.9183	.2931	.9128	.3624	.8933	.3334	.8434
36.25	.3057	.8980	.3065	.8978	.3239	.8912	.4000	.8672	.3669	.8064
41.25	.3443	.8671	.3451	.8668	.3648	.8584	.4496	.8278	.4091	.7518
45.00	.3722	.8409	.3731	.8405	.3944	.8306	.4848	.7949	.4388	.7071
48.75	.3993	.8120	.4002	.8116	.4230	.8001	.5185	.7589	.4665	.6594
53.75	.4338	.7690	.4348	.7685	.4593	.7548	.5609	.7061	.5004	.5913
57.50	.4584	.7330	.4594	.7324	.4851	.7170	.5906	.6627	.5234	.5373
61.25	.4818	.6935	.4828	.6929	.5096	.6758	.6183	.6158	.5440	.4810
65.00	.5038	.6501	.5048	.6494	.5325	.6305	.6440	.5652	.5624	.4226
70.00	.5308	.5848	.5319	.5841	.5604	.5630	.6745	.4913	.5831	.3420
75.00	.5547	.5087	.5558	.5079	.5850	.4849	.7006	.4085	.5994	.2588
75.52	.5570	.5000	.5581	.4992	.5873	.4762	.7031	.3994	.6008	.2501
80.00	.5901*	.3473*	.5901*	.3473*	.6055	.3916	.7216	.3136	.6111	.1737
85.00	.6129*	.1743*	.6129*	.1743*	.6212	.2707	.7366	.1986	.6182	.0872
90.00	.6205*	.0000*	.6205*	.0000*	.6299	0	.7439	.0000	.6205	.0000

α = winding angle
a = radius
* = spherical cap

3.1.2 Isotensoid Concepts

Another contour reviewed was that of the osotensoid configuration developed by the Aerojet General Corporation (see reference 3). Unlike the zero hoop stress contour this configuration includes the effects of polar openings. With this contour the individual glass filaments are loaded to a constant stress level throughout the structure and the resin matrix is assumed to have no strength. Theoretically the filaments must follow a geodesic path. This may pose a serious problem with current fabrication methods in that most manufacturers wind with a polar wrapping technique in which it is difficult to follow a true geodesic path. Another factor to be considered is that with current winding equipment identical contours and openings should be used on both ends to yield comparable results.

3.1.3 Determination of Optimum Contour

The zero shear contour developed in this program was evolved from a consideration of the important parameters which affect dome contours. It was recognized that two of the more important parameters were the winding angle and pattern and that an ideal or natural contour would be one in which the fibers are placed in the direction of the applied load and are stressed in pure tension. A survey showed analytical methods for establishing an optimum contour were very difficult and usually based on assumptions which were compromised by practical fabri-

cation techniques. For this reason the initial phase of this program was devoted toward evaluating the effects of various parameters on a natural contour. A unique method was devised in which the winding angle and pattern is made mutually compatible with the natural contour. This was accomplished by an analog technique in which resin-free glass fibers are wound over an inflated rubber bladder. The rubber bladder is initially spherical in shape. This configuration is then pressurized while the glass is still in a relatively limp condition. This yields a natural contour in which no shear, flexural strains or inflection points are present. The original spherical shape changes into a form approximating that of an oblate spheroid. In this method the fibers are free to deflect with minimum resistance since shear forces are non-existent. With controlled winding techniques the fibers are loaded uniformly in pure tension and the pressure load is distributed evenly throughout the dome closure. This was accomplished by winding the first layer of glass with low tension and then pressuring the structure until it was tensioned uniformly. Following this, the winding tension was increased and additional windings were placed over the inflated bladder. When completely wound the internal pressure in the bladder was increased further and the contour change was recorded at various pressures. A two piece telescoping shaft was

used inside the bladder to permit free contour adjustment. Figure 3 illustrates the method used in obtaining the ovaloid configuration. Contour changes were noted using a shadowgraph technique. It was found that the contour approached an asymptote at a relatively low pressure (approx. 22 to 30 psig.). Inasmuch as the fibers are free to adjust themselves, the winding pattern and contour are made mutually compatible.

3.1.4 Winding Angle Effects on Zero Shear Contour

The first step in the determination of a suitable optimum zero shear contour was the evaluation of winding angles and pattern effects. Initial studies showed that in any dome configuration the winding pattern and contour must be mutually compatible to insure that subsequent deflections during hydrostatic loading will not effect the original shape to the point where serious bending and inflection points are encountered. Figures 4 and 5 depict several contours which were obtained from ovaloid specimens. It should be noted that the polar fitting opening requirements were made compatible with the Polaris X-250 second stage requirements. The purpose of these specimens was to determine the effect of winding angle on the zero shear contour. In figures 4 and 5 the zero shear contours of five specimens wound with different winding angles are compared with various theoretical zero hoop stress contours. Each specimen was

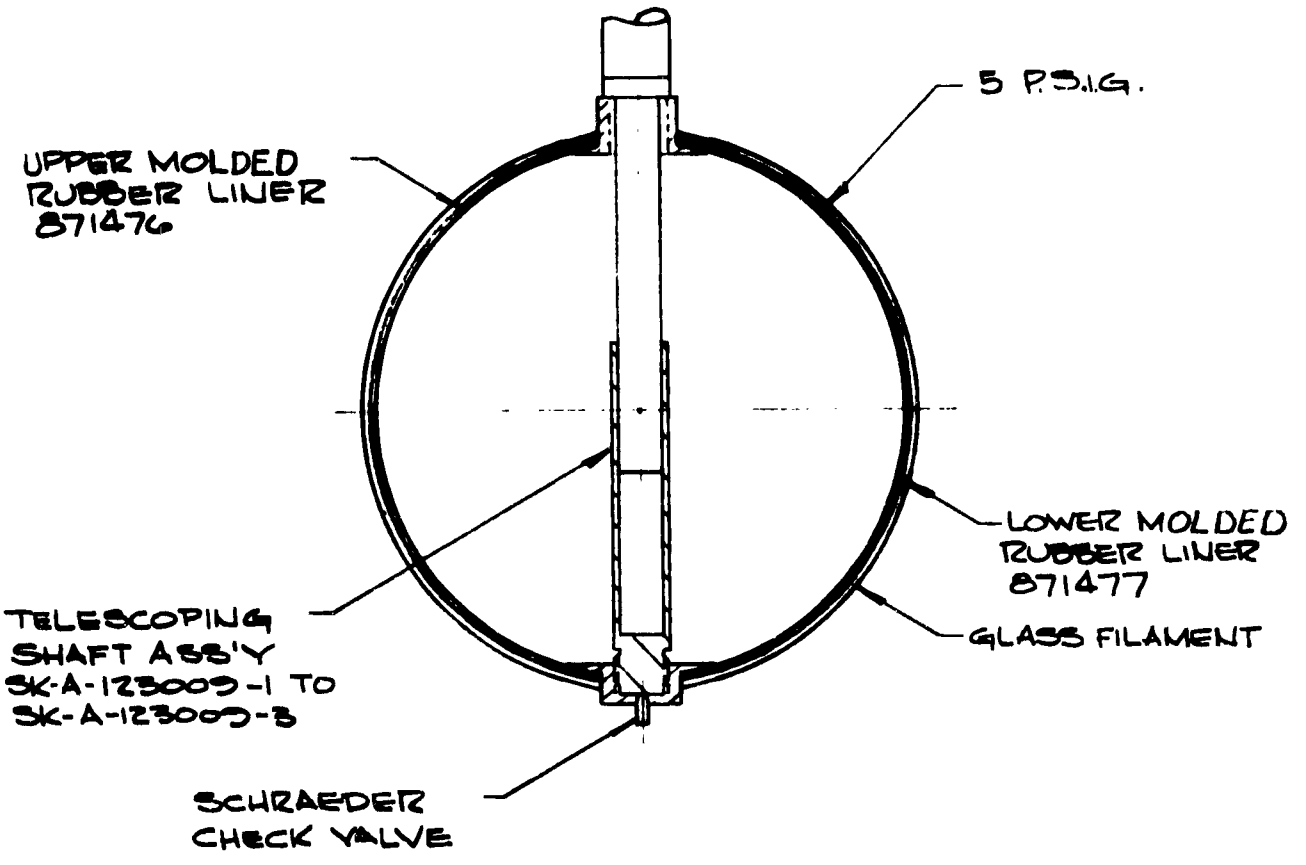

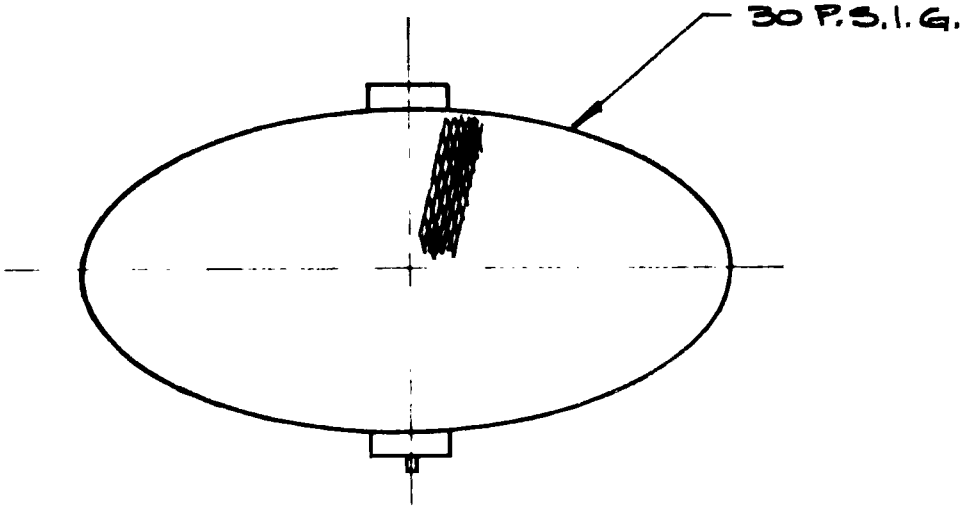

WINDING SET-UP FOR DETERMINING
ZERO SHEAR CONTOUR
SK-A-123009

FIGURE 3

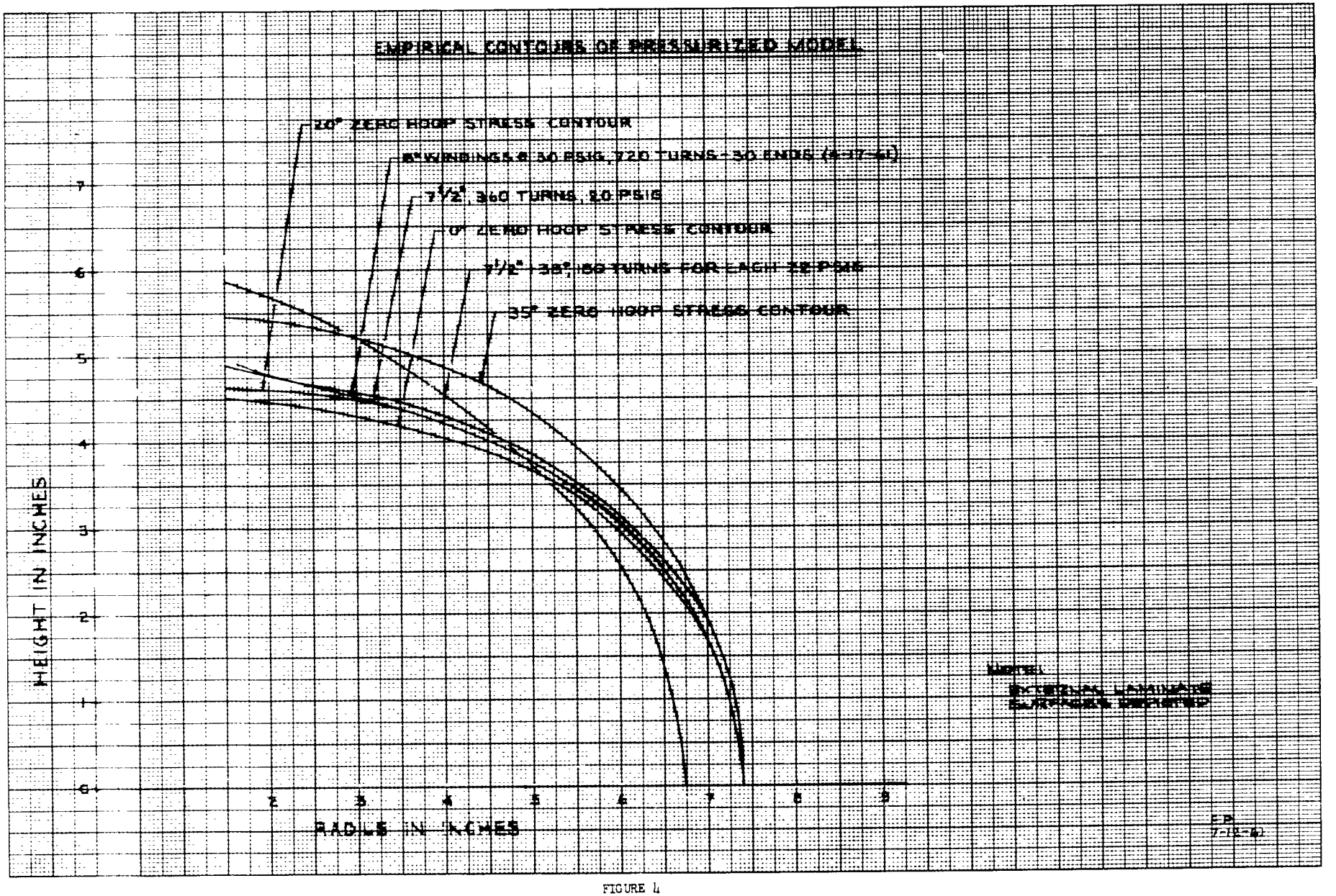
EMPIRICAL CONTOURS OF PRESSURIZED MODEL
20° ZERO HOOP STRESS CONTOUR
8" WINDINGS @ 30 PSIG, 720 TURNS - 30 ENDS (4-17-61)
7½", 360 TURNS, 20 PSIG
0° ZERO HOOP STRESS CONTOUR
7½", 35°, 180 TURNS FOR EACH 20 P SIG
35° ZERO HOOP STRESS CONTOUR
HEIGHT IN INCHES
RADIUS IN INCHES
E.P.
7-12-61

FIGURE 4

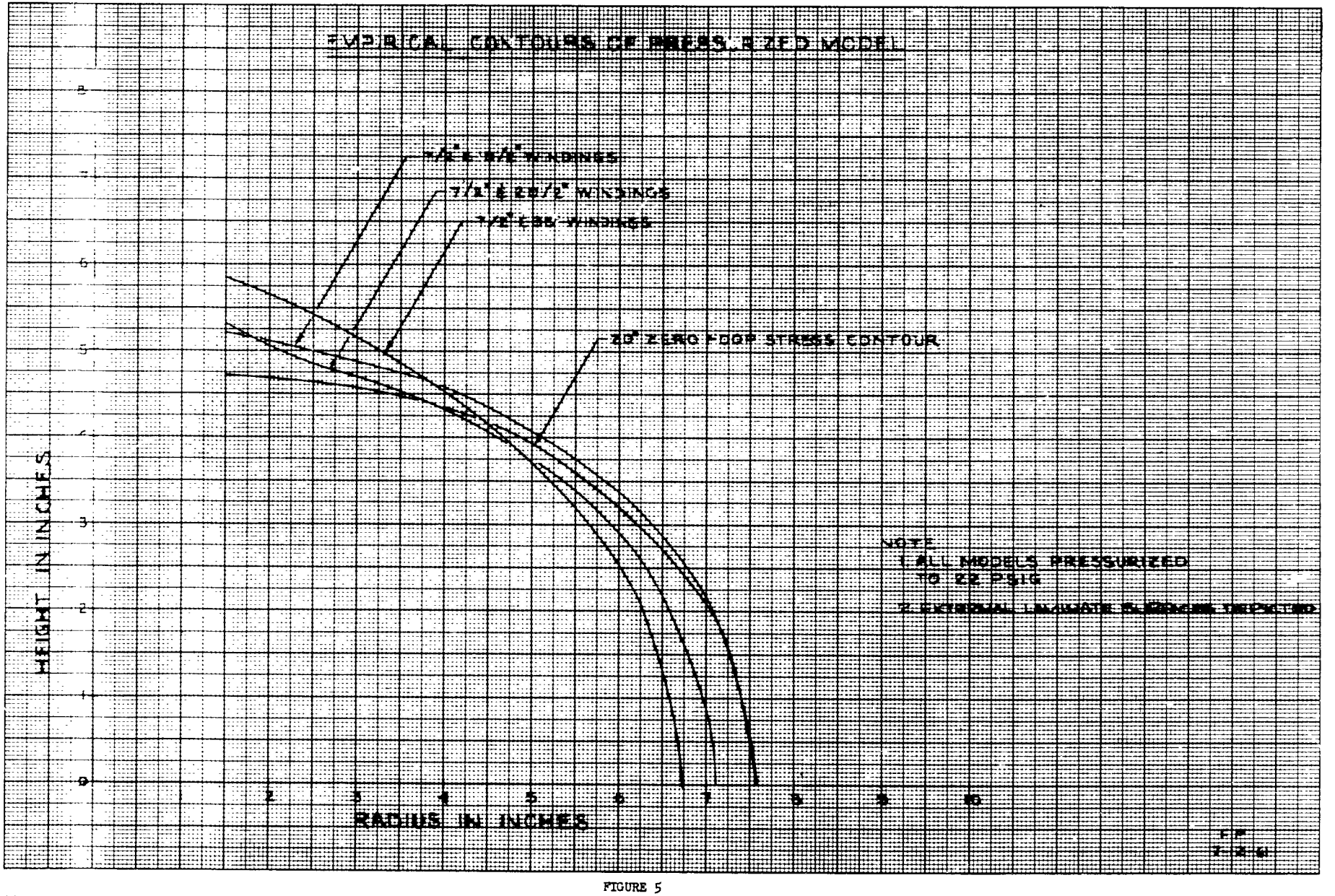
TYPICAL CONTOURS OF PRESSURIZED MODEL
7/8" & 5/8" WINDINGS
7/8" & 20/8" WINDINGS
7/8" & 35 WINDINGS
20" ZERO HOOP STRESS CONTOUR
HEIGHT IN INCHES
RADIUS IN INCHES
NOTE
1. ALL MODELS PRESSURIZED TO 22 PSIG
2. EXTERNAL LAMINATE SURFACES DEPICTED

FIGURE 5

wound with the same total amount of glass and pressurized to the same pressure. A comparison of the zero shear contours obtained for the 7 1/2° and 7 1/2° + 38° wound specimen with the theoretical zero hoop stress contours shows that the larger winding angles are more dominant in controlling the actual shape of the natural contour. An examination of the knuckle area for the 7 1/2° wound contour shows it tends to conform to the low angle theoretical zero hoop stress contour while the configuration wound with the same total amount of glass, but with the glass equally divided between the 7 1/2° and 38° winding angles, better agreement is found with the theoretical 35° zero hoop stress contour. This is illustrated by the parallelism which exists between the two curves in the knuckle region. It should be noted that the empirical contours shown actually depict the external surface of the specimens. In this study phase of the program it was not deemed necessary to obtain the inside laminate contour. Results were considered valid for comparison purposes in the knuckle area up to 50% of the maximum radius because no significant change in laminate thickness was evident. Figure 5 shows three empirical contours for different winding angle combinations plotted against the theoretical 20° zero hoop stress contour. Only one zero hoop stress contour is shown for clarity. It shows that the a/b ratio for the natural zero shear contours becomes smaller with an increase in winding

angle. This agrees with the trend for the theoretical zero hoop stress contours and is expected because additional fiber hoop strength in the knuckle area would increase its resistance to expand.

3.1.5 Effect of Multiple Winding Angles and Girth Reinforcement on Zero Shear Contours

Another area which was investigated involved the effect of girth reinforcement and combinations of winding angle on the zero shear stress dome contours. Based on the geometry of the Polaris second stage chamber two winding angles were selected as the most practical combination; namely 7 1/2° and 20°. The glass filament winding ratio for the 7.5° and 20° winding angle combination was varied between 0.33 and 3.0 which is a 9/1 overall change. This ratio was limited to this range because larger ratios would be impractical in the fabrication of rocket chambers which are stressed equally in the hoop and longitudinal directions. Figure 6 shows the radius of curvature in the knuckle area is smaller for the lower winding ratio. Figure 7 shows the effect of a 9/1 change in the winding ratio on a zero shear stress contour whose diametral growth is restricted by a girth reinforcement at the point of tangency. A gradual transition occurs in the slope of the curves in the area near the point of tangency until the curves become parallel at a point whose radius is approximately 90% of the maximum diameter. This indicates that the glass fiber winding ratio influences dome geometry

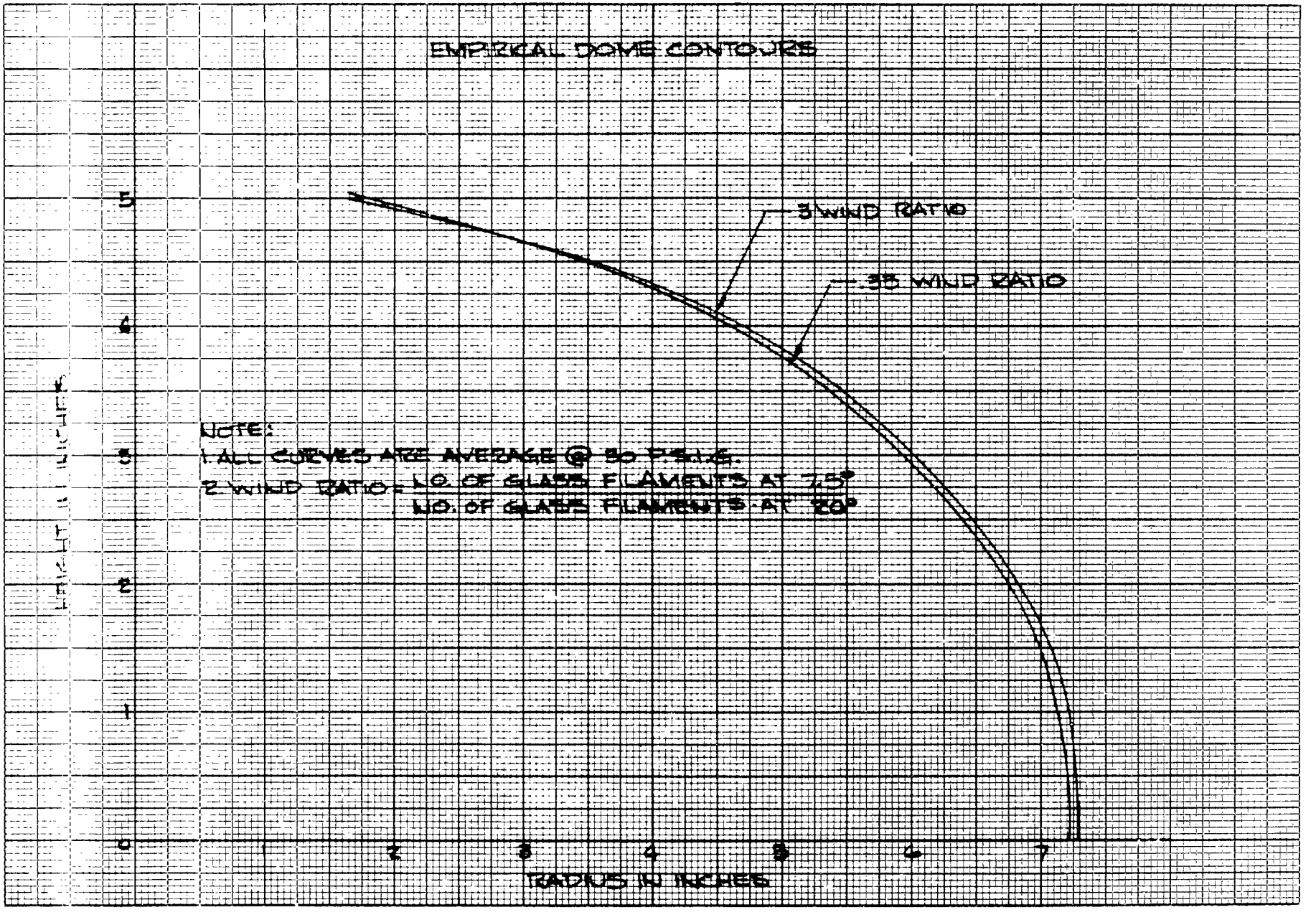
EMPIRICAL DOME CONTOURS
.5 WIND RATIO
.35 WIND RATIO
NOTES:
1. ALL CURVES ARE AVERAGE @ 50 P.S.I.G.
2. WIND RATIO = NO. OF GLASS FILAMENTS AT 75°
NO. OF GLASS FILAMENTS AT 20°
HEIGHT IN INCHES
RADIUS IN INCHES
0
1
2
3
4
5
6
7
8

FIGURE 6

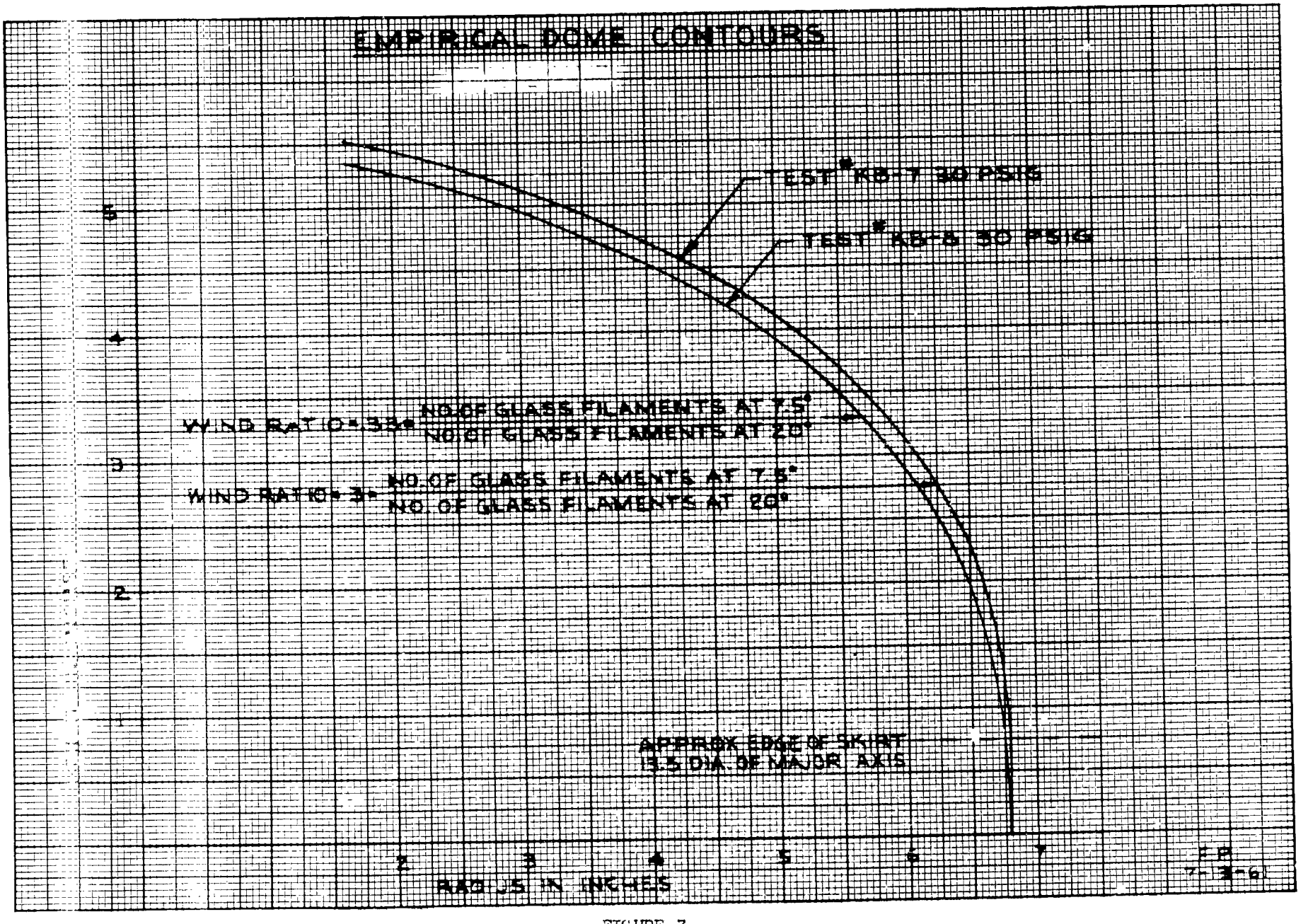
EMPIRICAL DOME CONTOURS
TEST # KB-7 30 PSIG
TEST # KB-8 30 PSIG
WIND RATIO = 3.33 = NO. OF GLASS FILAMENTS AT 7.5° / NO. OF GLASS FILAMENTS AT 25°
WIND RATIO = 3 = NO. OF GLASS FILAMENTS AT 7.5° / NO. OF GLASS FILAMENTS AT 25°
APPROX EDGE OF SKIRT
13.5 DIA. OF MAJOR AXIS
RADIUS IN INCHES
5
4
3
2
1
2
3
4
5
6
7

FIGURE 7

and will effect deflections and bending stresses in the knuckle area. Similar tests with a narrow and wide girth reinforcement showed there was a tendency for slight bulging in the area adjacent to the reinforcement.

3.1.6 Dome Closure Model Tests

Following the study of the important parameters affecting dome closure contours several hydrostatic deflection tests were performed on hardened ovaloid specimens to obtain data concerning 1. the influence of a girth reinforcement on the deflection characteristics of the zero shear dome contour and 2. to determine the deflection characteristics of a particular contour as affected by the winding angle.

Two different dome contour configurations were tested; i.e. contours compatible with a 7 1/2° winding angle and with a balanced winding angle combination of 7 1/2 and 20 degrees. A balanced winding angle combination is one in which the number of glass filaments are equally divided between the two winding angles. These two winding configurations were chosen because they best satisfied the X-250 geometry requirements. The specimens were fabricated with standard Owens-Corning single end glass ECG150-1/0 with an 890 finish. The resin formulation used consisted of Dow 332 resin and Sonite 41 catalyst. The cure cycle was six hours at 200°F, followed by four hours at 250°F.

3.1.6.1 Dome Closure Deflection Tests with the 7 1/2° +20° Ovaloid Configuration

Deflection measurements were taken at 100 psi increments until rupture occurred. Figure 8 illustrates a typical test set up. Figures 9 and 10 show the results obtained on specimens KB-9 and KB-10 which were wound to determine the effect of girth reinforcement on the deflection characteristics. Both specimens were wound over an air inflated bladder and cured while in the pressurized condition. Specimen KB-9 was unreinforced in the girth direction and ruptured in what appears to be a typical hoop failure at 925 psig. Meridional and hoop stresses at failure were 78000 psi and 6900 psi, respectively. Figure 8 shows the failure obtained on specimen KB-9. Based on membrane theory the 20° windings were loaded to 4.44 lbs. per end at failure while the 7 1/2° windings were only loaded to 2.58 lbs. per end. The calculations are shown in Appendix I. Although the failure occurred at a relatively low hoop stress this value is considered reasonable because the hoop forces which were imposed upon the laminate as the ovaloid deflected were resisted mainly by shear in the resin matrix. Specimen KB-10 was reinforced in the girth direction at the equator with a layer of circumferential windings 2 inches wide and approximately 3/16 inches thick.

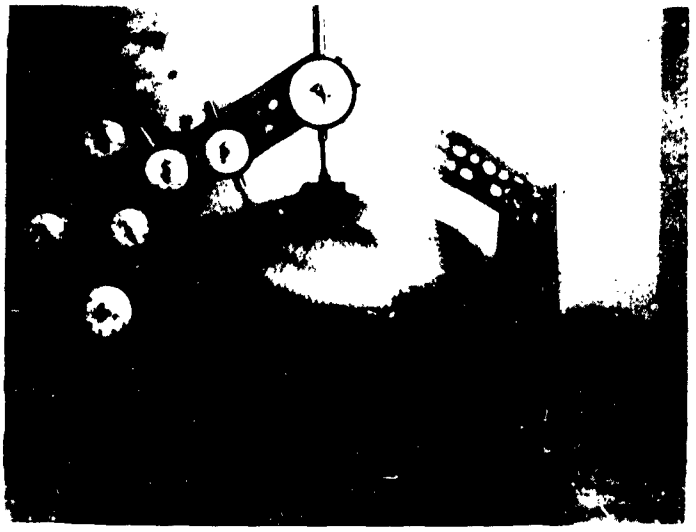

HYDROSTATIC TEST SET-UP
FIG 8 (a)

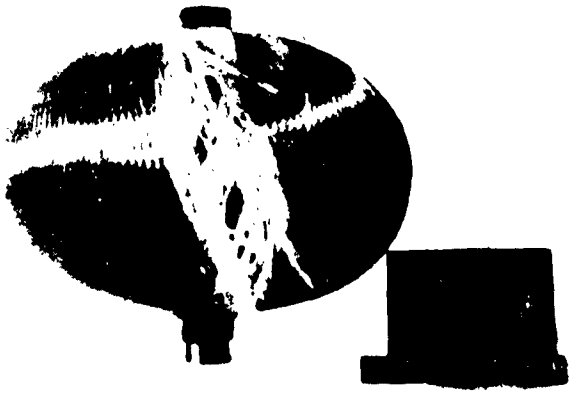

KB-9 OVALOID RUPTURE
FIG 8 (b)

FIGURE 8

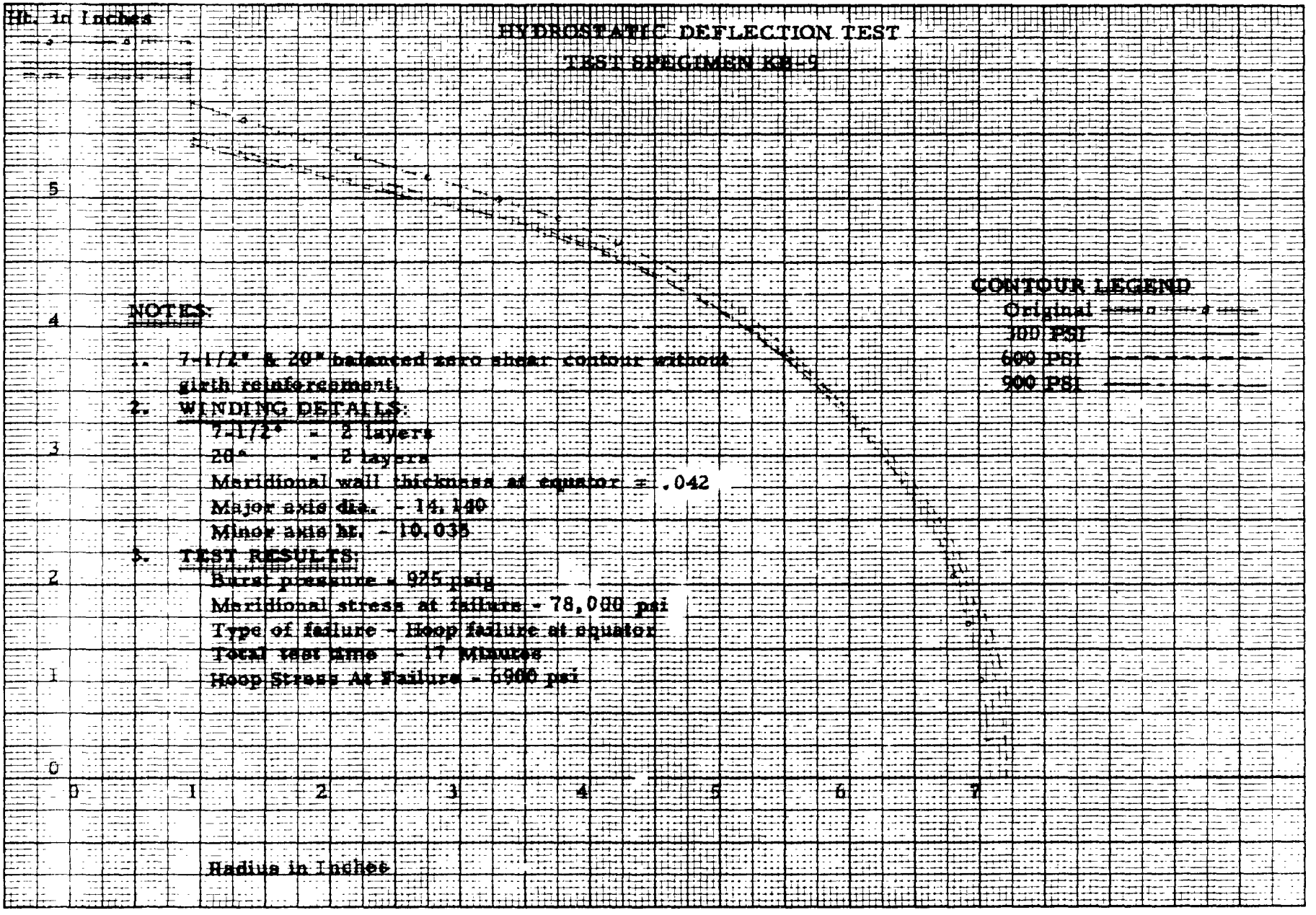
Ht. in Inches
HYDROSTATIC DEFLECTION TEST
TEST SPECIMEN KB-9
CONTOUR LEGEND
Original
300 PSI
600 PSI
900 PSI
NOTES:
1. 7-1/2" & 20" balanced zero shear contour without girth reinforcement.
2. WINDING DETAILS:
7-1/2" - 2 layers
20" - 2 layers
Meridional wall thickness at equator = .042
Major axis dia. - 14.140
Minor axis ht. - 10.035
3. TEST RESULTS:
Burst pressure - 925 psig
Meridional stress at failure - 78,000 psi
Type of failure - Hoop failure at equator
Total test time - 17 Minutes
Hoop Stress At Failure - 6900 psi
0
1
2
3
4
5
6
7
Radius in Inches

FIGURE 9

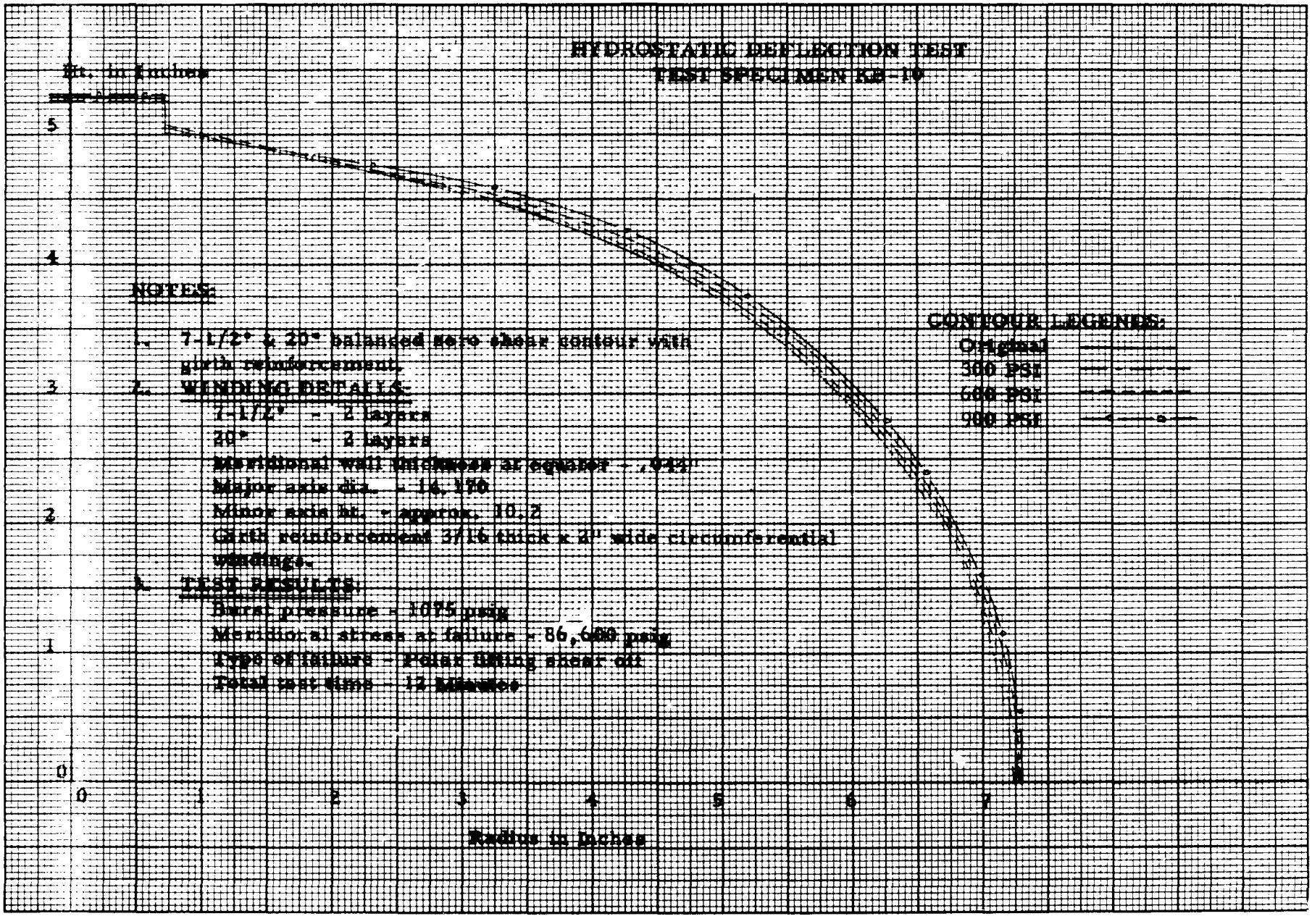
HYDROSTATIC DEFLECTION TEST
TEST SPECIMEN KE-19
Ht. in Inches
5
4
3
2
1
0
0
1
2
3
4
5
6
7
Radius in Inches
NOTES:
1. 7-1/2° & 20° balanced helo shear contour with girth reinforcement.
2. WINDING DETAILS:
7-1/2° - 2 layers
20° - 3 layers
Meridional wall thickness at equator - .044"
Major axis dia. - 14.170
Minor axis ht. - approx. 10.2
Girth reinforcement 3/16 thick x 2" wide circumferential windings.
3. TEST RESULTS:
Burst pressure - 1075 psig
Meridional stress at failure - 86,600 psig
Type of failure - Polar dome shear out
Total test time - 12 Minutes
CONTOUR LEGENDS:
Original
300 PSI
600 PSI
900 PSI

FIGURE 10

This approximated the actual Polaris dome configuration in that the unsupported dome height was proportional to that in the K-250 chamber. Specimen KB-10 failed at a pressure of 1075 psig when the polar fitting blew off in shear. Meridional stresses at the equator were 86,600 psi at the time of failure.

A comparison of test results between specimens KB-9 and KB-10 (see figures 9 and 10) shows:

1. The unreinforced specimen (KB-9) deflected in a positive outward direction at the equator and in a negative inward direction at the polar fitting. The inflection point occurred at a point corresponding to 85% of the maximum diameter.

2. Deflections at the equator and polar fitting are smaller with the girth reinforced configuration.

3. With the exception of the polar fitting, the girth reinforced specimen deflected in a positive direction.

4. Deflection characteristics are significantly different between the two specimens. Based on deflection tendencies bending is evident closer to the major axis for the reinforced specimen.

3.1.6.2 Dome Closure Deflection Tests with the 7 1/2° Ovaloid Configuration

Two hydrostatic deflection tests were performed on specimens KB-15 and KB-16 which were wound with a 7 1/2° winding angle and girth reinforcement. The purpose of these tests was to establish deflection tendencies with this winding angle and to determine the effect of winding over an air inflated bladder. The feasibility of winding thin walled dome contours was also checked as a prelude to the design and test of the 1/4 scale model rocket chamber. Both specimens were wound with less glass than the previous specimens to simulate the expected dome thickness on the 1/4 scale model case which was assumed to be approximately 0.015 inches.

Specimen KB-15 was wound over a plaster mandrel with special polar fittings which conformed to the established 7 1/2° zero shear contour while specimen KB-16 was wound over an air inflated bladder. Both specimens were instrumented with a single bending gage placed in the meridional direction in the knuckle area close to juncture between the dome and girth reinforcement. Figure 11 illustrates specimen KB-15. Deflection measurements were recorded at 100 psig increments until rupture occurred. Specimen KB-15 failed at a pressure of 700 psig at a point in the knuckle

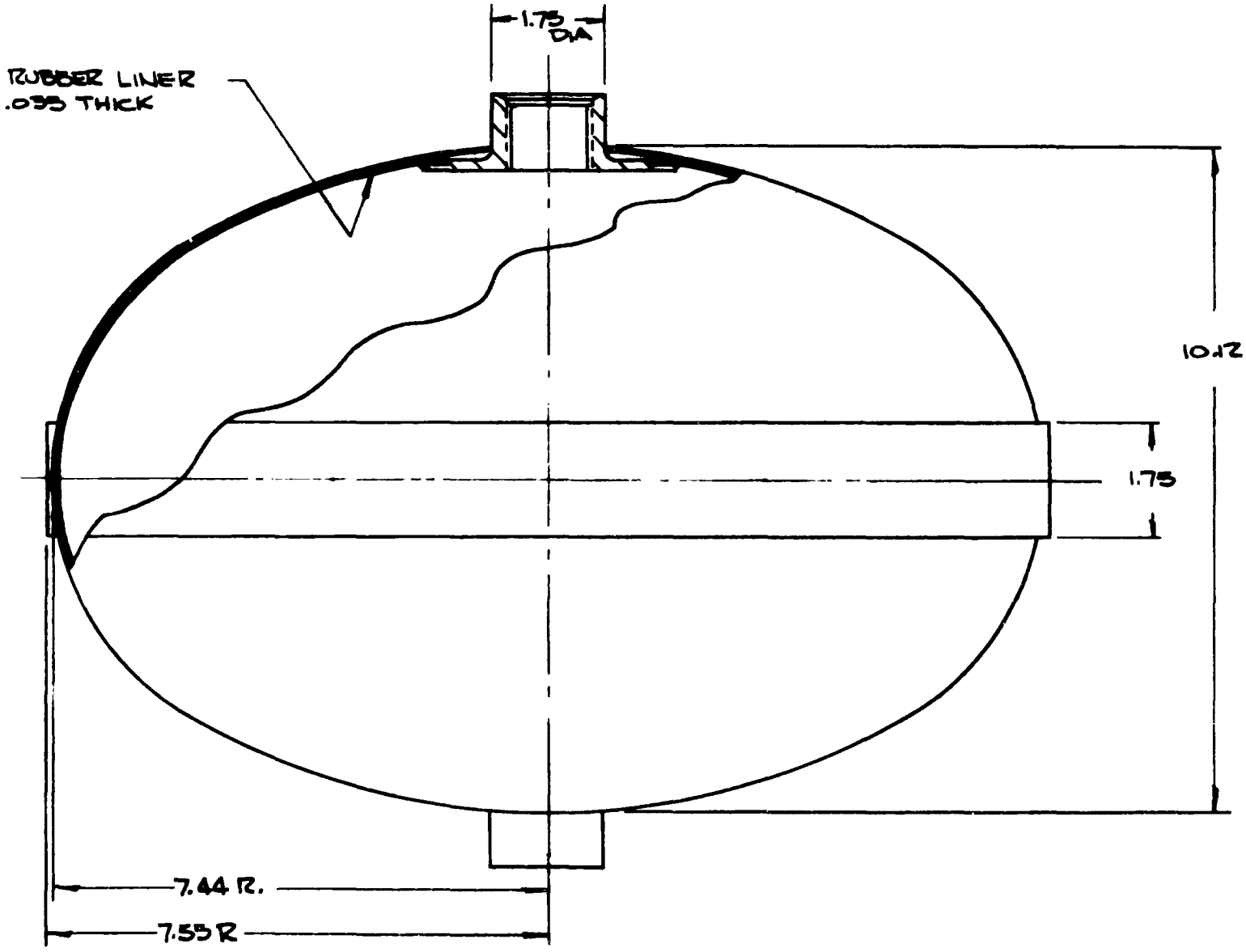

OVALOID
SPECIMEN KB-15
FIGURE 11

area corresponding to a 6.4 inch radius. This yields an average meridional wall stress in the dome at the point of failure of 107,300 psi with a glass loading of 4.32 lbs. per end. At the equator, meridional wall stresses were calculated to be 174,000 psi. Sample calculations for this specimen are found in Appendix II. A photograph of this failure is shown in figure 12.

Specimen KB-16 failed in a similar manner at a pressure of 800 psig. Meridional wall stresses at the point of rupture and equator were respectively, 112,600 psi and 199,000 psi, yielding a glass loading of 4.81 lbs. per end.

Figures 13 and 14 show the hydrostatic deflection test results obtained on specimens KB-15 and KB-16. A noticeable difference exists between the deflections obtained with the specimen wound over an air inflated bladder (KB-16) and the one wound over a rigid plaster mandrel. Deflections were greater on specimen KB-16 especially in the area of the polar fitting and knuckle area. The reasons for this difference are attributed to the following factors:

1. A difference between the polar fitting contours. In KB-16 standard spud and liner assemblies were

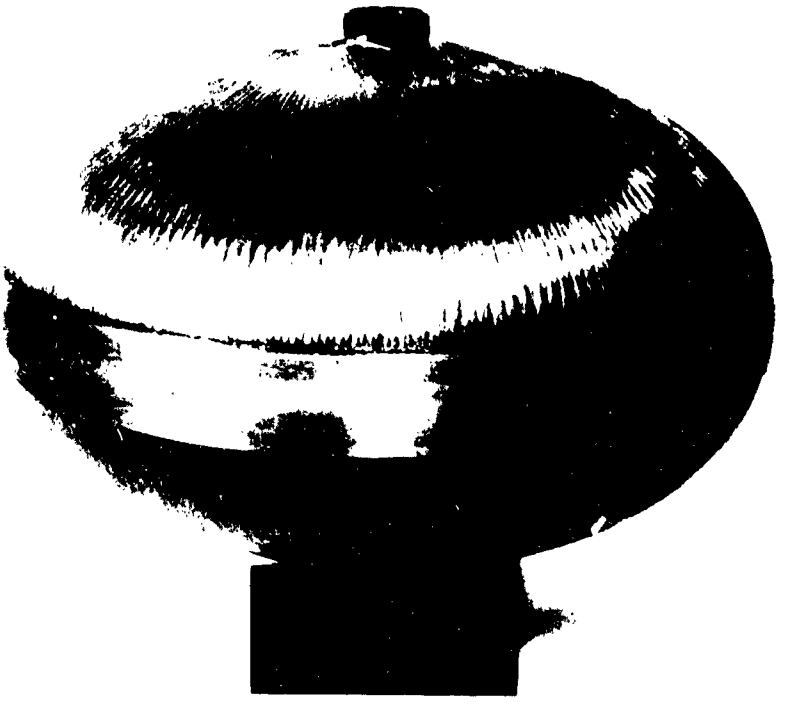

BEFORE TEST

AFTER HYDROSTATIC PRESSURE TEST
700 PSIG BURST PRESSURE

DOME CLOSURE MODEL TEST SPECIMEN # KB-15

FIGURE 12

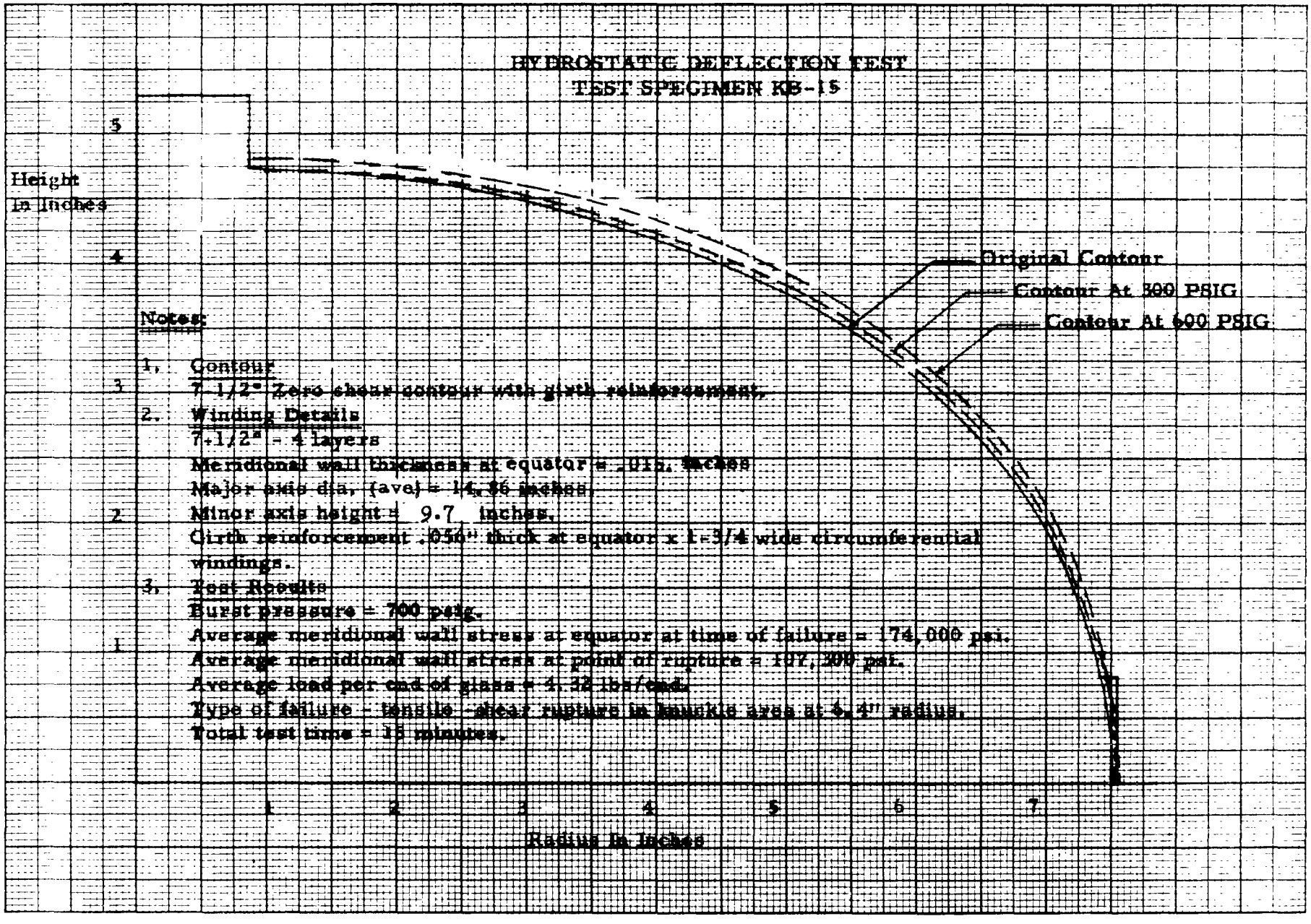
HYDROSTATIC DEFLECTION TEST
TEST SPECIMEN KB-15
Height
in Inches
5
4
3
2
1
Original Contour
Contour At 300 PSIG
Contour At 600 PSIG
Notes:
1. Contour
7 1/2" Zero shear contour with girth reinforcement.
2. Winding Details
7 1/2" - 4 layers
Meridional wall thickness at equator = .015 inches
Major axis dia. (ave) = 14.86 inches
Minor axis height = 9.7 inches.
Girth reinforcement .050" thick at equator x 1-3/4 wide circumferential windings.
3. Test Results
Burst pressure = 700 psig.
Average meridional wall stress at equator at time of failure = 174,000 psi.
Average meridional wall stress at point of rupture = 107,200 psi.
Average load per end of glass = 4.32 lbs/end.
Type of failure - tensile -shear rupture in knuckle area at 4.4" radius.
Total test time = 15 minutes.
1
2
3
4
5
6
7
Radius In Inches

FIGURE 13

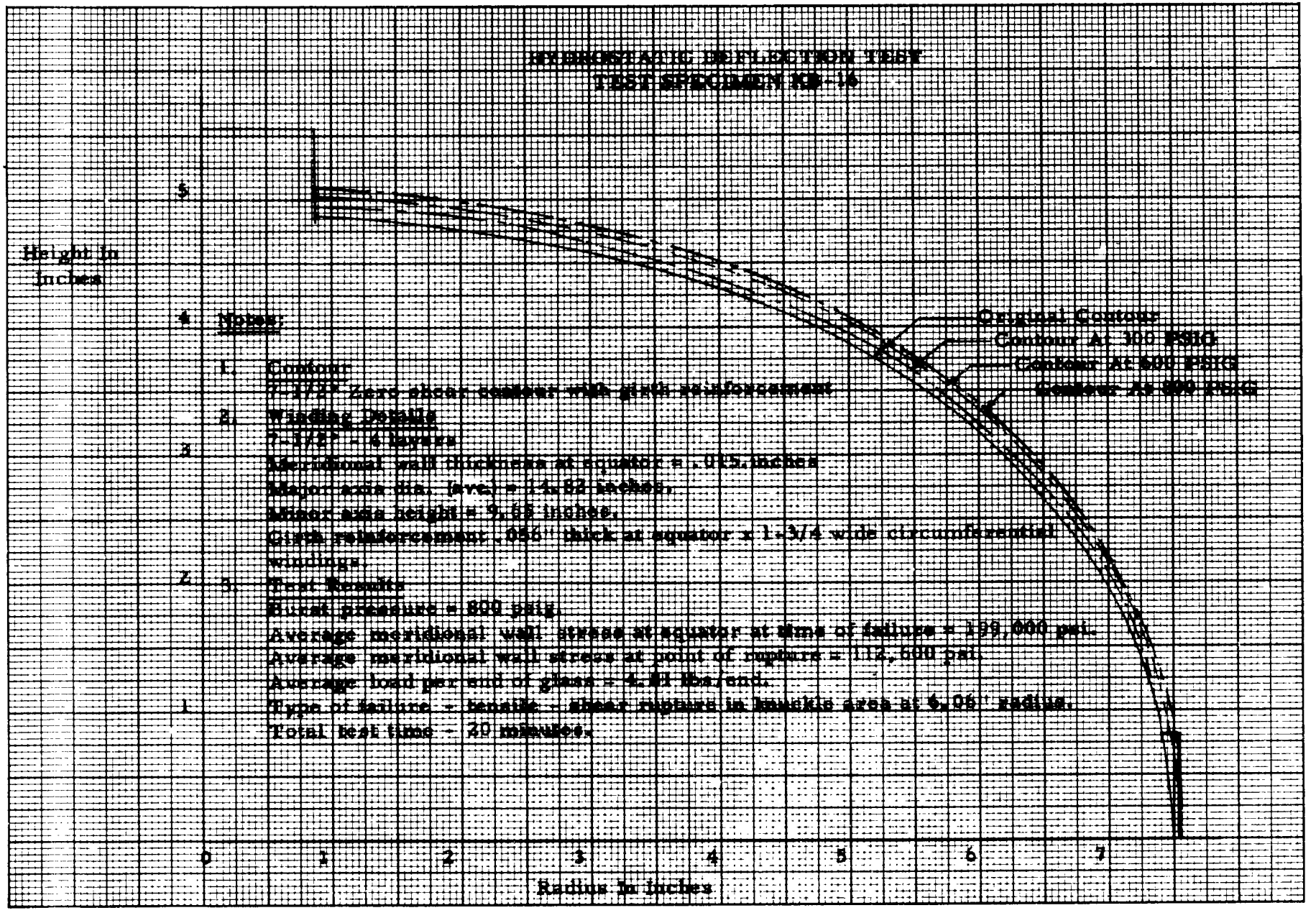
HYDROSTATIC DEFLECTION TEST
TEST SPECIMEN KB-16
Height in inches
Original Contour
Contour At 300 PSIG
Contour At 600 PSIG
Contour At 800 PSIG
Notes:
1. Contour:
7-1/2F Zero shear contour with girth reinforcement
2. Winding Details
7-1/2F - 6 layers
3. Meridional wall thickness at equator = .015 inches
Major axis dia. (ave.) = 14.82 inches.
Minor axis height = 9.65 inches.
Girth reinforcement .056" thick at equator x 1-3/4 wide circumferential windings.
4. Test Results
Burst pressure = 800 psig.
Average meridional wall stress at equator at time of failure = 199,000 psi.
Average meridional wall stress at point of rupture = 112,600 psi.
Average load per end of glass = 4.81 lbs/end.
Type of failure - bending - sheet rupture in knuckle area at 6.06" radius.
Total test time - 20 minutes.
0
1
2
3
4
5
6
7
Radius in inches

FIGURE 14

used in the air inflated bladder. In KB-15 special fittings were used which matched exactly with the zero shear contour.

2. A difference between the polar fitting flange diameters. The flange diameter on specimen KB-15 was 4" compared to 3" on specimen KB-16.

3. A difference in filament orientation over the dome contour. Inasmuch as specimen KB-16 was wound over an inflated bladder some reorientation of the filaments took place while in specimen KB-15 this was not possible.

3.1.6.3. Strain Gage Results

Meridional tensile and bending strains were measured near the girth build up with type C9-F20 Flexagages. Results are shown in Table 2. Very small positive bending strains were measured indicating deflections at this point were uniform with very little change in curvature. Since both specimens failed at points approximately 1.5" away from the gage position it becomes evident that if bending effects were the cause of these failures, they are very local and difficult to detect. Bending is manifested by a change in the radius of curvature and are not readily detected from the deflection curves. In

TABLE 2

Strain Gage Results - Test KB-15

Pressure Psig	Meridional Strain in μ in/in	Bending strain in μ in/in	Gage Location expressed as % of full diameter
100	2475	35	94.0
200	4853	87.5	"
300	7527	63	"
400	10476	84	"
500	13356	14	"
600	16151	49	"

Strain Gage Results - Test KB-16

100	2685	105	>4.0
200	5547	109	"
300	8249	91	"
400	11615	81	"
500	14242	88	"
600	17399	21	"
700	20052	28	"
800	23080	0	"

specimen KB-16 bending strains actually diminish with increased pressure until at maximum pressure no bending strain was detected. This shows that a shape change had taken place and if bending was still present it had gradually shifted to another point during pressurization. Appendix III presents equations for calculating bending strains.

3.1.6.4 Comparison With Full Scale Rocket Chamber Deflections

Table 3 and 4 is a qualitative comparison between ovaloid deflection test results and those obtained on full scale X-250 chambers. Table 3 presents scaled deflections obtained on ovaloid specimens KB-15 and KB-16 which correspond to similar locations on full scale X-250 cases for which hydrostatic deflection data is available. Table 4 contains a summary of deflection data for a number of X-250 cases which were tested between December 17, 1960 and June 17, 1961. Ovaloid deflections are shown for an internal pressure of 300 psig because this corresponds to a 74,700 psi meridional wall stress which is close to the value being attained in the full scale chambers. An examination shows that although equivalent ovaloid deflections at 300 psig are in general smaller than those obtained on full scale X-250 cases at proof pressure, no definite conclusions can be made. This

TABLE 3

Hydrostatic Deflection Test Results from Ovaloid Specimens

Gage Location expressed as % of full diameter		12.5	44.7	68.8	85.5	20.4	39.0	53.8	68.8
Actual ovaloid contour deflection at 300 psig (74,700 psi meridional wall stress)	Specimen KB-15	.0	.050	.060	.050	.010	.040	.055	.062
	Specimen KB-16	.070	.075	.070	.060	.090	.080	.060	.070
*Scaled ovaloid deflection (3.61x actual)	Specimen KB-15	.0	.180	.217	.180	.036	.144	.198	.224
	Specimen KB-16	.252	.270	.252	.216	.325	.289	.216	.252

*This evaluation ignores the difference in geometry between the ovaloid and full scale case and is made only for qualitative purposes.

TABLE 4

Average Hydrostatic Deflection Test Results for X-250 Cases Tested Between 12/17/60 and 6/17/61

Gage No.	A	B	C	D	E		G	H
Dome	Aft	Aft	Aft	Aft	Fwd	Fwd	Fwd	Fwd
Gage Location Expressed as % of full diameter	12.5	44.7	68.8	85.5	20.4	39.0	53.8	68.8
Average deflection in inches at Proof Pressure	.360	.329	.247	.180	.535	.553	.497	.332
Max. deflection in inches at proof pressure	.485	.450	.347	.389	.714	.686	.649	.496
Min. deflection in inches at proof pressure	.271	.259	.177	.128	.373	.353	.330	.235

is due to:

1. The wide range of deflections encountered on full scale cases and
2. Differences in the geometry and construction between the ovaloid specimens and full scale chambers.

It should be noted that smaller deflections are encountered on the aft end of the full scale chambers. This is to be expected because of the large metal dish which tends to limit axial growth.

3.1.7 Zero Shear Contour Determination

The first step in the determination of a suitable zero shear contour for the X-250 motor case was the selection of a winding angle and pattern which was compatible with the Polaris second stage design requirements. Detailed fabrication information on full-scale models was unavailable and it appeared that various vendors were utilizing different winding techniques. Two winding angles, 7 1/2° and 20°, were considered but it was finally decided to use a single winding angle of 7 1/2° for the scale model rocket case. A sequential winding pattern consisting of 181 flier turns per mandrel revolution was selected because it produced a minimum number of cross-over points, minimized slippage problems and appeared most compatible with geodesic requirements.

The analog technique discussed previously was used to establish the zero shear contour. Fitting diameters were chosen to simulate the Polaris second stage aft end closure. The actual contour requirement for the inside of the laminate was obtained by carefully cutting the ovaloid specimen into two halves. The contour was then carefully traced and measured to establish accurate coordinates. The coordinates were based on average readings obtained from the four quadrants. Figure 15 presents the zero shear contour for the 7 1/2° winding angle. A comparison of the derived zero shear contour coordinates with the theoretical Ideal Geodesic Contour is shown in Table 5. Very good agreement is evident. This substantiates the use of this experimental approach. The small deviations can be attributed to minor variations in taking measurements and to other process variables. Figure 16 is a comparison of the A-2 forward and aft dome contours with the zero shear and small angle zero hoop contour.

3.1.8 Summary and Conclusions For Phase I

Many important conclusions were derived from this first phase of the program and a significant insight was made into the parameters affecting the shape of optimum dome contours. The direct result of this phase was the establishment of a zero shear contour.

The following specific conclusions were derived from results and observations made in this phase of the program.

1. A different contour is required for each winding pattern and design configuration.
2. The analog technique for the determination of the zero shear contour yielded results which agreed with theoretical calculations (zero shear contour was practically identical to the Ideal Geodesic Contour).
3. A sequential winding pattern is preferred for use with the zero shear contour because it best conforms to the geodesic requirements and produces a minimum number of cross-over points.
4. The forward and aft polar ports should require identical openings to insure compatibility between the contour and winding pattern on both end closures.

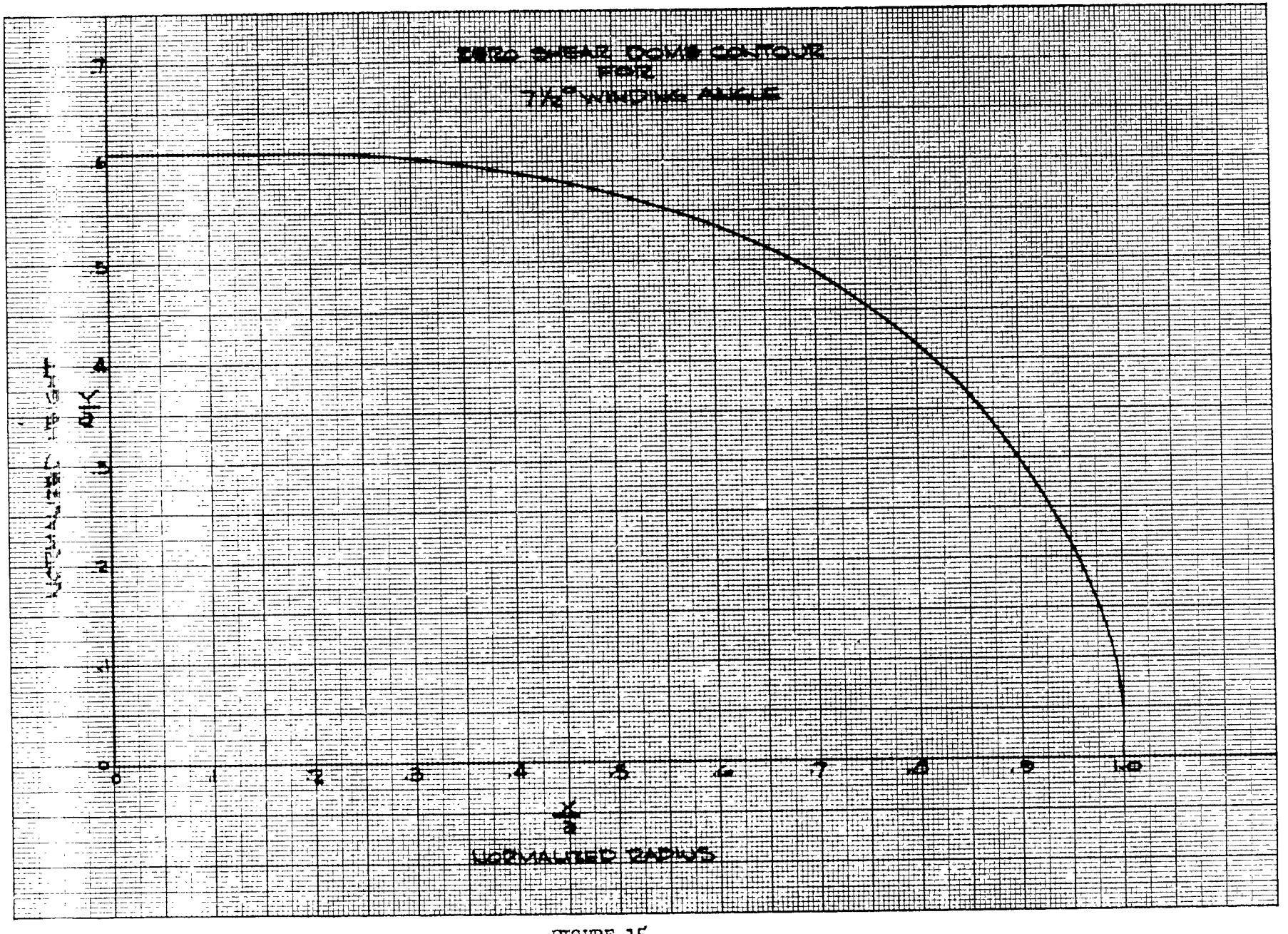
ZERO SHEAR DOWN CONTOUR
FOR
7½° WINDING ANGLE
NORMALIZED RADIUS

FIGURE 15

TABLE 5

COMPARISON OF GEODESIC AND ZERO SHEAR CONTOUR COORDINATES

NORMALIZED RADIUS x/a	NORMALIZED DOME HEIGHT - y/a α = 7 1/2°	
	ZERO SHEAR CONTOUR	IDEAL GEODESIC CONTOUR
.130	.605	.607
.200	.604	.603
.300	.599	.596
.400	.584	.583
.500	.563	.561
.550	.547	.546
.605	.528	.526
.650	.507	.507
.700	.483	.481
.760	.443	.443
.800	.412	.412
.855	.359	.358
.870	.340	.347
.890	.316	.318
.900	.303	.304
.905	.295	.297
.925	.265	.267
.950	.220	.219
.955	.209	.208
.980	.142	.141
.990	.105	.100
1.000	.0	0.00

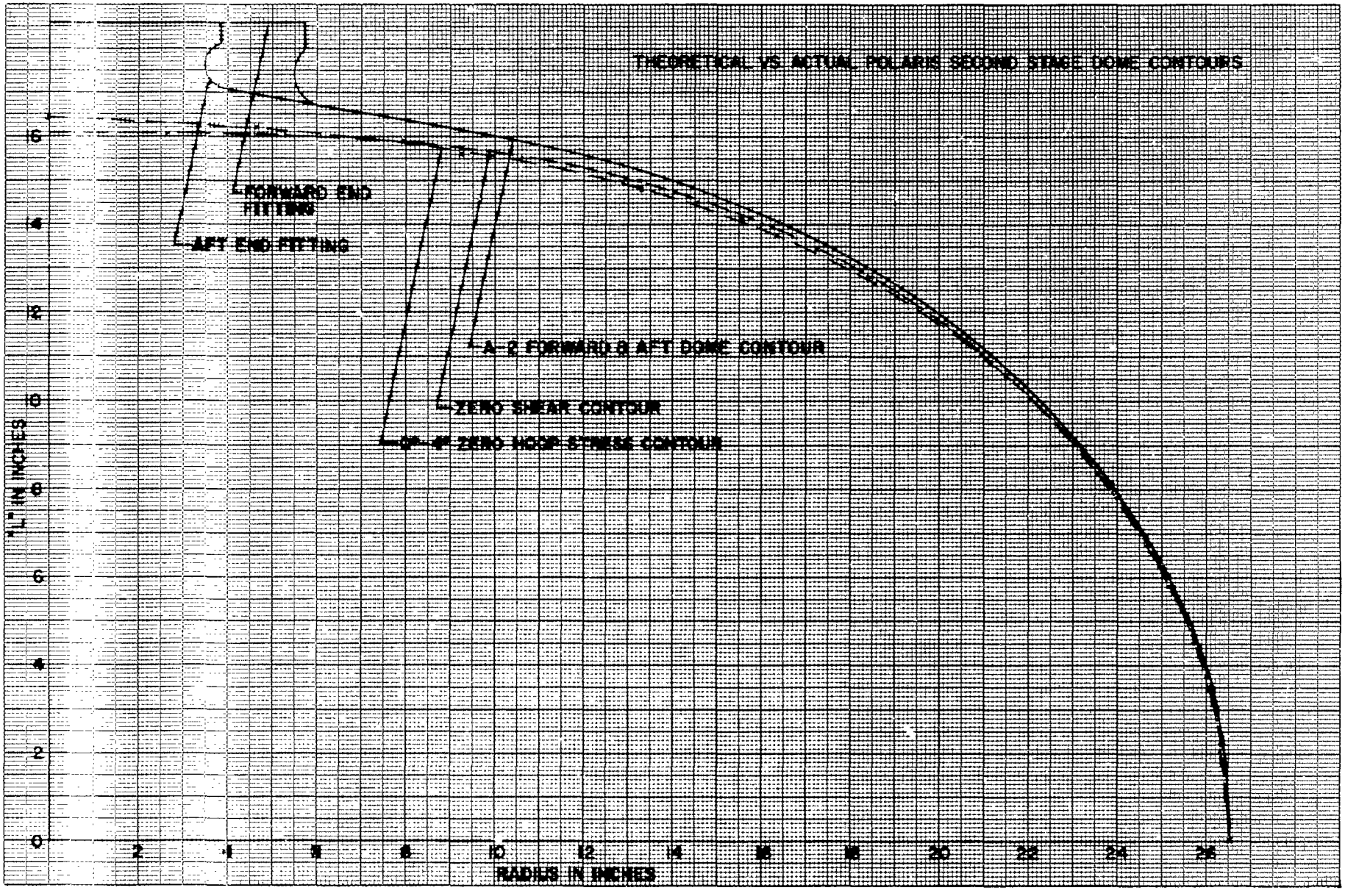
THEORETICAL VS ACTUAL POLARIS SECOND STAGE DOME CONTOURS
FORWARD END FITTING
AFT END FITTING
A-2 FORWARD & AFT DOME CONTOUR
ZERO SHEAR CONTOUR
ZERO HOOP STRESS CONTOUR
"L" IN INCHES
RADIUS IN INCHES
0
2
4
6
8
10
12
14
16
18
20
22
24
26

FIGURE 16

3.2.0 Phase II - Rocket Chamber Scale Model Design and Study

3.2.1 Design of 1/4 Scale Model

The first step in the design of the 1/4 scale model of the Polaris second stage chamber consisted of a dimensional analysis to obtain the necessary governing similarity relationships. Results of this study showed that ideally both geometric and loading similarity must be maintained between the model and full scale chambers. Similarity relationships were derived for the following two assumptions:

1. The fiberglass structure is such that the internal pressure results in glass fiber tension only.
2. The fiberglass structure is such that shear and bending stresses as well as direct stresses are introduced when the chamber is pressurized.

In the case of a rocket chamber each of the above assumptions result in somewhat different similitude requirements. Results are shown below:

Case 1. Glass Fibers in Tension Only

a. Stress Requirement

$$S/P = F\left[\frac{d_1}{d_2}, \frac{t}{d}\right]$$

b. Deflection Requirement

$$\delta/d_2 = F\left[\frac{P}{E}, \frac{d_1}{d_2}, \frac{t}{d_2}\right]$$

Case 2. Glass Laminate Resists Shear, Bending and Direct Stress

a. Stress Requirement

$$S/P = F\left[\frac{E}{P}, \frac{G}{P}, \frac{l}{d_2}, \frac{t}{d_2}\right]$$

b. Deflection Requirement

$$\delta/d_2 = F\left[\frac{E}{P}, \frac{G}{P}, \frac{l}{d_2}, \frac{t}{d_2}\right]$$

where S = Stress, (psi)

δ = deflection (inches)

P = internal pressure (psig)

d_1 = polar fitting diameter, (inches)

d_2 = cylinder diameter, (inches)

t = wall thickness

E = Elastic Modulus (psi)

G = Shear modulus (psi)

l = length of cylinder (inches)

F = "Function of"

Although the similitude requirements are different for the two basic assumptions, they do not contradict each other. Results show that if geometric and loading similarities are maintained, the following relationships exist between the scale model and prototype:

a) $S_m = S_p$

b) $\varepsilon_m = \varepsilon_p$

where S = stress (psi)

ε = strain (in/in)

m = subscript denoting model

p = subscript denoting full scale prototype

Geometric similarity is easily obtained by making the specimen a true scale model of the prototype with all linear dimensions reduced by the same scale factor. Loading similarity is maintained by using the same material and by testing the model at the same pressure as is required for the full scale chamber. Since both stresses and strains are simulated in the model the mode of failure should be duplicated. Test results have substantiated this premise. It should be noted that some differences did exist in the model because of the omission of the non-polar ports, and reinforcements.

The 1/4 scale polar ported chamber designed for test evaluation is shown in Figure 17 (Drawing SK-134943). All linear dimensions were obtained by taking 1/4 of the values shown on ABL drawing No. 250-2100 for the X-250 chamber. In those instances where dimensions were not given, their values were scaled. Based on polar port geometry a longitudinal winding angle of 7 1/2° was chosen. The forward and aft dome closure contours were designed to conform with the zero-shear contour developed in the first phase of this program. The stiffness of the aluminum skirt and reinforcement was simulated on the model by means of additional circumferential windings over a portion of the dome at the

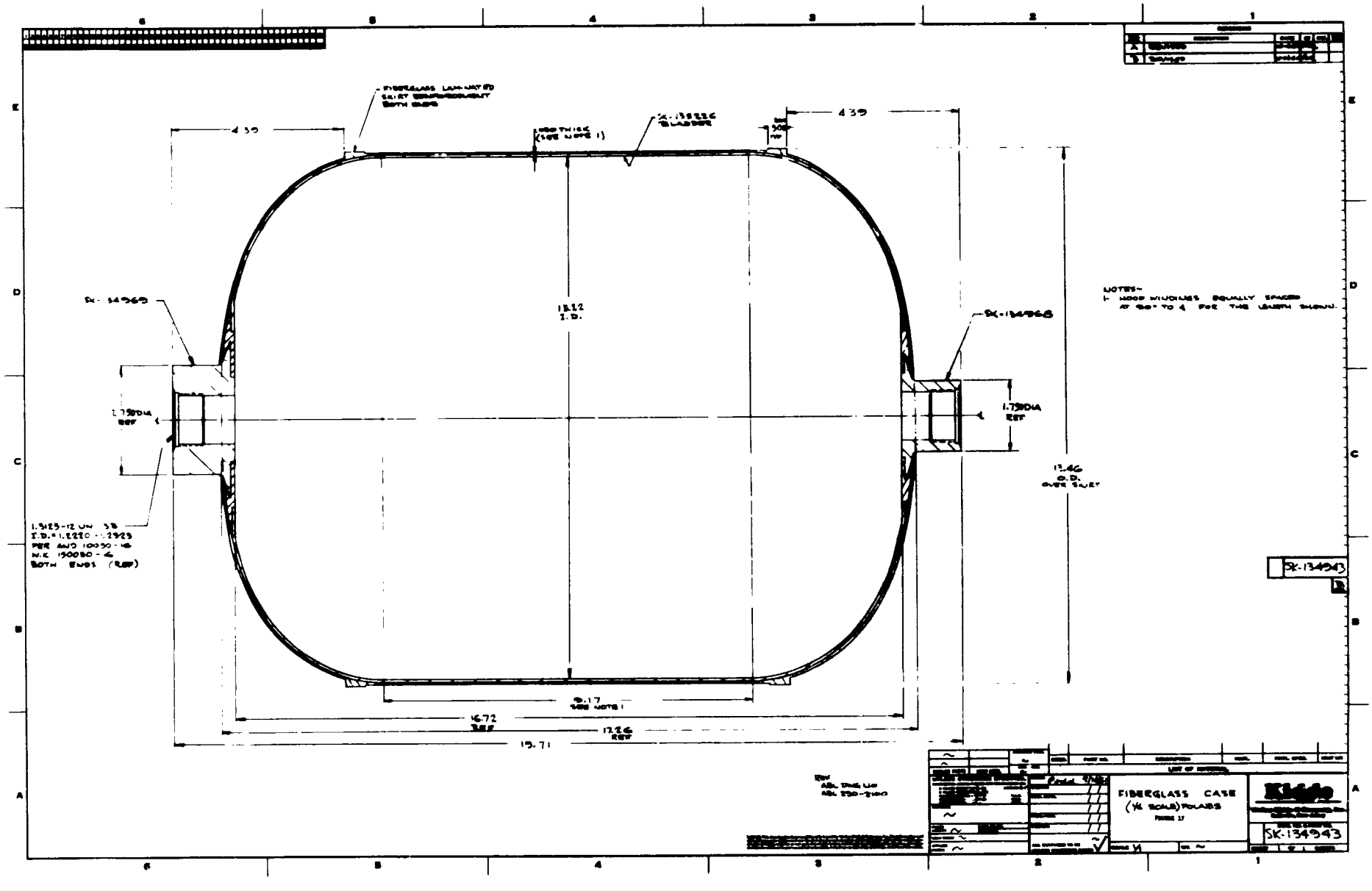
FIBERGLASS LAMINATED SILKY REINFORCEMENT BOTH SIDES
4.39
4.39
SK-134966 BLADDER
SK-134965
SK-134965
13.12 I.D.
1.750 DIA REF
1.750 DIA REF
1.5625-12 UN-3B I.D.=1.4220 - .2923 PER AMS 10050-16 M.K. 150050-16 BOTH ENDS (REF)
13.46 O.D. OVER SUET
9.17 REF NOTE 1
16.72 REF
17.26 REF
19.71
NOTES-
1- HOOP WINDINGS EQUALLY SPACED AT 90° TO 4 FOR THE LENGTH SHOWN.
SK-134943
FIBERGLASS CASE (1/4 SCALE) POLARIS
SK-134943

point of tangency. (See Appendix IV). The scale model dimensions for the skirt reinforcement windings were made compatible with the zero shear contour. Special adapters were used to provide a square shoulder. Design equations relating fiber forces, winding angles and number of ends for the cylindrical portion of a fiberglass container are presented in Appendix V. Equations are included for the special case where two or more angles are used. An equation relating winding angles and number of ends for a balanced design, i.e., equal fiber stress, is also given.

The actual design of the X-250 second stage Polaris case is given in Appendix VI. The number of turns (ends) of 7 1/2° and 90° windings are given for a 1/4 scale model as well as for the full size rocket case. The chamber was designed for equal strength in both the hoop and longitudinal directions to demonstrate the contour's greater efficiency and because available data indicated definite design requirements were not established. Since equal stress in both layers of windings produces equal strains in all directions it seemed reasonable to expect greater overall strength if uniform fiber loading were achieved. The chamber was designed to withstand a proof pressure of 450 psig at a glass loading of 4.8 lbs. per end. This basically agrees with results currently being obtained on the X-250 motor cases.

3.2.2 Specimen Fabrication

The specimens were wound with a polar type wrapping machine using a Cerro-tru (Cerro DePasco Corp. low melting temperature alloy) mandrel. The resin formulation consisted of 100 parts by weight of Epon 820 resin and 22 parts by weight of Sonite 41 catalyst. Cure temperatures were 8 hours at 210°F. The cerro-tru mandrel was cast in three sections, i.e., cylindrical center section, and forward and aft dome sections. The three sections were assembled and held in place by means of a shaft. The tapered outside diameter was then machined and a rubber liner was fitted over the assembly. Two end fitting assemblies were then cemented to the rubber liner using Bostik 1007 primer and 1008 adhesive. The end fittings contained rubber molded flanges to prevent leakage problems (see drawings SK-134968 and SK-134969). Prior to winding the case an air leak test was performed. To prevent bulging of the rubber liner a partial vacuum was created inside the mandrel assembly.

The longitudinal windings were first applied using a sequential winding pattern. A total of 675 flier revolutions were made using 10 ends in the roving. Single end glass filaments of ECG-150-1/0 890 were used. The applied tension was 0.4 lbs. per end for the longitudinals and 0.7 lbs. per end for the hoop windings. The hoop windings consisted of 627 ends per

inch of length over the cylindrical section. The girth reinforcement for simulating the skirt was applied using a fixture which provided a shoulder and prevented the windings from slipping over the dome. The total empty weight of the chamber was 4.84 pounds. The liner and fittings weighed 3.08 lb. Initial chamber volume was 2024 in^3.

3.2.3 Instrumentation & Test Procedures

A total of 13 strain gages were mounted on each chamber as shown in Figure 18. Nine gages were mounted on the aft dome. Four of those gages were Flexagages (manufactured by the Budd Co.) which were used to determine bending strains in the dome contour. The remaining gages were of the post yield type PA-3 manufactured by the Baldwin-Lima-Hamilton Co. Single gages were mounted on the cylinder midsection in the hoop and longitudinal directions.

Twenty-three dial indicators were mounted as shown in Figure 19. Both forward and aft dome closure deflections were measured. Cylinder radial expansion was measured at the mid section and at both ends near the point of tangency. With the exception of the indicators measuring cylinder growth and tilt, all indicators were mounted in one plane.

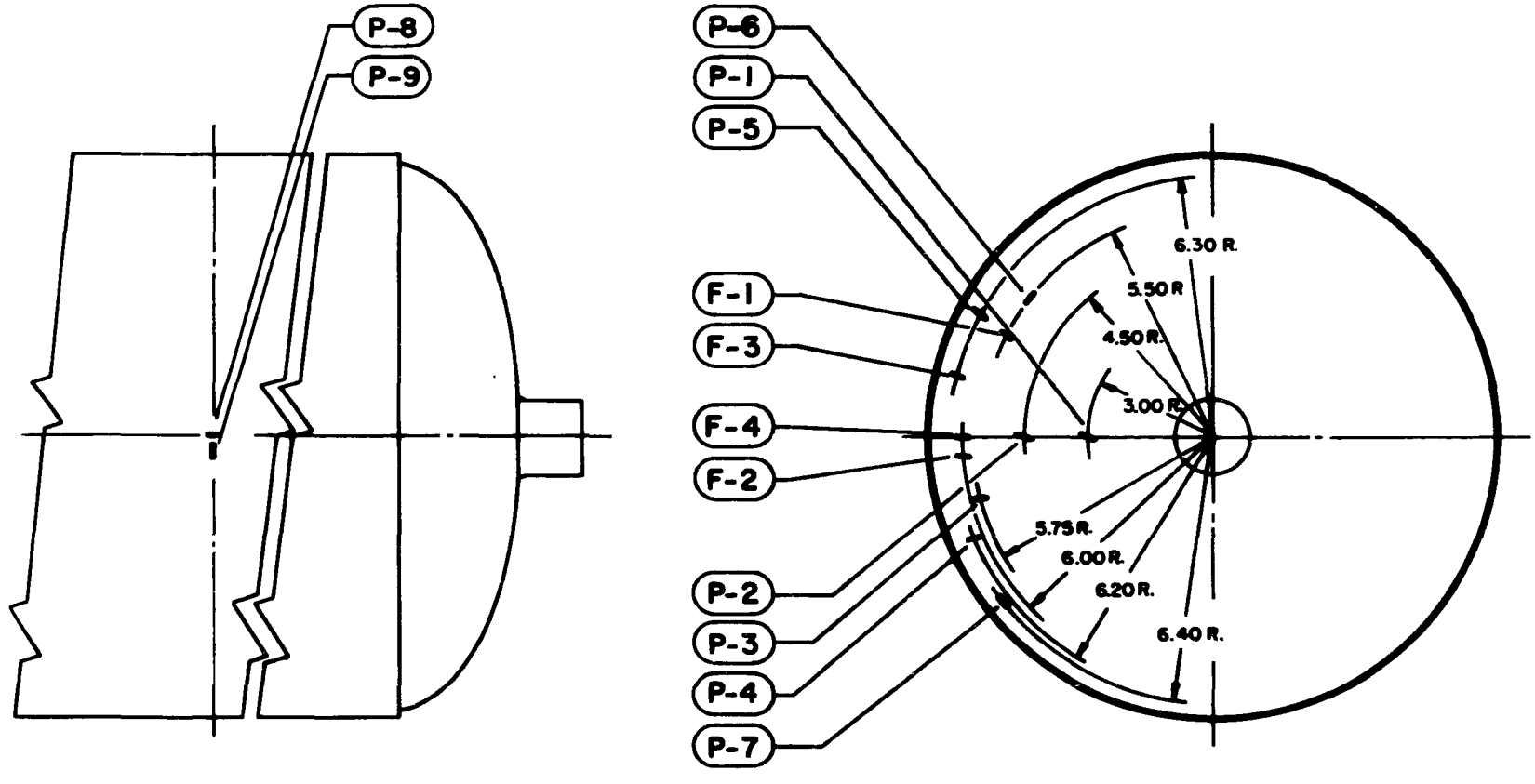

GAGE NOS. F-1, F-2, AND F-3 — FILAMENT PATH
GAGE NO. F-4 — MERIDIONAL PATH
GAGE NOS. P-1, P-2, P-3, P-4, AND P-5 — FILAMENT PATH
GAGE NOS. P-6 AND P-7 — HOOP DIRECTION
GAGE NO. P-8 — MID-CYL. LONGITUDINAL DIRECTION
GAGE NO. P-9 — MID-CYL. HOOP DIRECTION

HYDROSTATIC PRESSURE TEST
STRAIN GAGE INSTRUMENTATION
TYPICAL SET UP
FIG 18

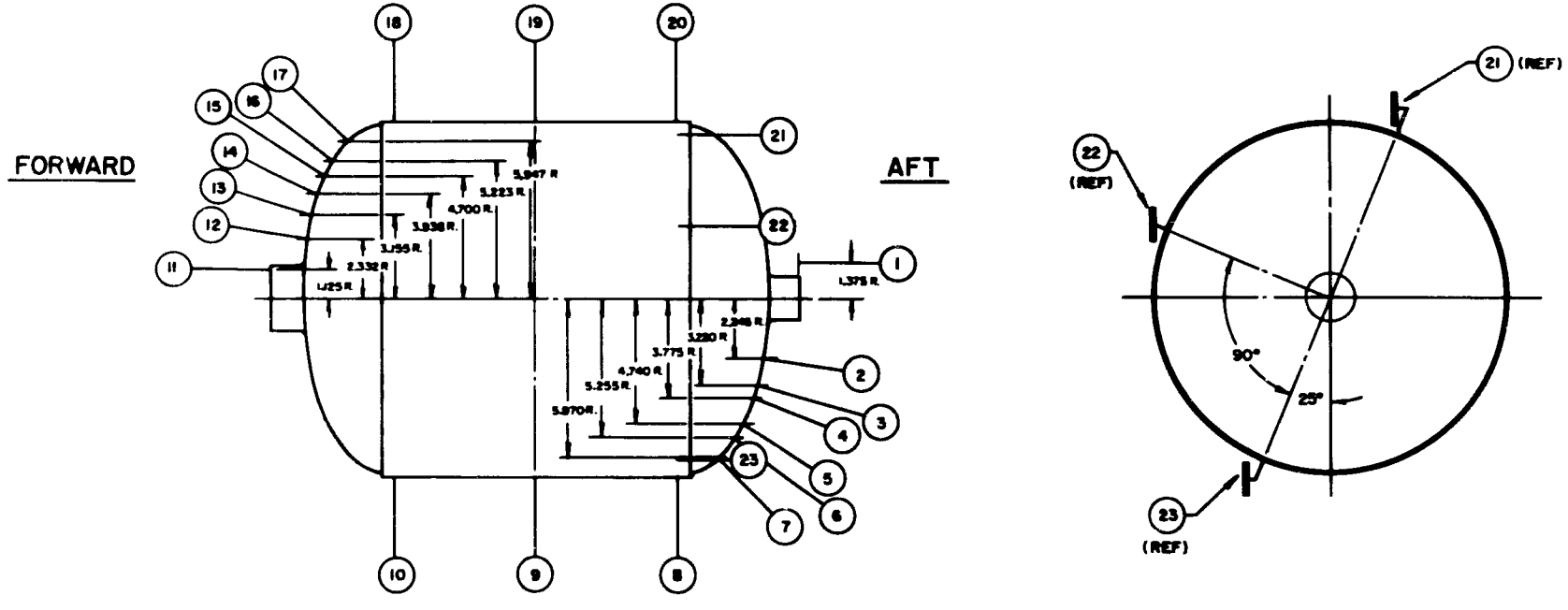

HYDROSTATIC PRESSURE TEST
DEFLECTION GAGE INSTRUMENTATION
TYPICAL SET UP
FIG 19

In test QP-1 a transducer was used to record internal pressures on the output side of the chamber and a Bourdon gage was used to indicate pressure on the input side. The former was continuously recorded on an oscillograph along with the strain gages. The dial indicator and Bourdon gage readings were continuously recorded by a movie camera. A timer and timing trace was used to synchronize all of the readings.

Test specimen QP-3 was similarly tested except that two transducers were used to provide oscillograph trace records of pressure on both ends of the case. A schematic diagram of the test set-up for specimen QP-3 is shown in Figure 20. Figures 21 and 22 are photographs of a typical test set up and strain gage instrumentation. The following are the test procedures followed:

1. The pressure transducers and strain gage circuitry was calibrated.
2. Dial indicator and strain gage zero readings were recorded before and after filling the chamber with water.
3. Internal chamber pressure was increased to 40 psig and then reduced to zero to check instrumentation. All readings were recorded.

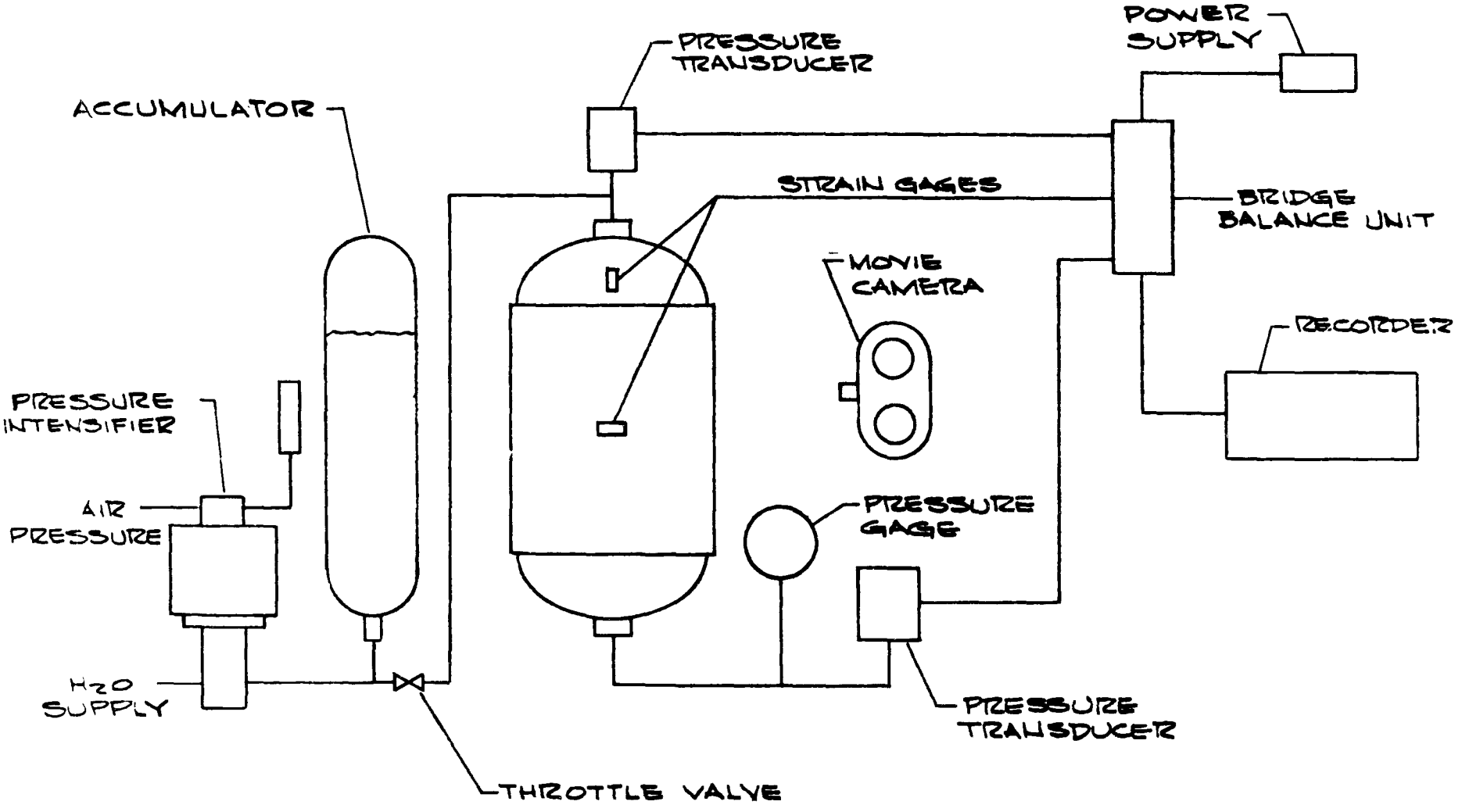

SCHEMATIC OF HYDROSTATIC TEST SET-UP

FIGURE 20

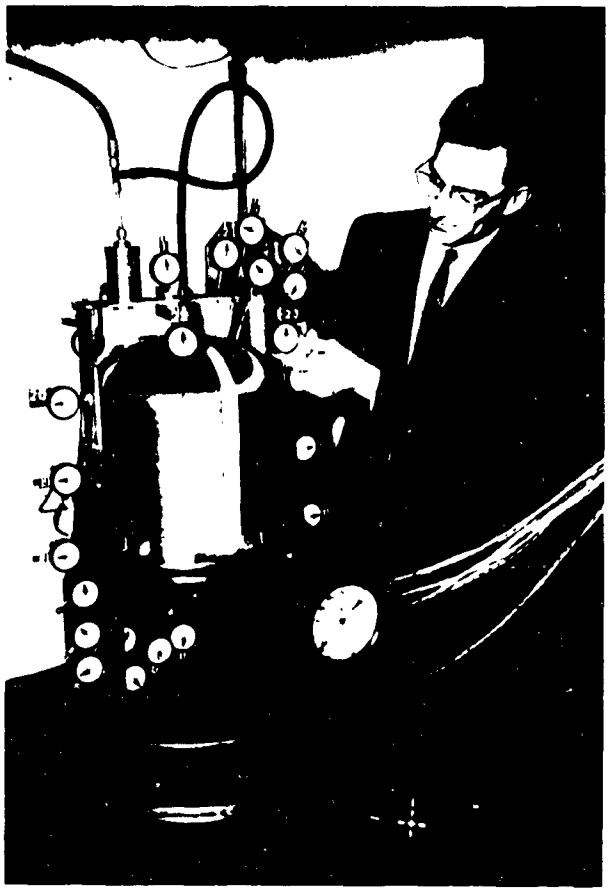

FIGURE 21

HYDROSTATIC PRESSURE TEST SET UP

FIGURE 22

STRAIN GAGE INSTRUMENTATION

4. The case was pressurized to 450 psig at a rate of 150 psi/per min. Pressure, strain, time and deflections were recorded continuously.
5. Chamber pressure was held at 450 psig for one minute. Intermittent readings of all data was recorded.
6. The internal pressure was reduced to approximately 50 psig while results were recorded.
7. The pressure was reduced to zero and all readings were recorded.

3.2.4 1/4 Scale Model Test Results

The purpose of these tests was to determine the deflection characteristics of the zero shear contour and establish whether bending and points of inflection are minimized with this dome configuration. Other objectives included the determination of skirt reinforcing effects.

Three hydrostatic pressure tests were performed on two 1/4 scale model rocket chambers, QP-1 and QP-3. Specimen QP-1 was first proof tested and then burst while specimen QP-3 was proof tested twice to check the repeatability of the test data. Both specimens were fabricated in identical fashion. The only difference between the two specimens

was the manner in which they were mounted in the test fixture. In the first specimen QP-1, the chamber was placed in a vertical position with the aft end up and was supported upon a segmented ring by the shoulder provided by the girth reinforcement on the forward dome. Specimen QP-3 was supported in a vertical position by means of aluminum tabs which were cemented to the cylindrical section just at the point of tangency. Specimens QP-1 was pressurized to a proof pressure of 390 psig at a rate of 150 psig per minute. Then the pressure was reduced to 50 psig to permit removal of several dial indicators which would be damaged during the subsequent burst test. The case was then repressurized at approximately 42 psig per second until burst occurred at 590 psig. This corresponds to a strain rate of 0.2%. The failure occurred at the dome skirt reinforcement juncture and extended about 220° around the dome perimeter. This duplicated results obtained with recent full scale chambers. A photograph of this rupture pattern is shown in Figure 23. Calculations show the composite hoop wall stress in the cylinder (based on total wall thickness) was 127,000 psi at failure yielding a hoop and longitudinal glass loading of 6.3 lbs/end and 6.2 lb/end, respectively. The strength to density ratio was calculated at 1.68×10^6. This chamber tilted to one side due to some mounting difficulties. Two factors

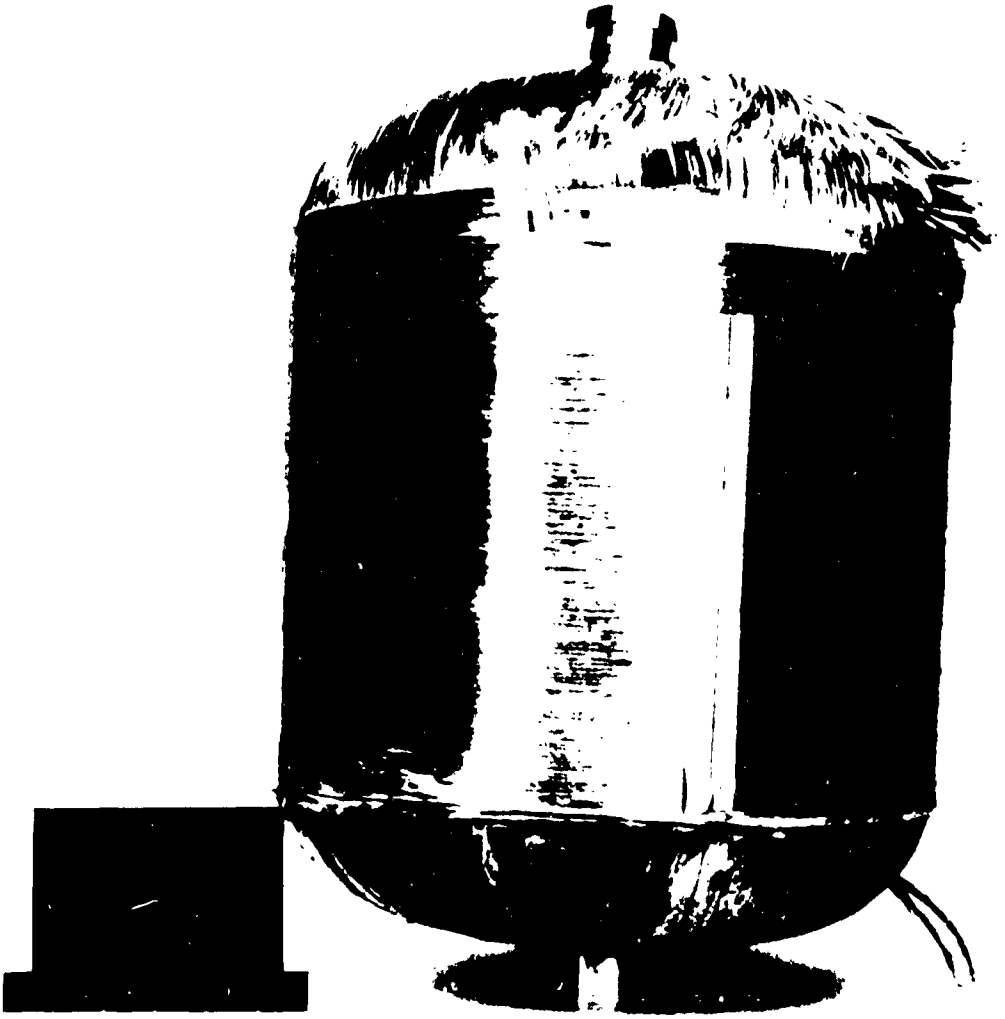

HYDROSTATIC PRESSURE TEST

1/4 SCALE MODEL CASE

FIGURE 23

were responsible for this condition. Additional clearance was required between the test rig and the forward dome, and one of the dial indicators measuring cylinder radial growth was jammed during installation.

Specimen QP-3 was not burst tested but was pressurized twice to a proof pressure of 450 psig which corresponds to a glass loading of 4.8 lbs/end with a composite wall stress in hoop of 97,200 psi and a meridional stress of 150,800 psi. The repeat test was performed to substantiate previous test data and to check whether deflections were influenced in a different manner on the second pressurization cycle. This simulates actual usage.

Figures 24 through 28 are graphs depicting the manner in which the forward and aft dome closure contours deformed during pressurization. Deflected contours are plotted for various pressures. Results show the maximum forward (.237 inches) and aft (.193 inches) dome deflections occurred at the polar fittings and diminished as the skirt is approached. An examination of the deflection curves shows bending-shear loads are present at the girth build-up. Tables 6 and 7 present a summary of the deflection data obtained on specimen QP-3. Forward dome deflections are larger than the aft dome deflections in the area of the polar fitting but tend to agree as the

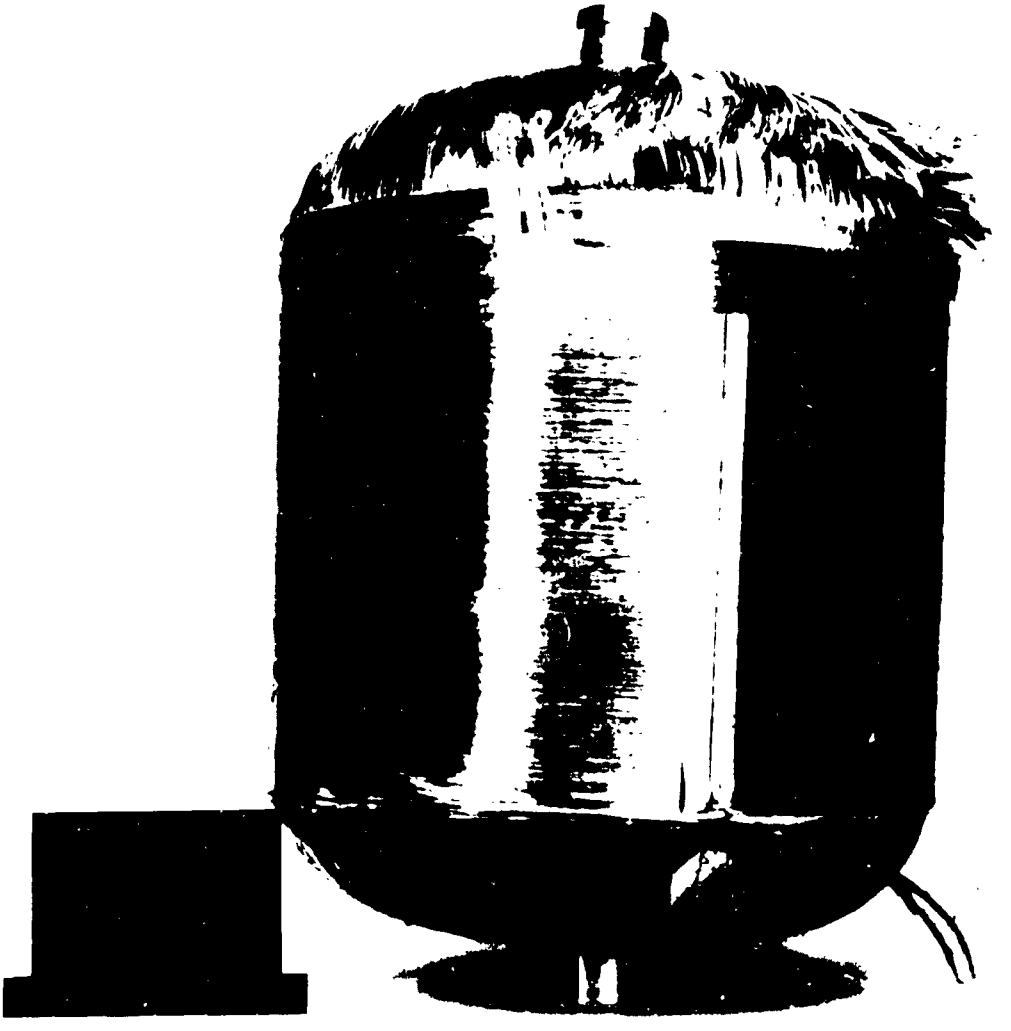

HYDROSTATIC PRESSURE TEST

1/4 SCALE MODEL CASE

FIGURE 23

were responsible for this condition. Additional clearance was required between the test rig and the forward dome, and one of the dial indicators measuring cylinder radial growth was jammed during installation.

Specimen QP-3 was not burst tested but was pressurized twice to a proof pressure of 450 psig which corresponds to a glass loading of 4.8 lbs/end with a composite wall stress in hoop of 97,200 psi and a meridional stress of 150,800 psi. The repeat test was performed to substantiate previous test data and to check whether deflections were influenced in a different manner on the second pressurization cycle. This simulates actual usage.

Figures 24 through 28 are graphs depicting the manner in which the forward and aft dome closure contours deformed during pressurization. Deflected contours are plotted for various pressures. Results show the maximum forward (.237 inches) and aft (.193 inches) dome deflections occurred at the polar fittings and diminished as the skirt is approached. An examination of the deflection curves shows bending-shear loads are present at the girth build-up. Tables 6 and 7 present a summary of the deflection data obtained on specimen QP-3. Forward dome deflections are larger than the aft dome deflections in the area of the polar fitting but tend to agree as the

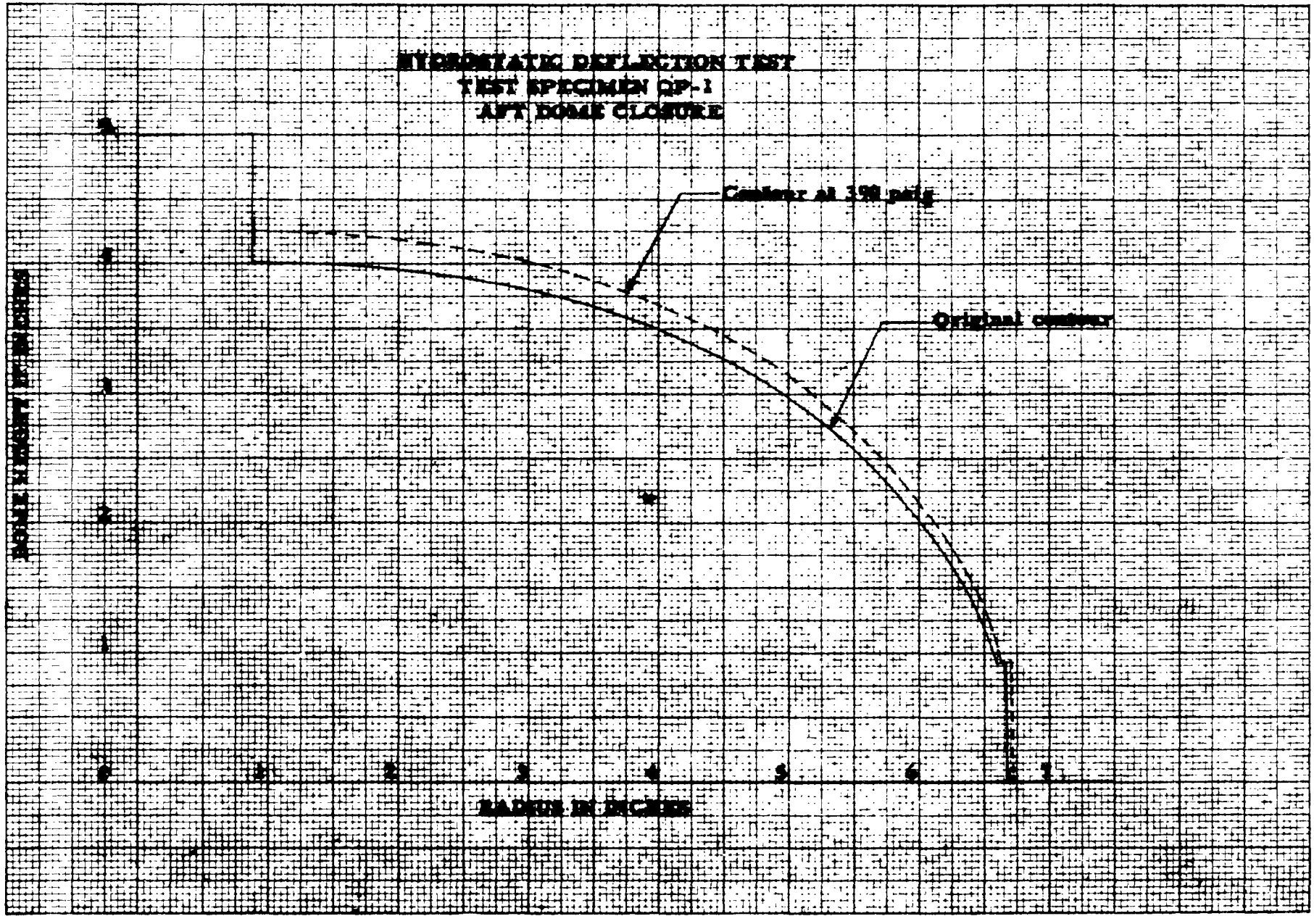
HYDROSTATIC DEFLECTION TEST
TEST SPECIMEN QP-1
AFT DOME CLOSURE
Canister at 398 psig
Original canister
RADIUS IN INCHES

FIGURE 24

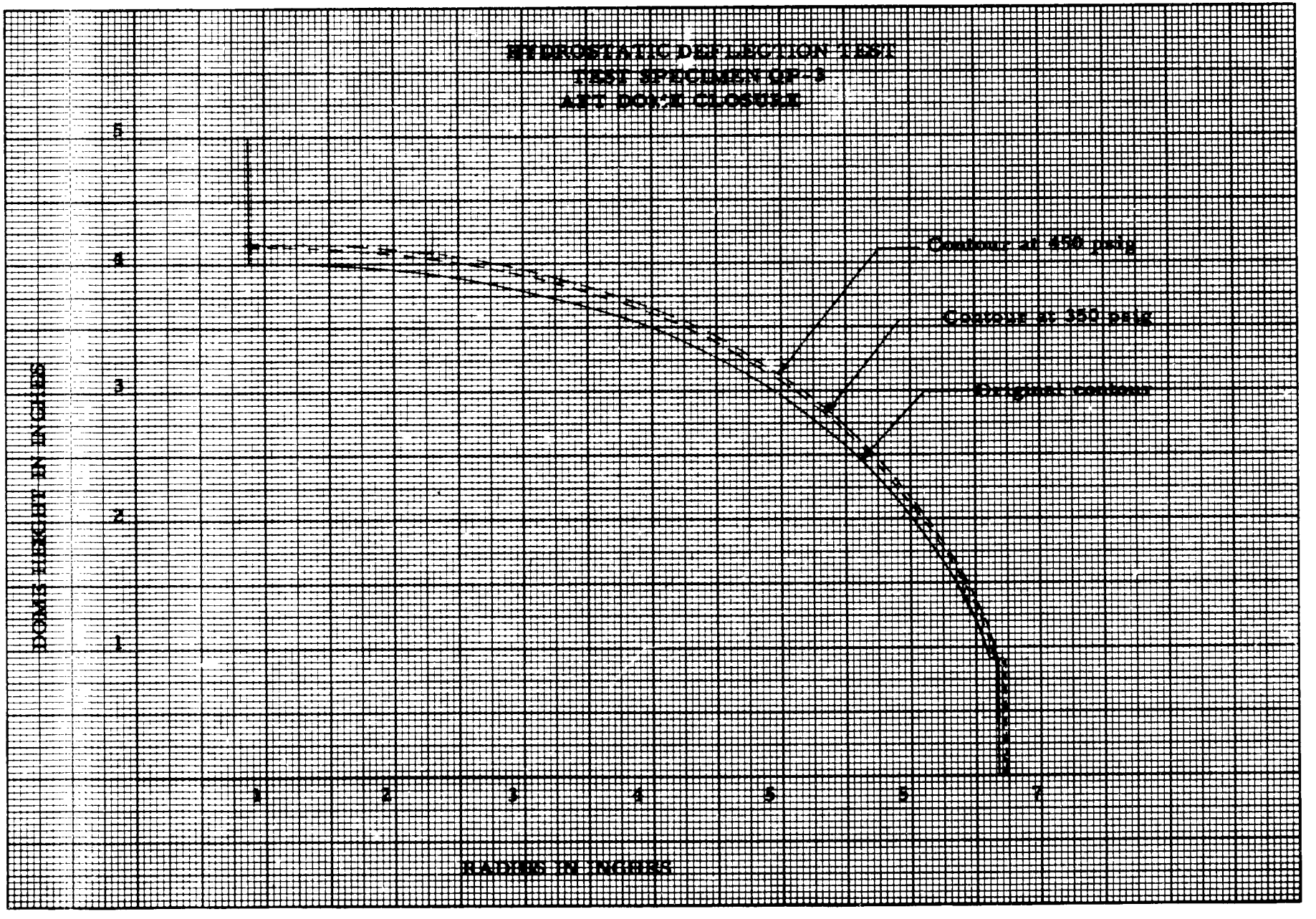
HYDROSTATIC DEFLECTION TEST
TEST SPECIMEN QF-3
ART DOME CLOSURE
Contour at 450 psig
Contour at 350 psig
Original contour
EXTERIOR HEIGHT IN INCHES
RADIUS IN INCHES
1
2
3
4
5
6
7
1
2
3
4
5

FIGURE 25

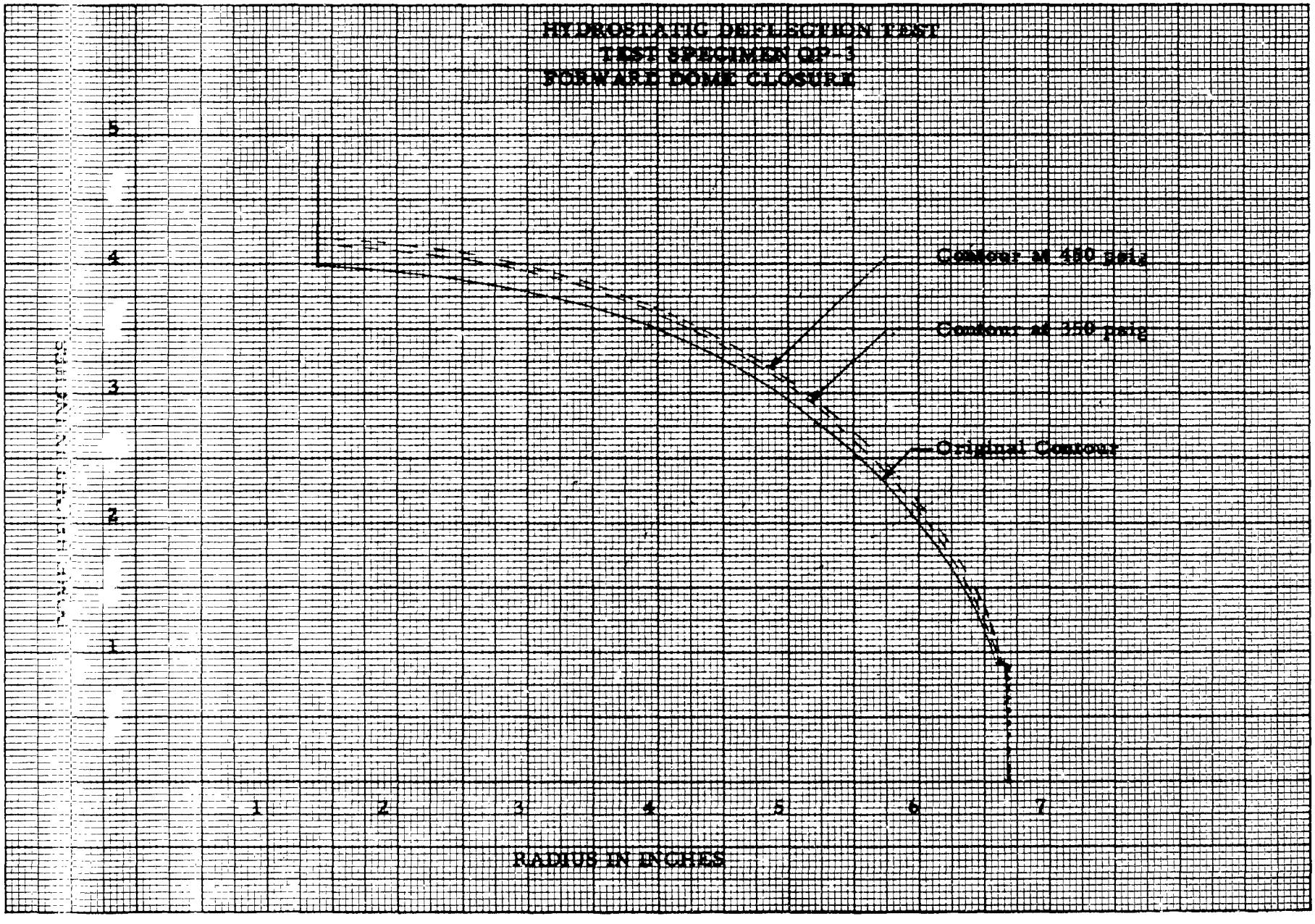
HYDROSTATIC DEFLECTION TEST
TEST SPECIMEN QP-3
FORWARD DOME CLOSURE
Contour at 450 psig
Contour at 350 psig
Original Contour
5
4
3
2
1
1
2
3
4
5
6
7
RADIUS IN INCHES

FIGURE 26

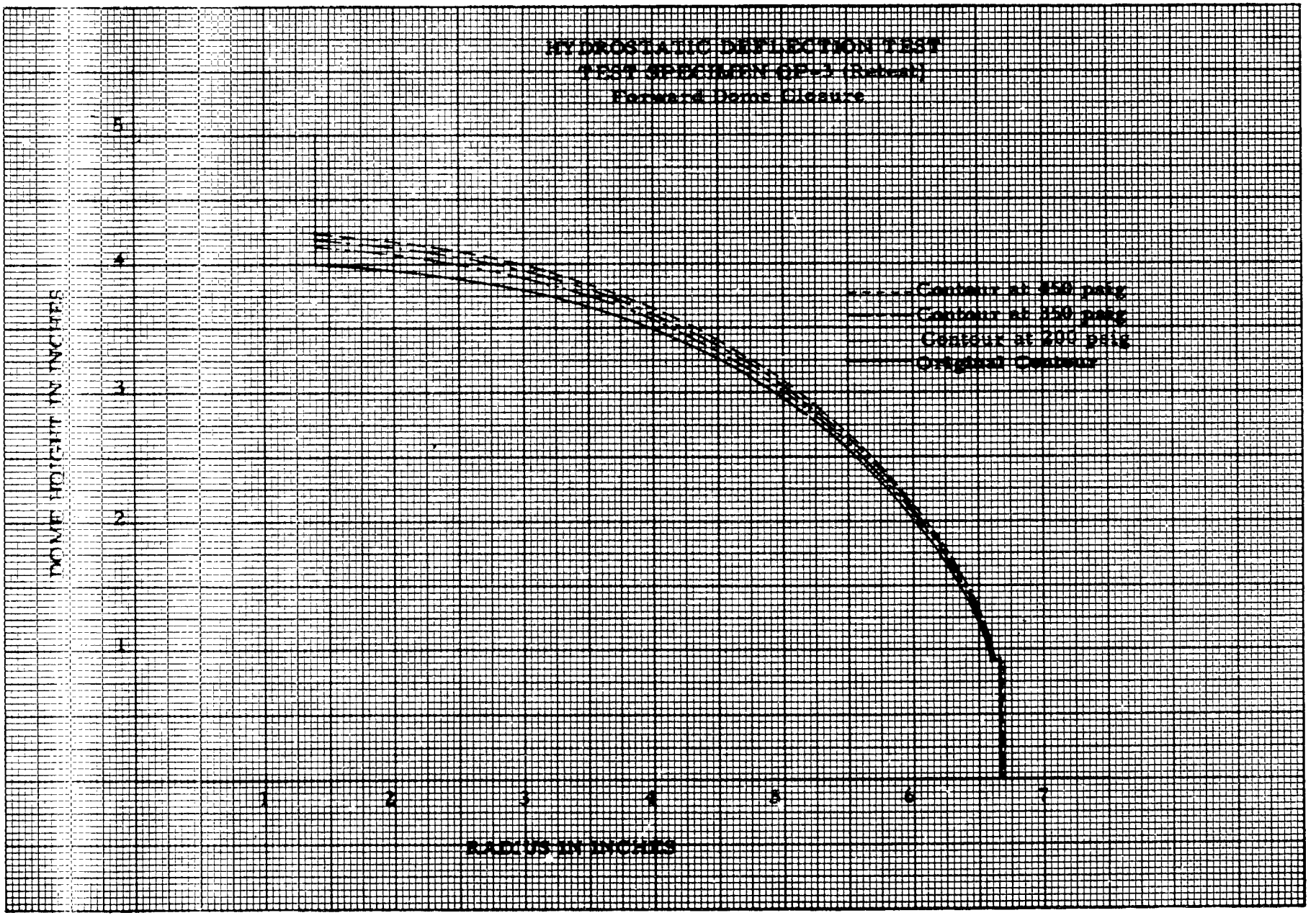
HYDROSTATIC DEFLECTION TEST
TEST SPECIMEN CF-3 (Retest)
Forward Dome Closure
Contour at 850 psig
Contour at 850 psig
Contour at 200 psig
Original Contour
INCHES IN HEIGHT
1
2
3
4
5
6
7
RADIUS IN INCHES

FIGURE 27

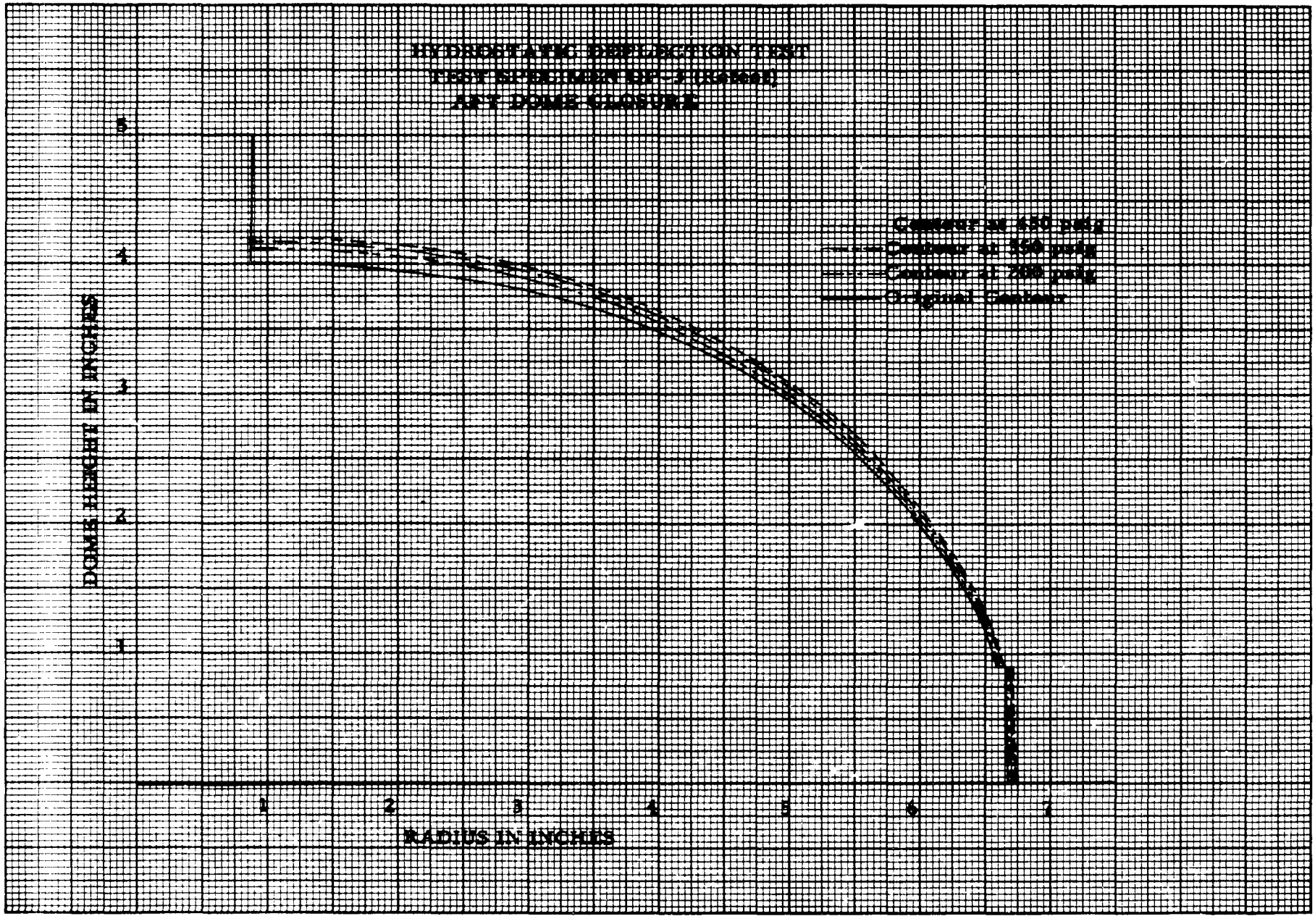
HYDROSTATIC DEFLECTION TEST
TEST SPECIMEN DFT-3 (Redesign)
AFT DOME CLOSURE
Canister at 650 psig
Canister at 550 psig
Canister at 200 psig
Original Canister
DOME HEIGHT IN INCHES
RADIUS IN INCHES
1
2
3
4
5
6
7

FIGURE 28

TABLE 6

Aft Dome Deflections on Specimen QP-3

Dial Indicator No.	1	2	3	4	5	6	7	8
Dome Contact Radius, in.	1.375 on fitting	2.245	3.220	3.775	4.740	5.255	5.970	6.7 Radial

Deflections in Inches

Press. in psig.	Test No 1	Test No 2	Test No 1	Test No 2*	Test No 1	Test No 2	Test No 1	Test No 2	Test No 1	Test No 2	Test No 1	Test No 2	Test No 1	Test No 2	Test No 1	Test No 2
100		.075		.091		.047		.038		.006		.007		.009		.008
200		.108		.122		.092		.078		.039		.047		.019		.020
300		.147		.164		.117		.101		.076		.074		.042		.038
350	.123	.156	.139	.194	.121	.142	.125	.121	.103	.084	.096	.091	.065	.064	.050	.050
400		.180		.199		.152		.133		.101		.093		.071		.062
450	.156	.193	.170	.216	.154	.167	.145	.148	.138	.116	.138	.115	.099	.079	.081	.075

* These points omitted on graph to form smooth curve.

TABLE 7

Forward Dome Deflections on Specimen QP-3								
Dial Indicator No.	11	12	13	14	15	16	17	18
Dome Contact Radius, in.	1.125 on fitting	2.332	3.155	3.938	4.700	5.223	5.947	6.7 Radial

Deflections in Inches																
Press. in psig.	Test No 1	2	Test No 1	2	Test No 1	2	Test No 1	2	Test No 1	2	Test No 1	2	Test No 1	2	Test No 1	2
100		.102		.085		.058		.041		.013		.013		.013		-.002
200		.137		.120		.085		.075		.040		.035		.025		-.001
300		.177		.160		.125		.105		.069		.064		.043		+.001
350	.178	.195	.161	.173	.137	.141	.123	.119	.099	.083	.082	.076	.057	.052	.0065	.0065
400		.211		.193		.160		.139		.097		.086		.063		.009
450	.218	.237	.197	.210	.175	.175	.161	.155	.129	.114	.113	.104	.082	.073	.0185	.0185

knuckle area is approached. This is attributed to the difference in the size of the polar opening and flange diameter between the forward and aft ends and indicates both contours should not be identically shaped unless identical fittings are used on both ends.

In addition a significant portion of the total deflection in the area of the polar fittings occurs during initial pressurization to the 100 psig level. A comparison of this phenomena between the forward and aft closures shows this low stress reorientation is greater on the forward dome at the polar fitting. This substantiates the conclusion that both contours must not be alike unless identical fittings are used.

With the exception of the aft polar fitting deflection, good correlation was achieved between the two tests on specimen QP-3.

Table 8 is a summary of the cylinder deflections on specimen QP-3. Although very good agreement is shown between the two tests it should be noted that the cylinder radial growth, as measured on opposite sides of the chamber at the forward and aft ends are not identical. These may be due to one of the following reasons:

TABLE 8

CYLINDER DEFLECTIONS ON SPECIMEN QP-3

Dial Indicator No.	8		20		9		19		10		18		21		22		23	
Location	Radial Aft End		Radial Aft End		Mid Cylinder		Mid Cylinder		Radial Forward end		Radial Forward end		Longi-tudinal		Longi-tudinal		Longi-tudinal	
	DEFLECTION IN INCHES																	
Pressure in psig	Test No 1	2	Test No 1	2	Test No 1	2	Test No 1	2	Test No 1	2	Test No 1	2	Test No 1	2	Test No 1	2	Test No 1	2
100		.008		.001		.026		.028		-.001		-.002		.064		.065		.065
200		.020		.008		.056		.058		..000		-.001		.111		.112		.112
300		.038		.020		.091		.088		.003		.001		.172		.173		.173
350	.050	.050	.033	.030	.117	.106	.104	.101	.010	.005	.004	.005	.190	.194	.192	.193	.190	.198
400		.062		.032		.126		.113		.012		.009		.221		.225		.225
450	.081	.075	.040	.040	.157	.146	.130	.128	.023	.020	.011	.009	.242	.242	.242	.251	.240	.251

1. Out of roundness in the cylinder.
2. Local differences in filament density and irregularities because measurements were made near the girth reinforcement.
3. Some misplacement between the gages in the axial direction of the cylinder. At the girth reinforcement and point of tangency accurate alignment is necessary because of the large change in laminate stiffness encountered in progressing from the girth reinforcement to the cylindrical section.

It is felt that the last reason is probably the cause of this phenomena. Table 9 presents chamber deflections obtained in the diametral and longitudinal directions on Specimen QP-3. Very good agreement was achieved between the two tests with the maximum diametral and longitudinal growth being 0.286 inches and 0.248 inches, respectively. Of interest was the fact that measurements taken before and after the first test indicated a permanent set at the cylinder mid-section of +.025 inches, however no permanent set occurred following the second pressurization at either the mid-cylinder or girth reinforcement locations. No definite permanent set was detected in the axial direction.

TABLE 9

COMPARISON OF QP-3 CHAMBER DEFLECTIONS

Pressure psig	Chamber Diametral Growth at mid cylinder, inches		Chamber Longitudinal Growth inches	
	Test No		Test No	
	1	2	1	2
100		.054		.065
200		.114		.112
300		.179		.173
350	.221	.207	.190	.195
400		.239		.224
450	.286	.274	.242	.248

Figures 29 and 30 are graphs of the forward and aft dome closure deflections for the various dial indicator stations. The graphs are plotted in non-dimensional form (where $Y_o = 6.7$) and show that following an initial shape change the deflections vary linearly with pressure.

3.2.5 Strain Gage Results

Aft dome closure strain gage results from specimens QP-1 and QP-3 are shown in Tables 10 and 11. Tensile strain measurements vary essentially linearly with pressure. Good agreement is evident between the various gages, indicating that tensile strains were fairly uniform throughout the dome structure. Bending strains were very small, in most cases being less than 1% of the surface tensile strain recorded (see Test QP-3). Negative bending strains were recorded by the meridional gages in both tests. In QP-1, two other bending gages (Flexagages) reflected some negative bending, however these values were probably influenced by the mounting difficulties encountered in this test.

The relatively small bending strains measured indicates bending is probably not a problem in the dome area of a polar ported dome closure. It should be noted that bending is probably present at the point of discontinuity adjacent to the girth reinforcement build-up but could not be detected with strain gages.

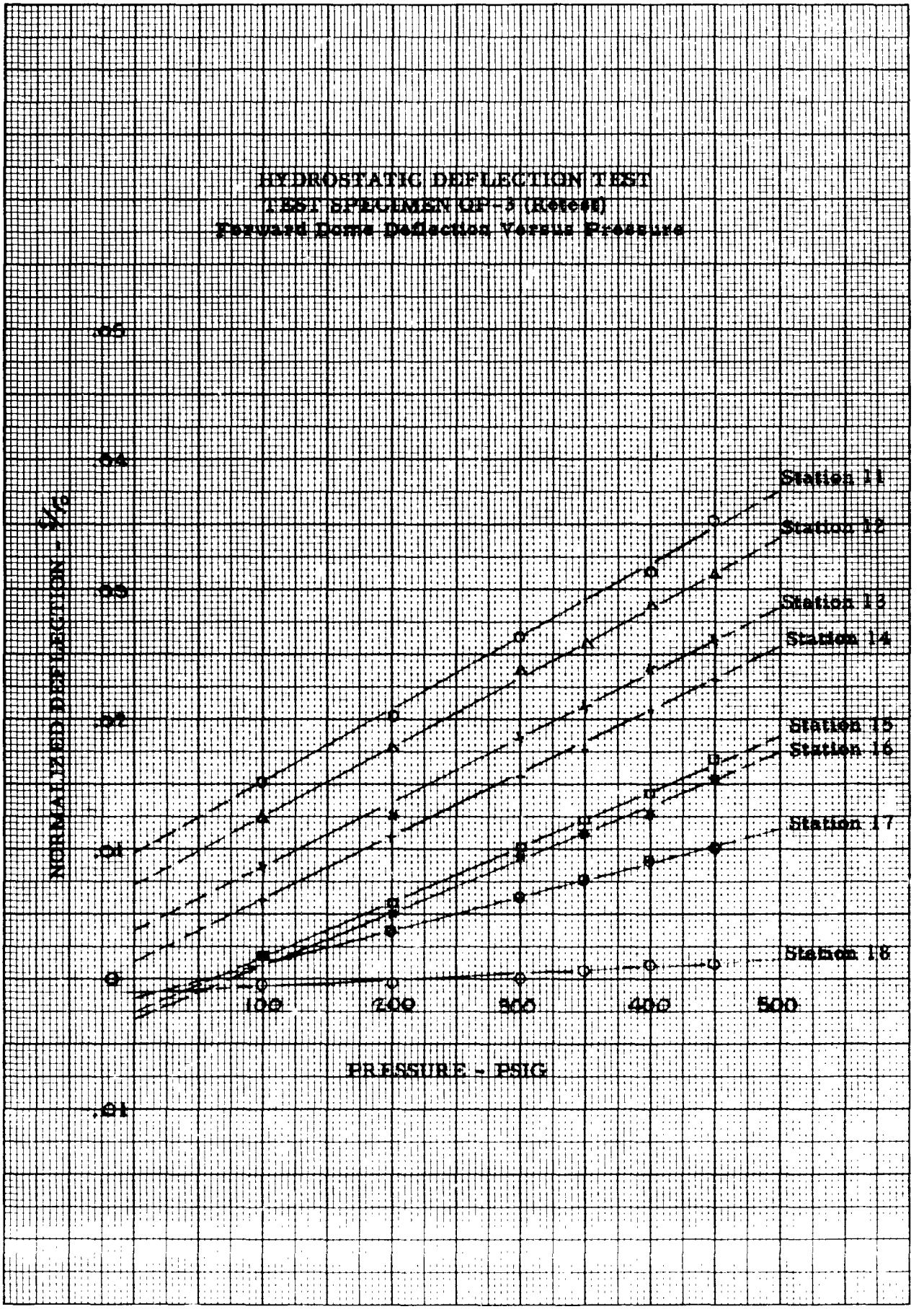
HYDROSTATIC DEFLECTION TEST
TEST SPECIMEN QF-3 (Retest)
Forward Dome Deflection Versus Pressure
NORMALIZED DEFLECTION - δ/t
.06
.04
.02
.01
0
100
200
300
400
500
PRESSURE - PSIG
Station 11
Station 12
Station 13
Station 14
Station 15
Station 16
Station 17
Station 18

FIGURE 29

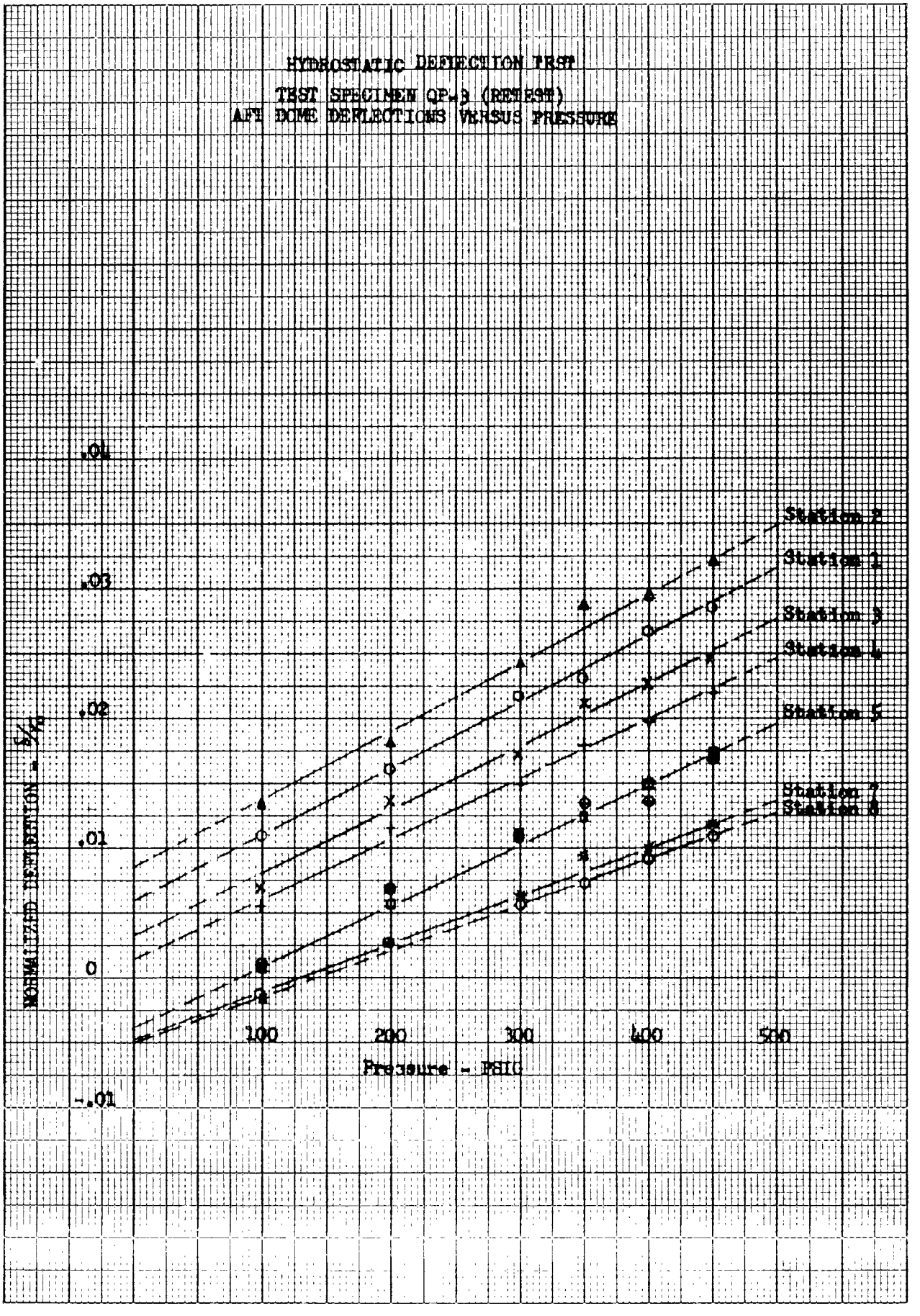
HYDROSTATIC DEFLECTION TEST
TEST SPECIMEN QP-3 (RETEST)
AFT DOME DEFLECTIONS VERSUS PRESSURE
.04
.03
.02
.01
0
-.01
NORMALIZED DEFLECTION - δ/a
100
200
300
400
500
Pressure - PSIG
Station 2
Station 1
Station 3
Station 4
Station 5
Station 7
Station 8

FIGURE 30

TEST SPECIMEN QP-1
1/4 SCALE MODEL SECOND STAGE POLARIS CASE (NON-PORTED)
AFT DOME CLOSURE STRAIN GAGE RESULTS
TABLE 10

GAGE NO			F-1		F-2		F-3		F-4		P-1	P-2	P-3	P-4	P-5	P-6	P-7	P-8	P-9
TYPE OF GAGE			C9-F20		C9-F20		C9-F20		C9-F20		PA-3	PA-3	PA-3	PA-3	PA-3	PA-3	PA-3	PA-3	PA-3
DIRECTION			FILAMENT PATH						MERIDIONAL[a]		FILAMENT PATH					DOME HOOP		MID CYL. LONG.	MID CYL. HOOP
RADIUS—IN.			5.5		6.0		6.3		6.0		3.0	4.5	5.75	6.2	6.3	5.5	6.4	6.7	6.7
LAMINATE TH'K UNDER GAGE—IN			.0125		.012		.010		.0115		.024	.0165	.0125	.010	.010	.0115	.010	.031	.031
	PRESSURE (PSIG)	TIME TO PRESSURE (SECONDS)	TENSILE STRAIN μ IN/IN	BENDING STRAIN μ IN/IN	TENSILE STRAIN μ IN/IN	BENDING STRAIN μ IN/IN	TENSILE STRAIN μ IN/IN	BENDING STRAIN μ IN/IN	TENSILE STRAIN μ IN/IN	BENDING STRAIN μ IN/IN	TENSILE STRAIN μ IN/IN	TENSILE STRAIN μ IN/IN	TENSILE STRAIN μ IN/IN	TENSILE STRAIN μ IN/IN	TENSILE STRAIN μ IN/IN	TENSILE STRAIN μ IN/IN	TENSILE STRAIN μ IN/IN	TENSILE STRAIN μ IN/IN	TENSILE STRAIN μ IN/IN
	390	180	18240	−470	16230	480	—	—	17310	−140	15910	16590	—	18420	17670	14100	6210	—	—
	345	138	14800	−390	13730	125	—	—	13990	−120	13230	14040	—	15020	14370	12510	3690	8730	14780
	300	125	14010	−460	12610	130	—	—	12510	−30	12130	12860	12920	13790	13300	11420	3270	8330	13660
	275	110	12370	−490	11040	140	—	—	11550	−150	10640	11490	11500	12040	11710	8340	2940	7180	11690
	160	64	6550	−370	5770	40	6060	−90	5830	−80	4970	5600	6000	6070	4790	3670	980	3710	5850
	990[b]	13	26530	−520	24840	170	—	—	23290	−240	—	17670	—	27060	24900	—	—	—	—

[a] 3 1/2° OFF MERIDION
[b] BURST PRESSURE

TEST SPECIMEN QP-3
1/4 SCALE MODEL SECOND STAGE POLARIS CASE (NON-PORTED)
AFT DOME CLOSURE STRAIN GAGE RESULTS
TABLE II

GAGE NO.			F-1		F-2		F-3		F-4		P-1	P-2	P-3	P-4	P-5	P-6	P-7	P-8	P-9
TYPE OF GAGE			C9-F20		C9-F20		C9-F20		C9-F20		PA-3	PA-3	PA-3	PA-3	PA-3	PA-3	PA-3	PA-3	PA-3
DIRECTION			FILAMENT PATH						MERIDIONAL		FILAMENT PATH					DOME HOOP		MID CYL.	
																		LONG.	HOOP
RADIUS - IN.			5.5		6.0		6.3		6.0		3.0	4.6	5.75	6.2	6.3	6.6	6.4	6.7	6.7
LAMINATE TH'K UNDER GAGE - IN.			.0125		.012		.010		.0118		.024	.0185	.0125	.010	.010	.0115	.010	.051	.051
	PRESSURE (PSIG)	TIME TO PRESSURE (SECONDS)	TENSILE STRAIN ~ IN/IN	BENDING STRAIN ~ IN/IN	TENSILE STRAIN ~ IN/IN	BENDING STRAIN ~ IN/IN	TENSILE STRAIN ~ IN/IN	BENDING STRAIN ~ IN/IN	TENSILE STRAIN ~ IN/IN	BENDING STRAIN ~ IN/IN	TENSILE STRAIN ~ IN/IN	TENSILE STRAIN ~ IN/IN	TENSILE STRAIN ~ IN/IN	TENSILE STRAIN ~ IN/IN	TENSILE STRAIN ~ IN/IN	TENSILE STRAIN ~ IN/IN	TENSILE STRAIN ~ IN/IN	TENSILE STRAIN ~ IN/IN	TENSILE STRAIN ~ IN/IN
	100	34	4070	75	4020	85	4130	30	4110	60	3480	3740	4080	4040	4230	1880	630	3080	4250
	205	78	8110	130	8110	160	8340	50	8430	10	7780	7880	8210	8080	8370	4440	2190	8320	8880
	305	119	12250	140	12130	210	12390	70	12910	-75	11780	11780	12340	12080	12280	7190	4320	12680	13270
	355	137	13940	140	14070	180	14250	70	15400	-140[a]	14370	13790	13880	13940	13830	8480	4270	14660	15600
	440	168	18140	200	——	——	18550	90	19470	-270[a]	18470	18030	18110	18280	17130	12020	4800	17890	20280
	450	180	18690	170	——	——	19310	100	19720	-140[a]	18770	18330	18310	18680	17820	12680	4480	——	——

[a] EXTRAPOLATED
[b] SAME AS QP-1

3.2.6. Empirical Equation For Dome Closure Deflections

An empirical equation was developed governing the deflection characteristics obtained on the polar ported 1/4 scale model chamber. With this equation dome deflections can be calculated for polar ported chambers of various sizes as long as scale factors are not violated. With additional tests the effect of port size and skirt reinforcement could quite possibly be included. The effect of the difference in port size between the forward and aft domes was not included in this study because of the scatter in data obtained for the low pressures and in the area near the dome-cylinder juncture.

The first step in the determination of this equation involved plotting the forward and aft dome deflection data for various pressures. This data was reduced to non-dimensional form by dividing both radius and deflection by the maximum outer dome radius. This was 6.7 inches for the 1/4 scale model. Results are plotted in Figure 31 for pressures of 100, 200, 300, 350, 400 and 450 psig. It shows that the test data can be approximated by a straight line having a slope of -0.03 yielding an equation of the following form: $\frac{\delta}{r_o} = b - 0.030\left(\frac{r}{r_o}\right)$

where δ = deflection normal to initial contour, inches

r_o = maximum outer radius of dome, inches

r = radius from dome centerline to point on surface, inches

b = intercept of deflection curve with the ordinate axis.

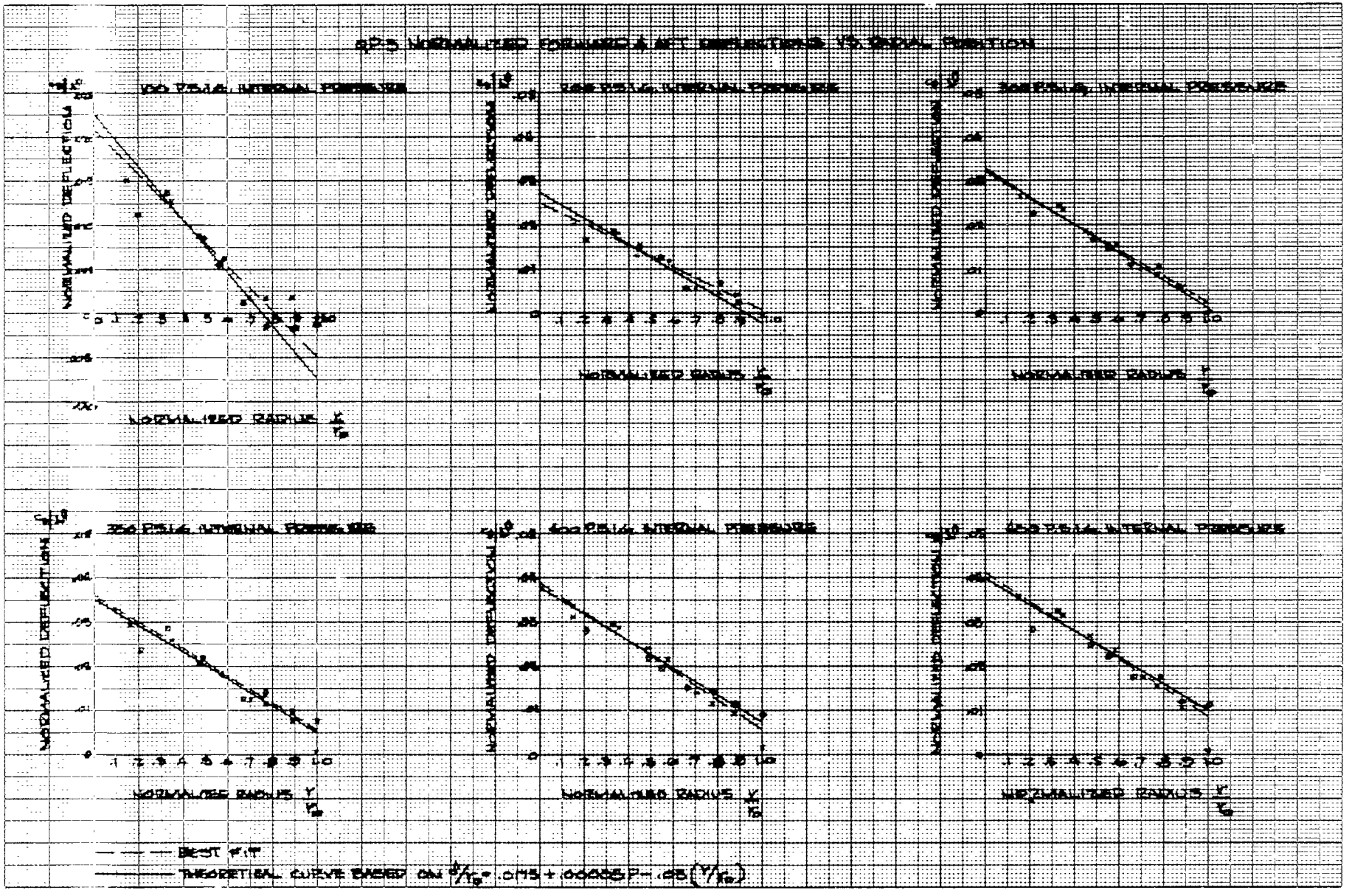

FIGURE 31

A study of the deflection data also shows the intercept "b" has a nearly linear relationship with pressure which can be written as

$$b = .0175 + 0.00005\ P$$

where P = internal pressure, psig.

This yields the following equation:

$$\frac{\delta}{r_o} = 0.0175 + 0.00005\ P - .030\left(\frac{r}{r_o}\right)$$

The accuracy of this derived equation is also shown in Figure 31. A comparison of the line obtained from the derived equation with the best fit shows the former yields good results for pressures above 200 psig and for values of r/r_o between 0.3 and 0.9. The deviation outside this range is due to test data scatter. Additional testing with more instrumentation is required to substantiate these results.

3.2.7 Full Scale Test Data and Results

A study of available full scale chamber test data, and failure characteristics was made in an attempt to establish some insight into the nature and causes of failures encountered in the field. A majority of the failures reviewed occurred at the dome cylinder juncture or around the off-center ports. The three basic reasons for these

failures appear to be:

1. The presence of discontinuities.
2. Bending and inflection points.
3. Insufficient and improper reinforcement to effectively accomplish the required load transfer.

An analysis of these failures is very difficult. Due to the unidirectional properties of the glass laminate standard analytical techniques are not adaptable. In practice, the use of various membrane analogies only yields a ball park estimate which must be confirmed through test.

Discontinuity failures are usually manifested by an abrupt and well defined rupture pattern. An example of this type of failure occurs on those specimens which failed under the build-up produced by the secondary winding angles (case YP-84) and on cases which failed at the dome-cylinder or girth reinforcement. Any change in uniform laminate construction tends to magnify discontinuities. For this reason all reinforcements must be designed to provide a gradual change in flexure properties and strain characteristics. In practice this is accomplished best by actual test.

A thorough investigation into the deflection characteristics of the X-250 cases posed a rather serious dilemma because the relatively large amount of deflection data could not be

equated to a particular design or fabrication method. Very little information was available regarding the design and fabrication of X-250 chambers. Inasmuch as our goal was the refinement of the X-250 and X-260 chambers it was decided to review both X-250 and X-260 test results. Much of the available data proved limited and inconclusive.

Typical deflection test results on X-260 full scale test chambers is shown in Figures 32, 33 and 34. It should be noted that in all instances no data is shown concerning the behavior of the specimen in the vicinity of the knuckle area or dome-cylinder juncture. This is because the skirt configuration obstructs this area. Although the deflection curves are incomplete their trend shows discontinuity and inflection points probably do exist in the knuckle area. It should be noted that the chambers depicted were manufactured by different vendors and yield widely divergent results. In Figure 33 the deflections measured between and across the nozzle ports are very much alike in magnitude while those in Figure 32 and 34 are distinctly different. This shows that there is considerable variation in dome stiffness between cases. Off-center port reinforcements must be designed to minimize this scalloping effect.

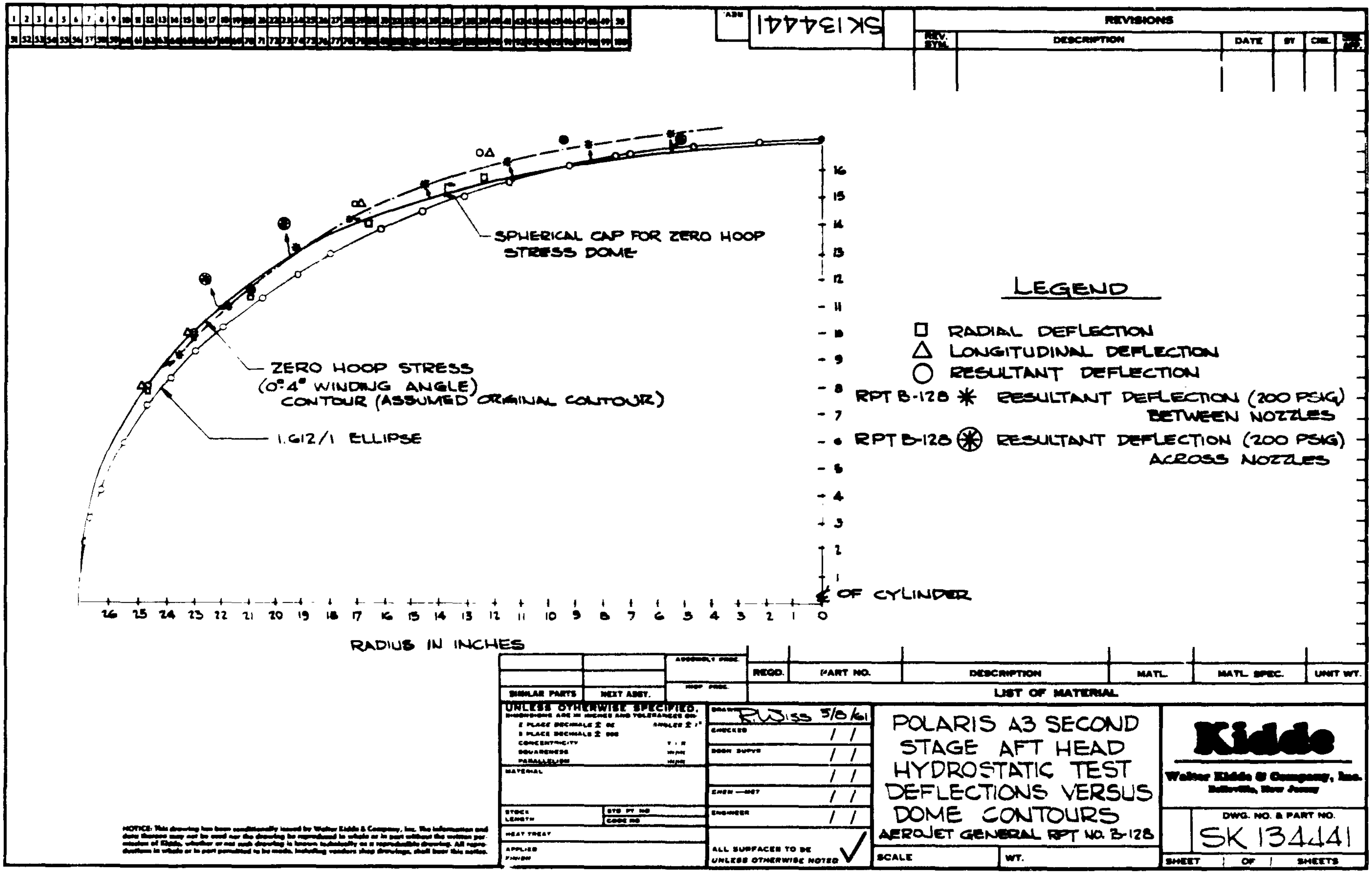
SK134441
REVISIONS
REV. SYM.
DESCRIPTION
DATE
BY
CHK.
SPHERICAL CAP FOR ZERO HOOP STRESS DOME
ZERO HOOP STRESS (0°4° WINDING ANGLE) CONTOUR (ASSUMED ORIGINAL CONTOUR)
1.612/1 ELLIPSE
LEGEND
□ RADIAL DEFLECTION
△ LONGITUDINAL DEFLECTION
○ RESULTANT DEFLECTION
RPT B-128 ✳ RESULTANT DEFLECTION (200 PSIG) BETWEEN NOZZLES
RPT B-128 ⊛ RESULTANT DEFLECTION (200 PSIG) ACROSS NOZZLES
℄ OF CYLINDER
RADIUS IN INCHES
REQD.
PART NO.
DESCRIPTION
MATL.
MATL. SPEC.
UNIT WT.
LIST OF MATERIAL
SIMILAR PARTS
NEXT ASSY.
UNLESS OTHERWISE SPECIFIED
POLARIS A3 SECOND STAGE AFT HEAD HYDROSTATIC TEST DEFLECTIONS VERSUS DOME CONTOURS
AEROJET GENERAL RPT NO. B-128
DRAWN R.Weiss 5/8/61
CHECKED
ENGINEER
ALL SURFACES TO BE ✓ UNLESS OTHERWISE NOTED
SCALE
WT.
Kidde
Walter Kidde & Company, Inc.
Belleville, New Jersey
DWG. NO. & PART NO.
SK 134441
SHEET 1 OF 1 SHEETS

FIGURE 32

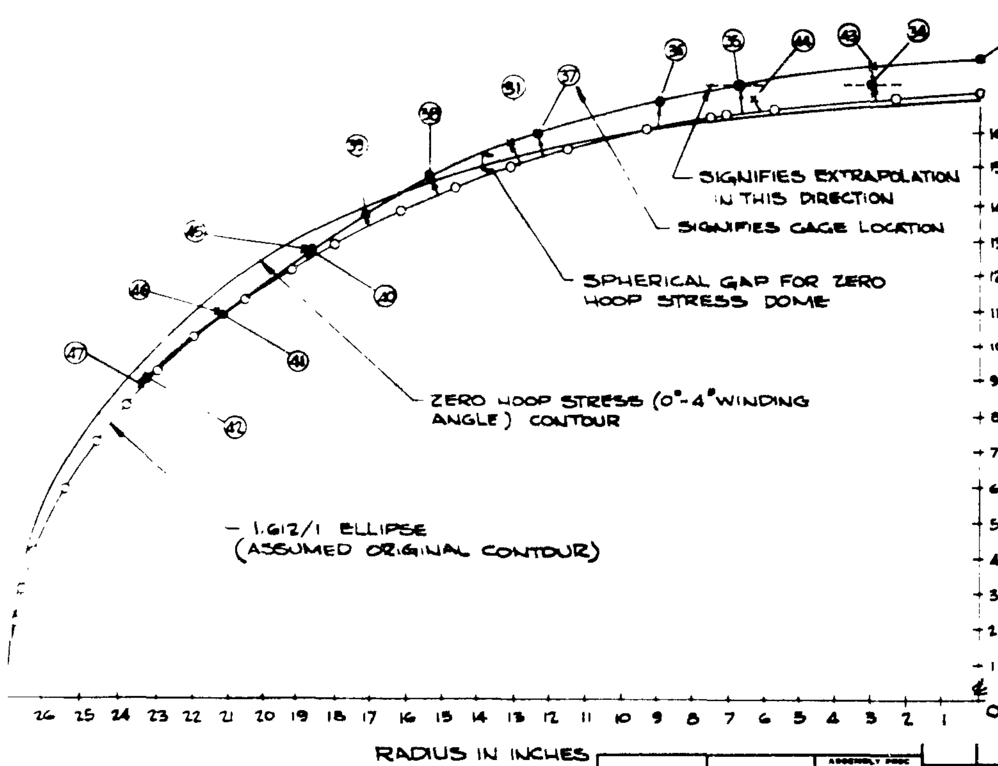

GAGE NO.	MERIDIONAL DEFLECTION	HOOP DEFLECTION
28	1.0	—
34	0.52*	0.06*
35	0.85	0.07*
36	0.63	0 *
37	0.62	0.7
38	0.52	0.73*
39	0.43	0.06
40	0.13	0
41	0.07	-0.05
42	0.12	-0.08
30		0.77N
31		0.60N
32		0.40N
33		0.57N
43	0.87	—
44	0.18	0.22
45	0.18	0.08
46	0.12	-0.04
47	0.08	-0.02

DEFLECTIONS PLOTTED FROM 1.612/1 ELLIPSE CONTOUR

⊗ RESULTANT DEFLECTION RPT B-124 POINTS MEASURED BETWEEN NOZZLES, 300 PSIG

× AS ABOVE BUT MEASURED ACROSS NOZZLE

✱ SIGNIFIES POINT WAS EXTRAPOLATED

N SIGNIFIES DEFLECTIONS NORMAL TO NOZZLE BOSS

POLARIS A3 SECOND STAGE AFT HEAD HYDROSTATIC TEST DEFLECTIONS VERSUS DOME CONTOURS

AEROJET GENERAL RPT NO. B-124

DRAWN R. Juss 5/8/61

DWG. NO. & PART NO. SK 134446

SHEET 1 OF 1 SHEETS

Walter Kidde & Company, Inc. Belleville, New Jersey

FIGURE 33

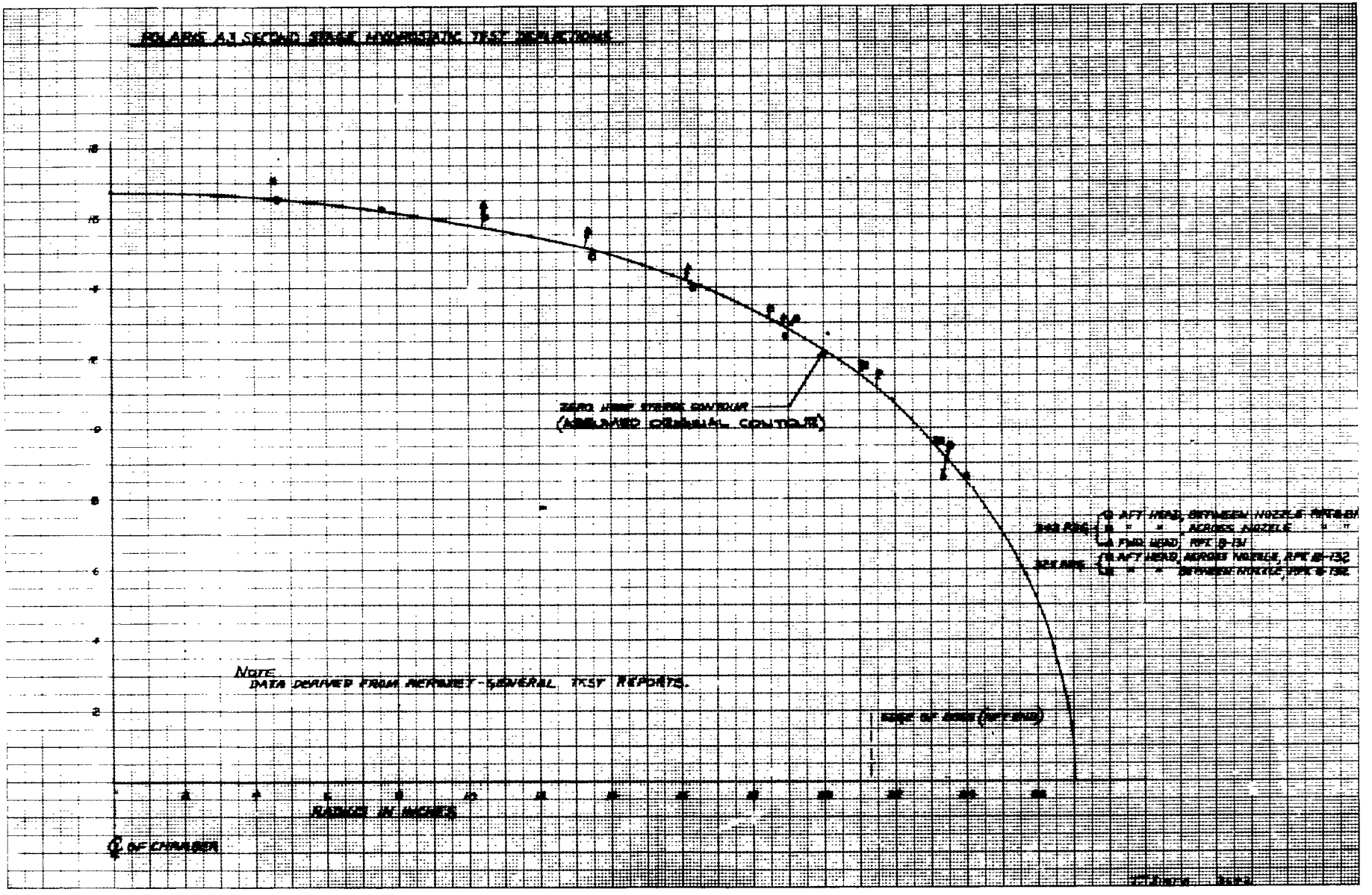
POLARIS A1 SECOND STAGE HYDROSTATIC TEST DEFLECTIONS
ZERO HOOP STRESS CONTOUR
(ASSUMED ORIGINAL CONTOUR)
AFT HEAD, BETWEEN NOZZLE
ACROSS NOZZLE
FWD HEAD, RPT B-131
AFT HEAD, ACROSS NOZZLE, RPT B-132
BETWEEN NOZZLE, RPT B-132
NOTE
DATA DERIVED FROM AEROJET - GENERAL TEST REPORTS.
RADIUS IN INCHES
℄ OF CHAMBER

FIGURE 34

The most feasible method for accomplishing this is to balance the dome flexural and strain properties in the vicinity of the ports while providing sufficient shear area between the reinforcement and meridional fibers to satisfactorily affect an efficient load transfer. Based on the complexity of this situation it is recommended that additional scale model testing be conducted to achieve a balanced design. Insofar as the dome-cylinder juncture is concerned, the best practical way to minimize this discontinuity is by adding strips of glass cloth reinforcement at the point of tangency which overlap the dome and cylinder juncture. Recent test results substantiate this approach.

3.2.8 Comparison of Model Tests with Full Scale Chamber Test Results

Another basic objective of this program was to make comparisons of deflections between the various models tested and the full scale chambers. The purpose of these comparisons was to determine whether bending or other adverse conditions are being minimized. As discussed previously, meaningful comparisons can only be made if both geometric and loading similarities are maintained.

Table 12 is a comparison of end closure deflections between the 1/4 scale model and several typical ported and non-ported

TABLE 12

COMPARISON OF END CLOSURE DEFLECTIONS BETWEEN 1/4 SCALE MODEL QP-3, TYPICAL FULL SIZE CHAMBERS, AND THEORETICAL VALUES

	Equivalent ¼ Scale Model Deflections (non ported), at 450 psig, inches		Full Scale Chamber (Non-ported) Deflections, at 430 psig, inches		Typical X-260 Chamber Deflections, at 410 psig, inches		X-250 Chamber Average Deflections in inches (See Note 1)		Theoretical Deflections based on δ/r_o = .0175 + .0000P-.03 (r/r_o) (See Note 3)	Theoretical Deflections based on δ/r_o = .0175+.00005P-.03 (r/r_o) (See Note 2)
Radius Inches	Forward Dome	Aft Dome	Forward Dome	Aft Dome	Forward Dome	Aft Dome	Forward Dome	Aft Dome		
3.3					.67	.61				.769
3.5	.87	.62	-	-						.763
5.5							.535	.360	.876	.703
10.5							.553	.329	.726	.553
12	.76	.60	.24	.46	.65	.41			.681	.508
14.5							.497	.247	.606	.433
16	.64	.58	.42	.48					.561	.387
18.5							.332	.180	.486	.312
20	.48	.56	.40	.45	.61	.30			.441	.267
24	.33	.35	.33	.34					.321	.102
25.5					.17	.08				

NOTE:

1. X-250 chamber deflections are average values at proof pressures of approximately 410 psig.
2. Theoretical deflections based on developed equation for polar ported scale model. Deflections calculated for 300 psig and a hoop stress of 65000 psi in the scale model.
3. Theoretical deflections based on developed equation for polar ported scale model. Deflections calculated for 430 psig.

chambers at similar pressure levels. A comparison is also made with the theoretical deflections which were computed using the empirical equation developed in this program.

Results show that the 1/4 scale model deflections are in agreement with the non-ported full size cases in the knuckle area but are larger at all other points. Better agreement in the vicinity of the dome-cylinder juncture is to be expected because of the greater influence exerted by the cylinder and girth reinforcements on dome deflections. Results substantiate the fact that such variables as methods of fabrication, winding pattern, and type of reinforcement affect deflections. The larger deflections in the area of the polar fitting are due to a difference in the ratio of longitudinal to hoop windings between the full sized chambers and the scale model. The full scale chambers were fabricated with a larger longitudinal to hoop glass ratio which stiffens the dome resulting in smaller deflections. A comparison of the theoretical deflections with the full scale non-ported chamber deflections also shows excellent agreement in the knuckle area.

A study was made of the available strain gage data accumulated from various X-260 motor cases. Results shown in Table 13 are limited to the region around the knuckle area and indicate there is a scarcity of data regarding bending strain levels in the critical knuckle area (no data available on X-250 cases). Both positive and negative bending strains are being encountered. Meridional strains at equivalent dome positions on the full scale chambers are in agreement with results obtained on the ovaloid and 1/4 scale model tests. (See Tables 10, 11 and 2). This study showed that additional instrumentation to measure bending and deflection should be utilized especially in the knuckle area.

A study was made to compare the various physical properties between the 1/4 scale model chamber used in this test program and several ported and non-ported full size chambers. Table 14 compares the most important properties at similar pressure levels. It shows that the 1/4 scale model chamber was a more efficient structure. Stresses in the model are higher for equal hoop and longitudinal glass loads.

TABLE 13

SUMMARY OF STRAIN GAGE TEST RESULTS ON X 260 MOTOR CASES

Case No.	Press. Psig.	Gage Position	Meridional Strain on aft dome in $in/in \times 10^{-6}$	Aft End Gage Location expressed as % of full dia.	Meridional Strain on forward end in $in/in \times 10^{-6}$	Forward End Gage Location expressed as % of full dia.	Meridional Bending Strain in $\mu in/in$	Meridional Strain in line of wrap in $\mu in/in$	Meridional bending strain in line of wrap $\mu in/in$	Remarks
RHL02	398	R6	11300	81.	9900	56.				Gages located between nozzle
RHL03	390	"	8300	71.	9400	94.				"
B601	385	"	6100	81.	10000	56.				"
RHL20	390	"	7800	81.	10100	75.				"
RHL21	390	"	7800	81.	10200	56.				"
RHL22	391	"	8300	81.	9700	75				"
B602	382	"	6700	81.	9700	56.				"
B801	379	"	6100	81.	8900	56.				"
9STU	320	19	2900	82.			530			"
9STU	320	22	6040	93.				3190		"
54-19	342	102		94				11270		"
54-19	342	103	9360	72						"
54-17	325	15		87				12620	-1058	"
54-17	325	16		90.				8630		"
54-14	320	5		80.				9500		)
"	375	5		80.				10000		No nozzle ports on case)
"	320	6		72.				8700		)
"	375	6		72				10000		)
"	320	11		72				8000		)
"	375	11		72				9100		)
"	320	12		80				9000		)
"	375	12		80				10300		)
9STU	320	8	7523	92			-260	293		Gage located across nozzle
54-19	342	77		88				10800		"
"	342	95		94				11570		"
54-17	325	20		79				4500	-2810	"
54-17	325	22		87				-730	-463	"

TABLE 14

COMPARISON OF PHYSICAL PROPERTIES BETWEEN SCALE MODEL AND TYPICAL FULL SIZE CHAMBERS

Type of Chamber	1/4 Scale Model			Full Scale	Full Scale	Full Scale
Model No.	QP-1		QP-3	X-260	X-260	X-260
Glass Type	ECG-150-1/0		ECG-150-1/0	ECG-150-1/0	ECG-150-1/10	ECG-150-1/10
Laminate Wt.	1.91		1.76	-	-	-
Hoop Glass ends per inch	627		627	2110	2110	2110
Longitudinal glass ends per inch	314		314	1465	1465	1465
Proof pressure, psig	390		450			
Burst pressure, psig		590		464	496	430
Time to pressure, seconds		13	180	11.5	38	28
Cylinder wall thickness inches	.031		.031	.140	.137	.133
Dome thickness at cylinder juncture, inches	.010		.010	-	-	-
Resin Content %	17.5% in. cylinder 31% in dome			19.9	18.6	-
Composite hoop stress in cylinder, psi	84300	127000	97200	89500	97,900	84700
Meridional stress at dome-cylinder juncture, psi	130000	197000	150800	109000	120,000	103800
Hoop load per end-lbs.	4.1	6.18	4.8	5.85	6.05	5.42
Longitudinal load per end-lbs.	4.16	6.3	4.83	4.37	4.75	4.10
Strength to density ratio-inches (10^6)	-	1.68		1.27	1.36	1.21
Girth Expansion-inches	.60	1.15	.90	-	3.27	2.50
Failure	Aft dome at girth built up juncture			Aft dome at juncture	Cyl. combined hoop & longitudinal	Dome
Dome Configuration	Zero-shear contour non-ported			ported	non-ported	non-ported
Hoop Windings-degrees	90°		90°	90°	90°	90°
Longitudinal Windings-degrees	7 1/2		7 1/2	8 1/2°	8 1/2°	8 1/2°

3.2.9 Summary and Conclusions For Phase II

This phase of the program showed the zero shear contour was effective in producing a more efficient dome configuration. Comparisons with full scale polar ported chambers (with non-polar ports) showed that although equivalent deflections on the scale model were larger, the burst pressure was higher for a smaller amount of glass. The mode of the scale model rupture was identical to that obtained on similar full scale chambers. At rupture the meridional glass loading was higher than the design load of 6 lbs. per end.

Test results were repeated and showed good agreement although some scatter was evident at the lower pressures and in the knuckle area. An empirical equation governing deflection characteristics on a polar ported chamber was derived.

3.3.0 Phase 3 Modified Dome Design

This section of the report outlines the steps necessary to refine the current Polaris second stage rocket chamber configuration. One objective of this program was to produce a more efficient structure within present envelope requirements. The scope of this program does not permit a complete redesign of every single component so that an attempt will only be made to specify the ground rules by which this goal may be achieved.

A simplified design procedure involves the following steps:

1. Select dome contour, winding angles and winding pattern from the geometry of the motor case. Note that the winding angle, and pattern must be made mutually compatible with the dome contour.

2. Calculate the length of the cylindrical section of the motor case for the above contour.

3. Calculate the number of turns (ends) required for each winding angle.

4. Design the non-polar port reinforcements.

5. Determine winding sequence.

6. Design skirt attachment.

The winding sequence and skirt attachment design is not considered in this report because specific fabrication procedures are involved for which there are numerous possibilities.

The example presented below is based on Hercules Powder Co. Drawing No. ABL-260-4002.

3.3.1 Dome Contour Selection

Since the X-250 chamber design is already frozen the design example presented is based on dimensions taken from Hercules Powder Co. drawings for the X-260 configuration. The zero shear contour derived during this program was for the 7 1/2° winding angle which applies to the X-250 chamber, whereas a 5.4° angle must be used for the X-260. Therefore a slight modification to the derived contour may be necessary especially if unequal polar port diameters are required. However, it is assumed that a small change in winding angle could probably be tolerated without causing a significant contour change. A study of the various contours and of data reported by other sources tends to substantiate this reasoning at least for the smaller winding angles. It is however recommended that the chamber designs be changed to incorporate equal polar opening diameters. Of course the contour presented is compatible with the present X-250 design configuration (which utilizes a 7 1/2° winding angle) and probably would result in a significant improvement in efficiency if it could be incorporated into the design. Design requirements for a polar ported X-250 chamber are shown in Appendix VI of this report.

3.3.2 Determination of Modified Zero Shear Contour

Figures 29 and 30 show non-dimensionalized deflections for the 1/4 scale model dome closure plotted against pressure for the

various gage locations. Deflections vary linearly with pressure especially at the higher pressures, however none of the straight lines pass through the origin when extrapolated to zero pressure. If all the fibers in the dome are equally stressed, there is no apparent reason for the functional relationship between deflection and pressure to change. It can therefore be assumed that the original contour did not produce uniform fiber stresses and as the specimen was initially pressurized an initial shape change took place without significant straining. This produced deflections which were not proportional to pressure. This reorientation took place at very low pressures. As the pressure was increased linear deflections occurred caused by straining of the glass fibers.

Based on this phenomena it is apparent that the original contour could be corrected by the amount of this "zero pressure" deflection, i.e., the intercept of the deflection curve with the δ/r_e ordinate at zero pressure. In this manner the contour is corrected to coincide with the deflection tendencies and subsequent deflections should progress in a more uniform manner. Figure 35 presents the "zero pressure deflection as a function of radial position. Due to the scatter, the data, for both domes is averaged. Results show a definite trend is established. It indicates that the new contour must have a slightly smaller ratio of major to minor axis. The coordinates and contour for the modified zero shear dome are presented in Figure 36. Figure 37 is a comparison of the original and modified zero shear contours.

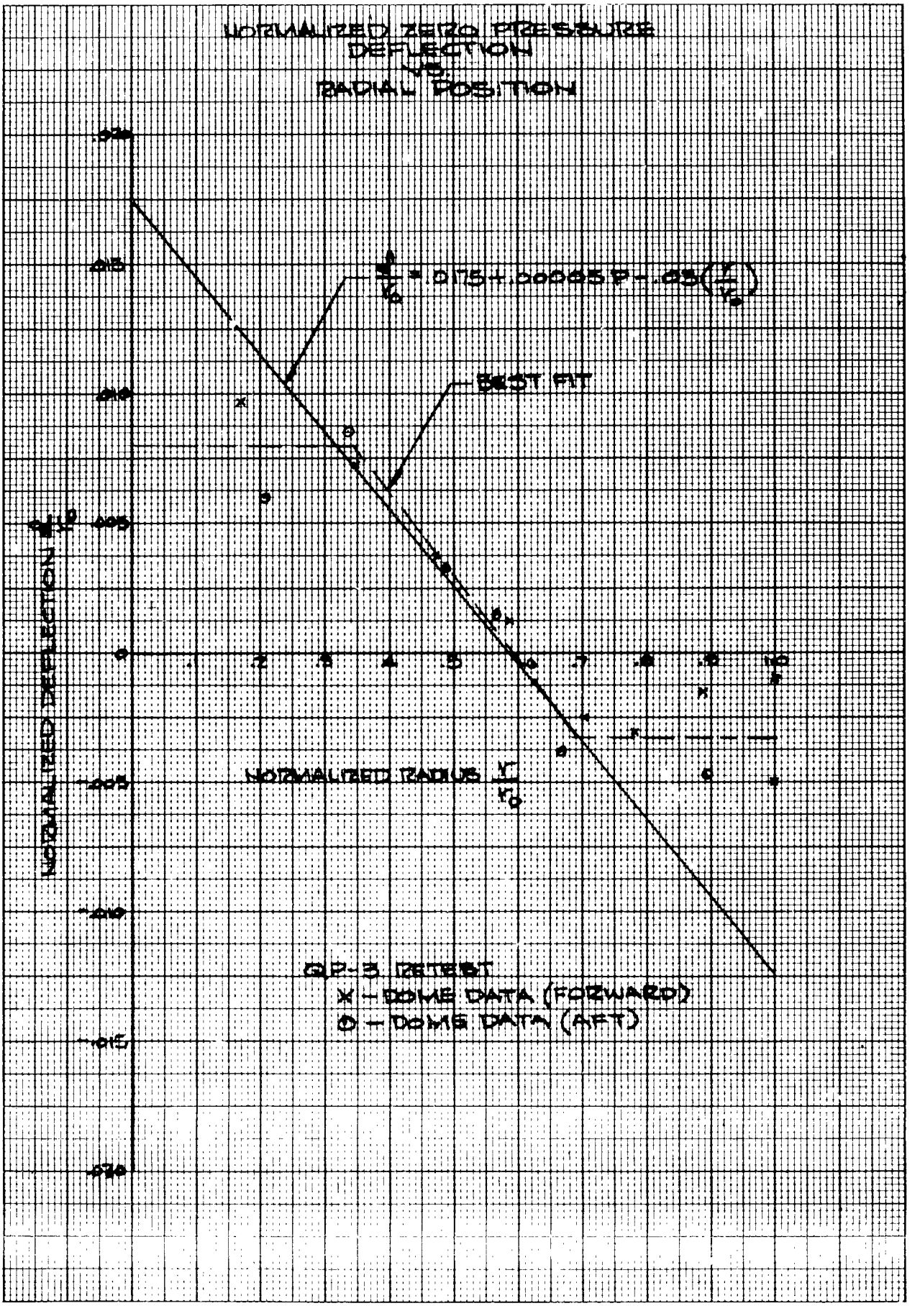
NORMALIZED ZERO PRESSURE
DEFLECTION
VS.
RADIAL POSITION
BEST FIT
NORMALIZED RADIUS
GLP-3 RETEST
X - DOME DATA (FORWARD)
Φ - DOME DATA (AFT)

FIGURE 35

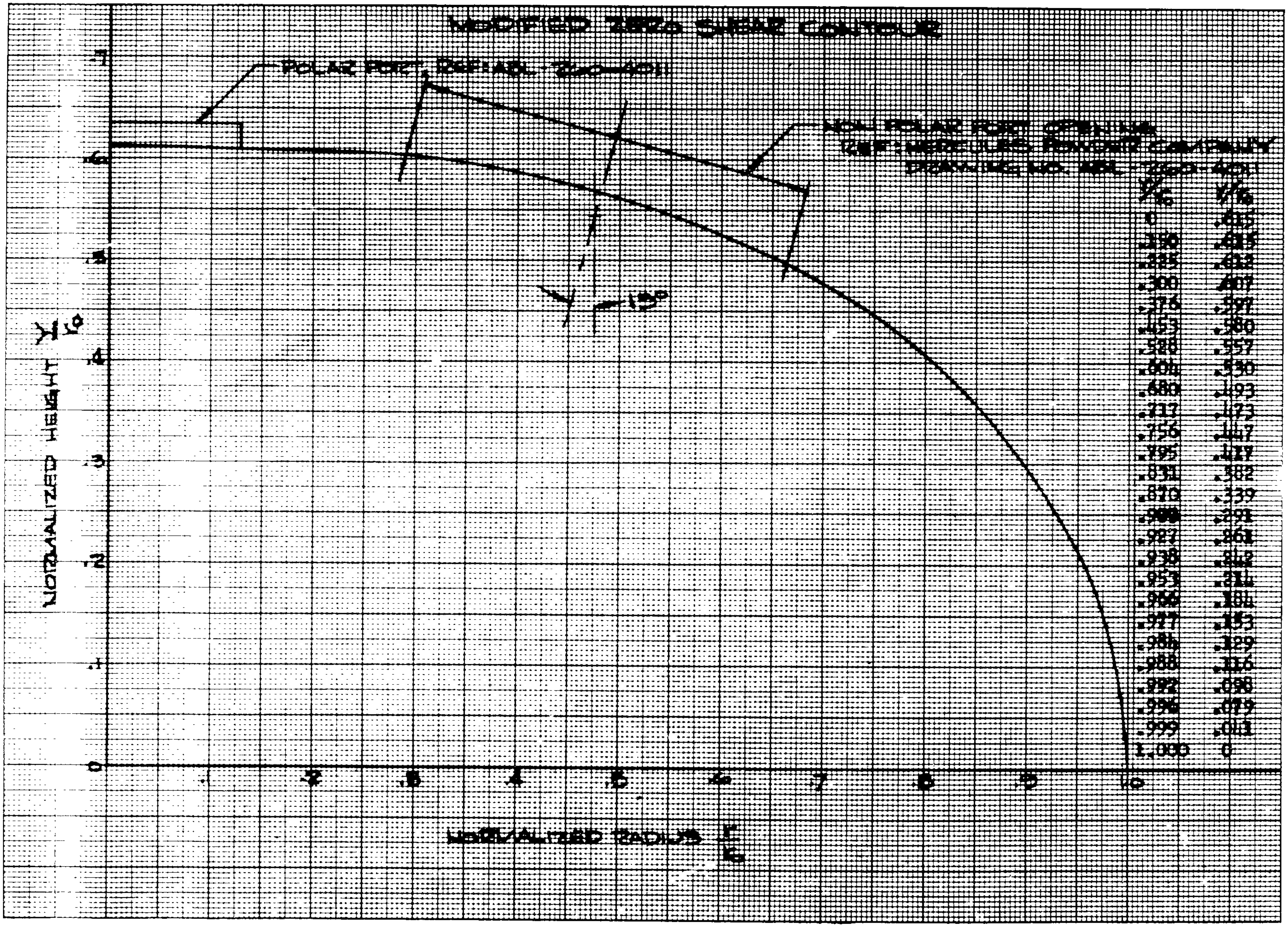
MODIFIED ZERO SHEAR CONTOUR
POLAR PORT, REF: ABL-ZZO-4011
NON-POLAR PORT OPENING
REF: HERCULES POWDER COMPANY
DRAWING NO. ABL-ZZO-4011
15°
NORMALIZED HEIGHT
NORMALIZED RADIUS
0
.1
.2
.3
.4
.5
.6
.7
.8
.9
1.0
X/c Y/c
0 .615
.150 .615
.225 .612
.300 .607
.376 .597
.453 .580
.528 .557
.604 .530
.680 .493
.717 .473
.756 .447
.795 .417
.831 .382
.870 .339
.927 .261
.938 .242
.953 .214
.966 .184
.977 .153
.984 .129
.988 .116
.992 .098
.996 .079
.999
1.000 0

FIGURE 36

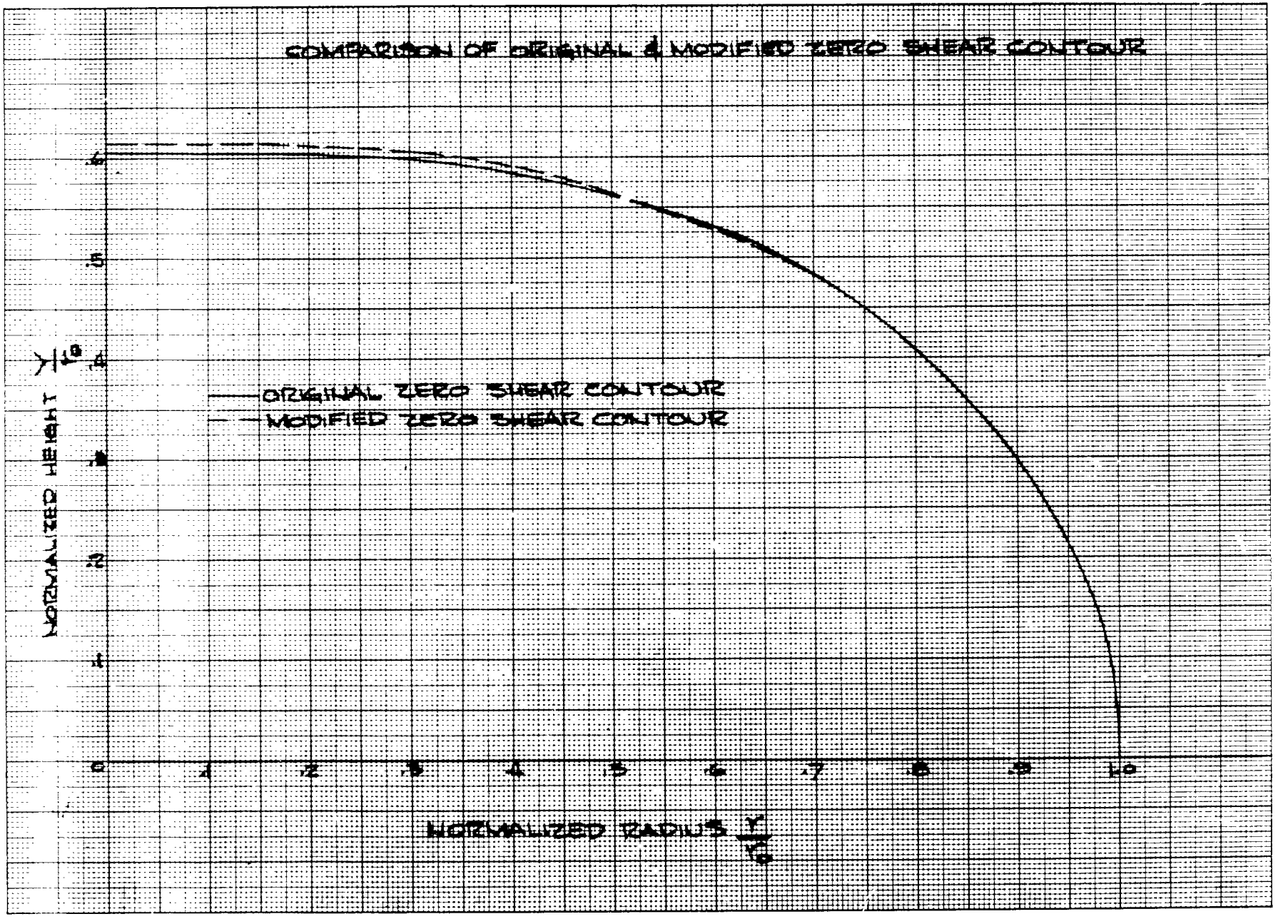
COMPARISON OF ORIGINAL & MODIFIED ZERO SHEAR CONTOUR
ORIGINAL ZERO SHEAR CONTOUR
MODIFIED ZERO SHEAR CONTOUR
NORMALIZED HEIGHT
NORMALIZED RADIUS

FIGURE 37

Further testing of a scale model using this corrected contour is necessary to confirm uniform deflections. The advantage to be gained is reduced deflection due to distortion which would aid in the elimination of undesirable bending stresses and permit uniformaly distributed loading of the filaments.

3.3.3. Winding Angles

The winding angles are determined from the geometry of the chambers. For the X-260 configurations sketched in figure 38 the polar wrap angle is found as follows:

$$\tan \alpha = \frac{r_F + r_a}{l - 2b} = \frac{7}{75.72 - 2(.625)}$$

$$\tan \alpha = .094$$

$$\alpha = 5.4°$$

Only two winding angles are recommended. Hoop strength in the cylinder is obtained by placing circumferential windings at an angle approximating 90°.

3.3.4 Length of Cylindrical Section of Motor Case

The length of the cylindrical section is found by matching the zero shear contour with the basic rocket case at the outside diameter of the polar fitting.

From figure 35 at $r/r_o = \frac{3.5}{26.84} = .130$

$$y/r_o = 0.614$$

$y = (.615)(26.84) = 16.48"$

Overall length = $L = l + 2(y+h) - 75.72 = + 2(16.48 + .645) + l$

$l = 41.51$ inches = length of cylindrical section

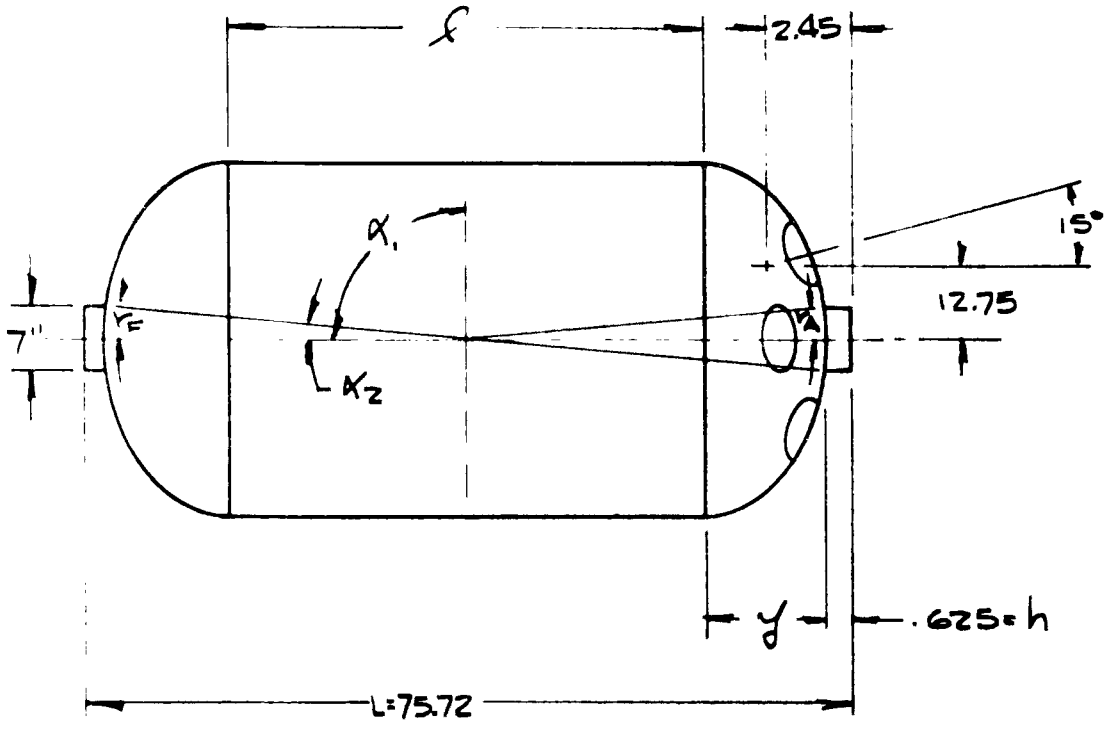

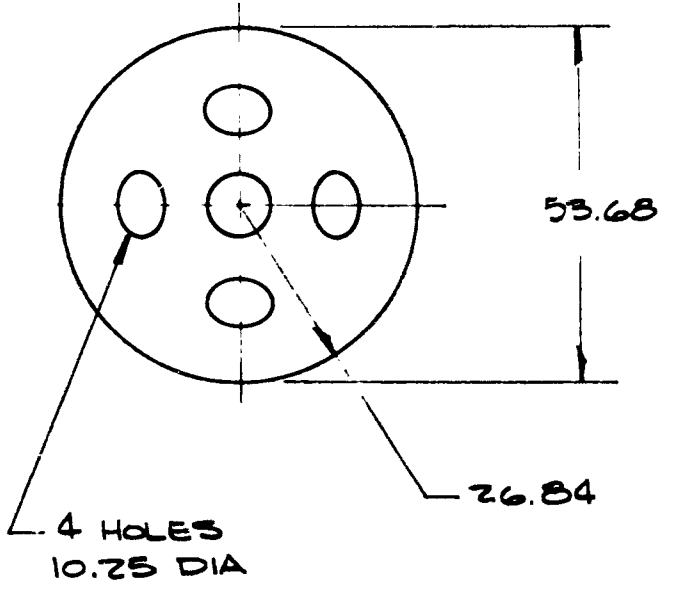

$d = 53.68$
$\ell = 41.51$
$\alpha_1 = 90°$
$\alpha_2 = 5.4°$

X-260 DESIGN DATA

REF:
ABL 260-4002
ABL 260-4010
ABL 260-4011

FIGURE 38

3.3.5 Glass Filament Requirements

The amount of glass fibers required to withstand a test pressure of 370 psig is next calculated for uniform fiber loading using equations derived in Appendix V.

a) For equal fiber loads in both directions:

$$N_1 \cos\alpha_1 - \frac{\pi d}{4\ell} M_1 \sin\alpha_1 = -\left[N_2 \cos\alpha_2 - \frac{\pi d}{4\ell} M_2 \sin\alpha_2\right]$$

where N = no. of fibers crossing circumference πd

M = no. of fibers crossing length 2ℓ

$\alpha_1 = 90°$ and $\sin\alpha_1 = 1$ $\cos\alpha_1 = 0$

$$\therefore \quad \frac{\pi d}{4\ell} M_1 = N_2 \cos\alpha_2 - \frac{\pi d}{4\ell} M_2 \sin\alpha_2$$

where $M_2 = \frac{2\ell}{\pi d} N_2 \tan\alpha_2$

$$\therefore \quad \frac{M_1}{N_2} = \frac{2\ell}{\pi d}\left[2\cos\alpha_2 - \tan\alpha_2 \sin\alpha_2\right]$$

where $\sin\alpha_2 = .094$

$\cos\alpha_2 = .996$

$\tan\alpha_2 = .094$

$$\frac{M_1}{N_2} = \frac{2\,(41.51)}{\pi(53.68)}\left[2\,(.996) - .094(.094)\right]$$

$$\frac{M_1}{N_2} = 0.975$$

b) $$P\,\frac{d}{4} = \frac{1}{\pi d}\left[N_1 f_1 \cos\alpha_1 + N_2 f_2 \cos\alpha_2\right]$$

where $\cos\alpha_1 = \cos 90° = 0$

$$N_2 = \frac{\pi d^2 p}{4 f_2 (\cos\alpha_2)}$$

where P = proof pressure - 370 psig

f_2 = working load per end = (.9)(6)=4.8 #/end

$$N_2 = \frac{\pi(53.68)^2(370)}{4(4.8)(.996)}$$

N_2 = 175500 ends crossing circumference πd

and $M_1 = .975\ N_2 = .975(175{,}500) = 171{,}000$ ends crossing length 2ℓ

This corresponds to a winding pattern consisting of 87,750 end turns with a 5.4° winding angle and 85,500 end turns with a 90° winding angle.

3.3.6 Design of Non-Polar Port Reinforcements

The design of the reinforcements for the non-polar ports is a difficult task because in the application of currently established techniques and equations for isotropic materials various assumptions must be made which often lead to erroneous and impractical solutions. The problem is to accomplish an efficient load transfer across the cut-out opening without introducing critical secondary bending and shear stresses. With the present state of the art this is best accomplished by a combined analytical and test program. An example of the assumptions which are possible include the following:

1. All of the load transfer is accomplished through shear between the various layers of reinforcements and meridional windings.
2. All of the load transfer across the opening must be accomplished through the reinforcement medium. If reinforcing rings are considered then all the load is transmitted through them.
3. The load transfer is achieved through a combination which produces an optimum configuration in which the flexural and strain properties of the reinforcement match those of the dome structure

so that secondary forces are minimized.

Two analyses were made for sizing the non-polar port reinforcements. One was based on load transfer requirements and the other on strain requirements. Both analyses were based on the following assumptions:

1. dome contours grow uniformly under pressure
2. bending effects are neglected
3. no residual or discontinuity stresses are present
4. all fibers are loaded uniformly

The first approach selected for analysis consisted of doilies made of hoop windings in the form of rings to which the entire load is transmitted through shear. This type of reinforcement was selected because it would be made of continuous glass fibers thereby maintaining its structural integrity and enabling a better load transfer. A simplified analysis was made in which the laminate was considered as flat and bi-directional. The fiber loads were assumed to be transmitted directly to the reinforcing ring at the outside radius. Results of this analysis are shown in Appendix VII. Expressions for the radial and tangential loads are derived in terms of the winding angle and glass fiber tension. A study of the results shows that the resultant (radial-tangential) load is maximum at the upper edge of the port nearest the polar fitting and acts in a radial direction. This corresponds to a value equal to twice the unit fiber load. The maximum hoop load occurs at the lateral edges of the ring.

Detailed design procedures for calculating the required amount of ends were established based on shear requirements. The analysis is based on small angle windings which yields maximum loads and is therefore conservative.

The second analysis considered was based on matching the meridional and hoop strains between the dome shell and the reinforcing ring. With this method the meridional and hoop strains around the reinforcement at proof pressure would be equal to those encountered in an undisturbed dome. This would result in uniform growth and minimize secondary bending and shear stresses.

Results of both analyses indicate the latter approach is more feasible from both theoretical and practical considerations. There are two basic possibilities for attaching these rings to to the dome structure. One method is to bond the reinforcing ring to the outside of the shell with adhesive and then cut away the longitudinal fibers to form the desired opening. The second, and preferred method is to intersperse the required amount of reinforcement between the longitudinal layers of glass filaments. It is felt that a more effective load transfer can be accomplished with this approach. Care must be exercised in the design of these rings to minimize discontinuity effects. This is achieved best by varying the diameter of each layer in such a manner that an effective flexural gradient is obtained across the reinforcement. The edges should be tapered to blend in with the desired contour and overlapping

glass mat used in reinforcing the dome cylinder juncture and in the area between the nozzle ports.

3.3.7 Sizing Non-Polar Port Reinforcement Based on Load Requirements

The following illustrates the method for sizing the aft port reinforcements based on the X-260 configuration.

1. The first step involves calculating the maximum number of fiberglass ends per inch perpendicular to the fiber direction which are cut for the port opening.

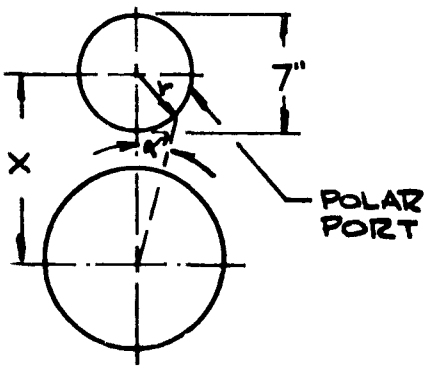

where γ = polar port radius, inches

x = distance between centers of polar and nozzle ports, inches

α' = angle between tangent to polar port and center of nozzle port

From figure 36

a) $\frac{x}{\gamma_o} = \frac{x}{26.84} = .481$

$x = 12.9"$

b) $\sin\alpha' = \frac{3.5}{12.9} = .271$

$\alpha' = 15.72°$

$\tan\alpha' = .281$

$\cos\alpha' = .963$

c) $(N)\ \text{max.} = \frac{\text{no. of ends crossing circumference}}{2\pi x} \times \frac{1}{\cos\alpha'}$

$= \frac{175,500}{2\ (\pi)\ (12.9)} \times \frac{1}{.963}$

(N) max. = 2250 ends per inch $\perp$ to fiber direction.

2. The maximum load per inch (T) perpendicular to the fibers is then calculated based on the design fiber load of 4.8 lb. per end.

$$(T)\ \text{max.} = PN = 4.8\ (2250)$$

$$= 10800\ \text{lbs per inch} \perp \text{to fibers.}$$

3. The minimum outside diameter for the rings is determined from equation 3 of Appendix VII.

$$r_2 = r_1 + \frac{+T}{n f_{sa}}$$

Where n = no. of reinforcement rings

f_{sa} = allowable interlaminar shear, psi.

Assume n = 4

The value of "n" is chosen as 4 to permit an effective reinforcement distribution.

$f_{sa} = 5000$

and $r_1 = 5.125$ inches

then

$$r_2 = 5.125 + \frac{10800}{4(5000)} = 5.125 + .54$$

$r_2 = 5.665$ inches minimum.

Inasmuch as the distance between the edges of the polar and non-polar ports is 4.3 inches, the outer radius of the reinforcing ring may be as much as 9.425 inches. For best design an outside diameter of 7.625 inches will be considered to yield a 2 1/2" wide ring.

4. The final step is to calculate the required number of circumferential ends per layer of reinforcement. This is obtained from

$$S = (r_1 + r_2) \frac{T}{np^1}$$

where S = No. of circumferential ends per layer

T = load per in $\perp$ to fibers

n = no. of reinforcement layers

p^1 = allowable load per end in circumferential reinforcement fibers.

$$S = (5.125 + 7.625) \frac{(10800)}{(4)(4.8)}$$

S = 7150 ends per layer of reinforcement.

This would result in each ring being 0.10 inches thick, yielding a total cross-sectional area of approximately 1.0 square inch. This number of glass filaments appears unfeasible from a practical standpoint and shows that this design approach is too conservative. It is felt that with this configuration the reinforcing ring would be too stiff and would result in high secondary bending and shear stresses. Under pressure loading the shell would not maintain its contour and high discontinuity stresses would be encountered.

3.3.8 Sizing Non-Polar Port Reinforcements Based on Strain Requirements

This method illustrates the method for sizing the aft port reinforcements based on the X-260 configuration. Since the zero shear dome contour has been shown to coincide with the geodesic contour formulae and data presented in references number 5, 6, 9 and 10 can be applied.

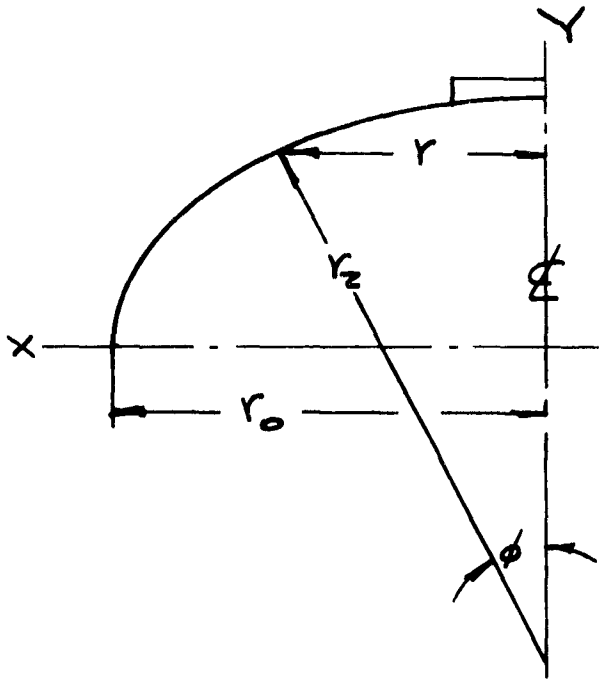

where r_o = dome radius, inches

r_o = 26.84"

r = radius to center of nozzle, inches

α_T = angle filament makes with the longitudinal axis at point of tangency, degrees = 5.4°

α = filament helix angle between filament direction and dome meridional plane at center of nozzle port, degrees.

Φ = angle between normal to dome contour and centerline of dome.

r_2 = radius of curvature normal to meridian, inches.

1. The first step is to determine the filament helix angle at the center of the nozzle port. From figure 36, r/r_o is 0.48 at this point and

$$r = .48(26.84) = 12.883 \text{ inches}$$

From reference 5

$$\sin \alpha = \frac{\sin \alpha_r}{r/r_o} = \frac{.09411}{.48} = .19606$$

and $\alpha = 11.3°$

2. The angle ϕ is calculated from

$$\phi = \arctan \frac{-x^3}{\left[(1-x^2)\left\{x^2(1+x^2)-\tan^2\alpha_r\right\}\right]^{\frac{1}{2}}} \quad \text{(see ref. 5)}$$

where $x = \frac{r}{r_o} = .48$

$$\phi = \arctan \frac{-.11059}{\left[(1-.2304)\left\{.2304(1+.2304)-.0089359\right\}\right]^{\frac{1}{2}}} = \arctan .24059$$

$$\phi = 13.525°$$

3. The radius of curvature r_2 is obtained from

$$r_2 = \frac{r}{\sin\phi} = \frac{12.883}{.2339}$$

$$r_2 = 55.079 \text{ inches}$$

4. The radius of curvature r_1 in the meridional plane is calculated from

$$r_1 = r_o R_c$$

where Rc = instantaneous radius of curvature at the center of the nozzle port

$$R_c = \frac{\left[1+\left(\frac{dy}{dx}\right)^2\right]^{3/2}}{\frac{d^2y}{dx^2}}$$

where $\frac{dy}{dx} = \tan\phi = .24059$

$$\frac{d^2y}{dx^2} = \frac{3x^2}{\sqrt{A}} - \frac{(x^4 - 3x^8 + Cx^4)}{\sqrt{A^3}}$$

$A = x^2 - x^6 - C\,(1-x^2)$

$C = \tan^2 \alpha_r = .0089359$

$X = .48$, $x^2 = .2304$

substituting we have

$A = .2304 - (.2304)^3 - .0089359(1-.2304)$

$A = .2113$

$$\frac{d^2y}{dx^2} = \frac{3(.2304)}{\sqrt{.2113}} - \frac{\left[(.2304)^2 - 3(.2304)^4 + .0089359(.2304)^2\right]}{\sqrt{(21133)^3}}$$

$$\frac{d^2y}{dx^2} = 1.038$$

therefore

$$Rc = \frac{\left[1+(.24059)^2\right]^{3/2}}{1.038} = 1.048$$

and $r_1 = 26.84 \times 1.048 = 28.128$ inches

5. The meridional (N_ϕ) and hoop (N_θ) loading is obtained from conventional pressure vessel formulae.

Meridional load $N_\phi = \frac{Pr}{2\sin\phi} = \frac{370(12.883)}{2(.2339)} = 10{,}187$ lb/in

$N_\phi = 10{,}187$ lb/in

Hoop Load $N_\theta = N_\phi\left(2 - \frac{r_2}{r_1}\right)$

$= 10187\left(2 - \frac{55.079}{28.128}\right)$

$N_\theta = 407.1$ lb/in

6. The corresponding dome meridional (ε_ϕ) and hoop (ε_θ) strains are calculated as follows:

meridional strain $\varepsilon_\phi = \dfrac{N\phi}{E\,t\cos^2\alpha}$

hoop strain $\varepsilon_\theta = \dfrac{N\theta}{E\,t\,\sin^2\alpha}$

$$t = \frac{t_r r_o \cos\alpha_r}{r\cos\alpha}$$

$$= \frac{(.040)(12.883)(.98061)}{(26.84)(.99556)}$$

$t = .0846$ inches

where E = modulus of elasticity
= 6.5 (10^6) psi (assumed)

t = laminate thickness corresponding to center of nozzle port.

t_r = meridional thickness at equator
= .040" (based on scale model)

$$\therefore \varepsilon_\phi = \frac{.10187}{6.5(10^6)(.0846)(.98061)^2}$$

$\varepsilon_\phi = .01928$ in/in

likewise

hoop strain $\varepsilon_\theta = \dfrac{407.1}{6.5(10^6)(.0846)(.1966)^2}$

$\varepsilon_\theta = .01928$ in/in

7. The cross-sectional area of the required reinforcing ring is then obtained based on making the ring and dome strains equal.

The reinforcing ring stress is

$$\sigma = \frac{N\phi\,(2R_R)}{2A_r}$$

and for equal ring and dome strains

$$\sigma = \varepsilon_\phi E$$

where R_R = radius of non-polar port opening, inches
= 5.125 inches

A_r = required cross-sectional area of ring, in^2

σ = ring stress, psi

E = modulus of ring, psi
= 7.5 (10^6) (assumed)

equating and substituting

$$\frac{N_\phi R}{A_r} = \varepsilon_\phi E$$

$$A_r = \frac{1.0187(5.125)}{.01928(7.5)(10^6)} = .362 \text{ in.}$$

$$A_r = .362 \text{ in.}$$

A similar analysis for the X-250 second stage configuration shows the required reinforcing ring area is .449 in^2.

3.3.9 Summary and Conclusions For Phase III

This phase of the program presents a method for refining the contour of a dome configuration based on established deflection tendencies. With this technique future modifications may be possible with other designs. The zero shear contour was modified to conform with the pressurized dome laminate shape. This should insure an even better load distribution. Further experimental work is recommended.

A design example for the X-260 chamber is presented. The design is based on an optimum configuration in which all glass fibers are loaded equally. This should result in a significant weight saving. Two different analyses for designing the required non-polar port reinforcements are presented, one based on load transfer requirements and the other on matching the dome meridional and hoop strains. The basic shape of this reinforcement is in the form of circumferentially wound rings. A comparison of the two approaches indicates the latter method is more feasible.

3.40 RECOMMENDATIONS AND CONCLUSIONS

The primary objectives of this program were successfully achieved. Many recommendations and conclusions are made possible as a result of this study program. The modified zero shear contour is recommended for use in both the X-250 and X-260 second stage dome configurations. The use of the zero shear contour on the scale model end closure contours produced a highly efficient structure in which the longitudinal and circumferential glass fibers were loaded equally. A strength to density ratio of 1.68×10^6 inches was attained. Empirical methods for the determination of optimum contours were proven feasible and present a practical method for obtaining future design variations. Results show dome contour, winding angle, pattern, and reinforcement are all inter-related factors. The empirically determined zero shear contour was shown to be in agreement with the theoretical Geodesic contour. A study of the various contours shows little variation, especially for the smaller winding angles. It should be noted however that these contours may only be practical for thin walled domes. For heavier walls some modification may be required. For future applications it is recommended that the effect of dome thickness be studied. The forward and aft adapter ports should require identical openings to insure compatibility between the contour and winding pattern on both closures. A sequential winding pattern is recommended where successive rovings are placed adjacent to each other. This minimizes the number of cross-over points and with a polar wrapping pattern more closely approximates geodesic requirements.

Deflection characteristics of a polar ported model were found to be essentially linear with pressure, indicating costly contour changes can

be first checked on scale models. A method is presented for adjusting dome contours based on deflection tendencies. In this fashion the contour is made to comply with deflections. Girth reinforcements for attaching the skirt were found to stiffen the knuckle area and formed an abrupt discontinuity. It should be noted that even with this discontinuity present, a much more efficient dome structure was achieved with this contour. It follows that present dome-cylinder juncture failures may also be influenced by the non-polar port reinforcements. The discontinuity effect is magnified by the use of secondary overwinds terminating in this region. It is recommended that the skirt attachment be made directly to the cylinder. A layer of glass cloth is better than pure circumferential windings for reinforcing the dome-cylinder juncture area because it would be more flexible and compatible with deflection tendencies. A gradual change in stiffness should be designed into this area.

The design of the reinforcements for the non-polar ports is a difficult task and must be supplemented with tests. The most efficient port reinforcement will be one in which the natural strain and deflection tendencies of the dome contour are matched in the reinforcement.

A review of available data on full scale chambers indicates considerable variation exists between cases manufactured by various manufacturers. Limited test data shows scalloping and points of inflection are present. To minimize contour and deflection incompatibility the metal inserts and reinforcements should conform to the contour requirements.

REFERENCES

1. Development of a Generatrix for Pressure Vessel Dome Closures With Minimum Hoop Stresses in the Surfaces.

   By: C. C. DeHaven, Allegany Ballistics Laboratory, Cumberland, Maryland, AB/X-39, June 1959.

2. Design Considerations for Spiralloy Glass - Reinforced Filament-Wound Structures as Rocket Inert Parts.

   By: A. H. Kitzmiller, Jr., C.C. DeHaven and R.E. Young A.R.S. Report 953-59

3. Isotensoid Pressure Vessels, December 1960

   By: John Zickel, Aerojet-General Corporation, Sacramento, California

4. Allegany Ballistics Laboratory X-250 Hydrotest Data Sheets 1 through 5.

5. The Ovaloid Problem - A definition and geodesic solution. Hercules Powder Co., Inc., Young Dev. Div. of Allegany Ballistics Laboratory

   By: J. H. Nourse

6. The Ideal Geodesic Ovaloid - Report No. 2

   By: J. H. Nourse

7. Allegany Ballistics Laboratory X-260 Non Insulated Ported Burst Chamber Results - Sheets 1 and 2.

8. Applied Elasticity - Wang, McGraw-Hill Co.

9. End Closures of Filament Wound Motor Cases - Optimum Dome Contour & Stress Distribution for winding angles other than zero

   By: A.F. Foerster, Goodyear Aircraft Corp., Report No. GER-10253, June 9, 1961

10. Design Study to Improve the Structural Efficiency of ABL-X-250 Motor Cases. Progress Report No. 4, GER-10250, Rev. C., Dec. 7, 1961, Goodyear Aircraft Corp.

11. Aerojet-General Test Report No. B-124. B-128, B-131, B-132.

Appendix I

KB-9 O-Shear Container - Evaluation of Test Data

KB-9 Test Data

Two layers of laminate wound at 7.5° and 20° respectively

Total wall thickness at equator = .042

d = 14.14 in. (external dimension)

h = 10.035 in. (external dimension taken from another specimen)

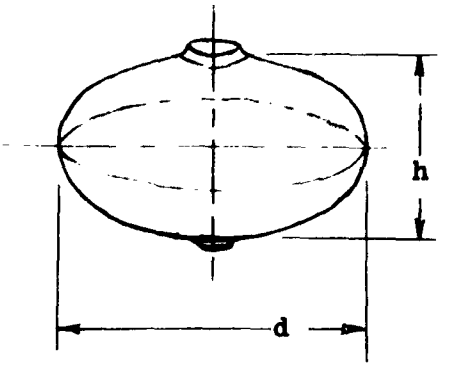

No. of ends per layer = 10,800 (same for both 7-1/2 and 20° winds)

No. of layers = 2 (same for both winds)

Percent resin by weight = 23.5

Burst pressure = 925 psig

Failure occurred at the equator.

Ref: Wang, "Applied Elasticity," McGraw-Hill, 1953, p. 329

Assuming the container to be acting as a membrane, we have the following equations:

$$2\pi r_o N_\varphi \sin_y + R = 0$$

$$N\theta = -\frac{ro}{\sin\varphi}\left[\frac{N\varphi}{r_2} + P_3\right]$$

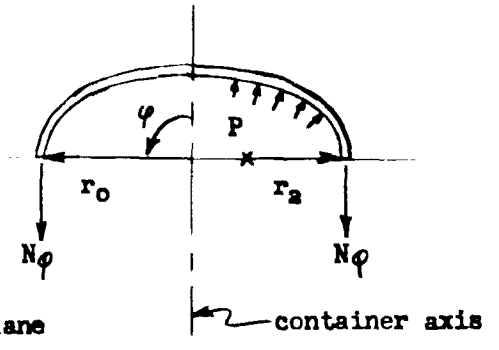

where r_o = radius of container at equator

r_2 = radius of curvature of surface in plane intersecting axis of container

R = resultant of forces acting on shell

φ = angle as shown

P_3 = external pressure acting on shell

N_φ = load per inch in longitudinal direction

Nθ = load per inch in hoop direction

Solving for N_φ

$$N_\varphi = - \frac{R}{2\pi r_o \sin\varphi}$$

But $R = - \pi r_o^2 P$

$\varphi = 90°$

$\sin\varphi = 1$

$$\therefore N_\varphi = \frac{Pro}{2} = \frac{(925)(7.07)}{2}$$

$N_\varphi = 3{,}270$ lb/in.

Solving for N_θ and substituting values:

$$N_\theta = - \frac{r_o}{\sin\varphi} \left[\frac{N_\varphi}{r_2} + P_3 \right]$$

But $r_2 = 3.7"$ {This value was found by graphical methods

$$\therefore N_\theta = - \frac{7.07}{1} \left[\frac{3{,}270}{3.7} - 925 \right] = -7.07 \, [884 - 925]$$

$N_\theta = - (7.07)(-41)$

$N_\theta = 290$ lb/in.

The membrane stresses corresponding to the above values of N_φ and N_θ are:

$$f_\varphi = \frac{N_\varphi}{t} = \frac{3{,}270}{.042} = 78{,}000 \text{ psi}$$

$$f_\theta = \frac{N_\theta}{t} = \frac{290}{.042} = 6{,}900 \text{ psi}$$

Consider a small element of the fiberglass laminate at the equator (only one layer is shown for clarity)

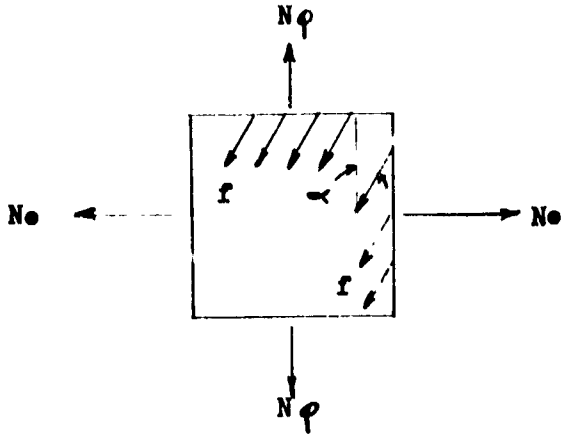

$$f_1 n_1 \cos\alpha_1 + f_2 n_2 \cos\alpha_2 = N\varphi$$

$$f_1 m_1 \sin\alpha_1 + f_2 m_2 \sin\alpha_2 = N\theta$$

where f = fiberforce per end (lbs/end)
n = no. of ends per inch crossing equator
m = no. of ends per inch crossing meridian at the equator
1, 2, = subscripts denoting layers with 7-1/2° and 90° winding angles respectively

m and n are related as follows:

The no. of ends crossing length 1 is equal to the no. of ends crossing length $1/\text{Tan}\alpha$,

$$n \cdot 1 = m \frac{1}{\text{Tan}\alpha}$$

$$\frac{m}{n} = \text{Tan}\alpha$$

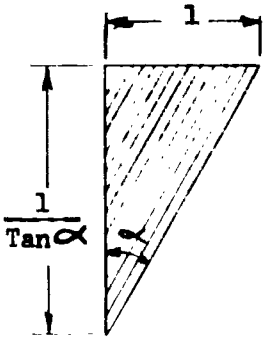

The equations for $N\varphi$ and Ne may therefore be rewritten

$$f_1 n_1 \cos\alpha_1 + f_2 n_2 \cos\alpha_2 = N\varphi$$

$$f_1 n_1 \sin\alpha_1 \operatorname{Tan}\alpha_1 + f_2 n_2 \sin\alpha_2 \operatorname{Tan}\alpha_2 = Ne$$

$$\therefore f_1 = \frac{N\varphi - f_2 n_2 \cos\alpha_2}{n_1 \cos\alpha_1} = \frac{Ne - f_2 n_2 \sin\alpha_2 \operatorname{Tan}\alpha_2}{n_1 \sin\alpha_1 \operatorname{Tan}\alpha_1}$$

Solving for f_2:

$$\therefore f_2 = \frac{Ne\cos\alpha_1 - N\varphi \sin\alpha_1 \operatorname{Tan}\alpha_1}{n_2 [\sin\alpha_2 \operatorname{Tan}\alpha_2 \cos\alpha_1 - \sin\alpha_1 \operatorname{Tan}\alpha_1 \cos\alpha_2]}$$

letting $\alpha_1 = 7.5°$ $\alpha_2 = 20°$

$\sin\alpha_1 = .13053$ $\sin\alpha_2 = .34202$

$\cos\alpha_1 = .99144$ $\cos\alpha_2 = .93969$

$\operatorname{Tan}\alpha_1 = .13165$ $\operatorname{Tan}\alpha_2 = .36397$

Also; $n_1 = n_2 = \frac{(10,800)(2)}{(\pi)(14.14)} = 486$ ends/inch

Substituting values

$$f_2 = \frac{(290)(.99144) - (3,270)(.13053)(.13165)}{486 [(.34202)(.36397)(.99144) - (.13053)(.13165)(.93969)]}$$

$f_2 = 4.44$ lbs/end { For 20° layer

$$f_1 = \frac{3,270 - (4.44)(486)(.93969)}{(486)(.99144)}$$

$f_1 = 2.58$ lbs/end { For 7.5° layer

Appendix II

Specimen KB-15 Stress and Load Calculations

A. At the Equator

1. Meridional load in lbs./inch = $N_m = \frac{Pr_o}{2}$ = where P = internal pressure in psig

r_o = Maximum radius

$$N_m = \frac{700}{2}(7.43)$$

$$N_m = 2610 \text{ lbs./in.}$$

2. Average meridional wall stress at equator = $S_m = \frac{N_m}{t}$ where t = laminate thickness at equator, inches

$$S_m = \frac{2610}{.015}$$

$$S_m = 174{,}000 \text{ psi}$$

3. Load per end, $T = \frac{N_m}{M}$ where M = ends per inch of circumference at equator

α = winding angle

$$M = \frac{\text{Total flier revs.} \times \text{ends/roving} \times 2}{2\pi r}$$

$$M = \frac{720 \times 20 \times 2}{2\pi(7.43)} = 617 \text{ ends/inch of circumference}$$

$$T = \frac{N_m}{M\cos\alpha} = \frac{2610}{617(.991)} = 4.27 \text{ lbs/end}$$

Appendix II (Cont'd.)

B. At Point of Failure

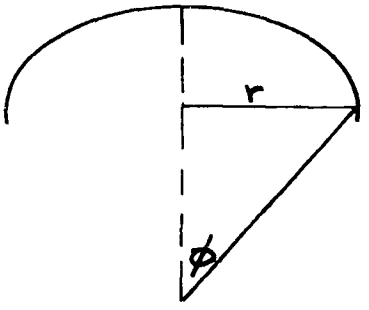

1. Meridional Load = $N_m = \frac{Pr}{2 \sin \phi}$

where P = internal pressure psig

r = radius, in inches = 6.4" } Obtained graphically

ϕ = 46° }

$$N_m = \frac{700\ (6.4)}{2\ (\sin 46°)} = \frac{700\ (6.4)}{2\ (.72)}$$

N_m = 3110 lbs./inch

2. Average meridional wall stress, $S_m = \frac{N_m}{t} = \frac{3110}{.029}$

where t = laminate thickness at point of failure on dome, inches = .029"

S_m = 107,300 psi

Appendix III

Equations For Calculating Bending Strains Using Flexagage

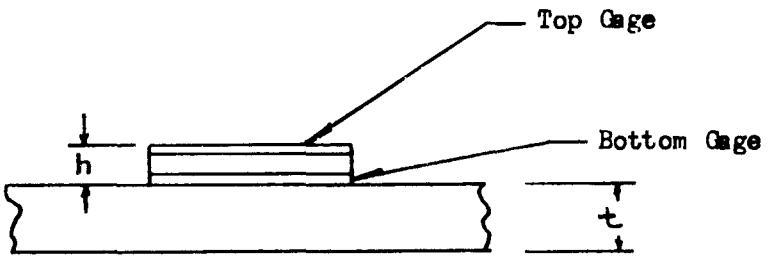

1. $$\varepsilon_b = (\varepsilon_1 - \varepsilon_2)\frac{t}{2h}$$

2. $$\varepsilon_a = \varepsilon_2 - \varepsilon_b - \frac{t_c}{h}(\varepsilon_1 - \varepsilon_2) = \varepsilon_2 - \varepsilon_b - K$$

where

ε_a = actual axial strain at laminate surface

ε_b = actual bending strain on laminate surface

ε_1 = strain reading at top gage

ε_2 = strain reading at bottom gage

t = laminate thickness

h = effective thickness of Flexagage

t_c = distance bottom gage is from laminate

Appendix IV

Simulation of Aluminum Skirt Stiffness with Equivalent Layers of Fiberglass Laminate

$$E = \frac{S}{\epsilon} = \frac{F}{A\epsilon} = \frac{Fd}{\delta A}$$

where F = load - lbs
d = length - in.
δ = elongation - in.
A = area - sq in.

For equal strain at given load (i. e. same stiffness)

$$\frac{F}{\delta} = \left(\frac{AE}{d}\right)_{Al} = \left(\frac{AE}{d}\right)_{gl}$$

or

$$A_{gl} = A_{Al}\left(\frac{E_{Al}}{E_{gl}}\right)$$

Assuming that only the portion of aluminum skirt which is bonded to rocket case, contributes to the stiffness of the rocket case, we have:

For the full-scale case: (t = .090 in.)

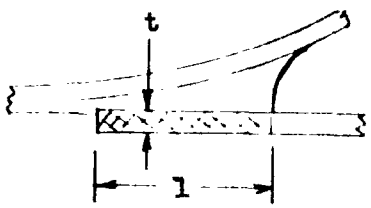

$A_{Al} = (2)(.09) = .180$ in.^{2}

Also

$E_{Al} = 10 \times 10^6$ psi

$E_{gl} = 7 \times 10^6$ psi

$$A_{gl} = (.180)\ \frac{10}{7} = 0.257 \text{ sq. in.}$$

For same length, i. e., 2.0 in.

$$t_{gl} = \frac{0.257}{2}$$

$t_{gl} = .13$ in.

For 1/4 scale model

$t_{gl} = .033$ l = 0.5

Appendix V

Design Equations for a Cylindrical Container Wound With Two or More Winding Angles

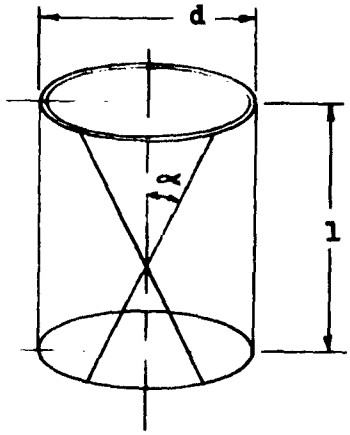

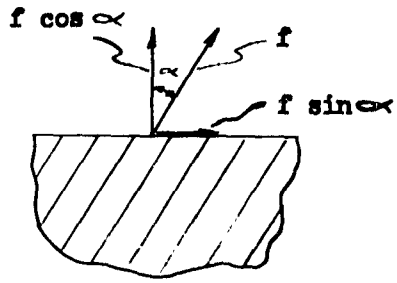

Longitudinal Force

$F_L = Nf \cos \alpha$

where: N = no. of ends crossing circumference πd

f = fiber force per end (lbs.)

But, $F_L = \frac{\pi d^2}{4} p$

where: d = diameter of cylinder (in.)

p = internal pressure (psi)

Also, $N_L \triangleq \frac{F_L}{\pi d}$ = longitudinal force per inch of circumference (lb. per in.)

$$N_L = \frac{F_L}{\pi d} = \frac{Pd}{4} = \frac{Nf}{\pi d} \cos \alpha \qquad \text{Eq. 1 a}$$

For k layers,

$$N_L = \frac{F_L}{\pi d} = \frac{Pd}{4} = \sum_{1}^{k} \frac{Nifi}{\pi d} \cos \alpha_i \qquad \text{Eq. 1 b}$$

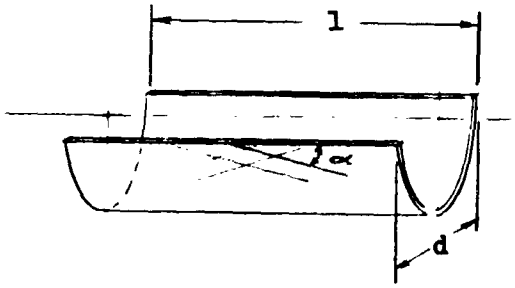

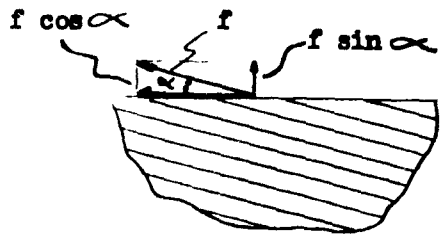

Hoop Force

$F_H = M f \sin \alpha$

where: M = No. of ends crossing length 2 l
f = fiber force per end (lbs.)

But, $F_H = dlP$

where: d = diameter of cylinder (in.)
l = length of cylinder (in.)
p = internal pressure (psi)

Also, $N_H \triangleq \frac{F_H}{2l}$ = hoop force per inch of length (lb. per in.)

$$\therefore \quad N_H = \frac{F_H}{2l} = \frac{Pd}{2} = \frac{Mf}{2l} \sin \alpha \qquad \text{Eq. 2 a}$$

For k layers,

$$N_H = \frac{F_H}{2l} = \frac{Pd}{2} = \sum_{i}^{k} \frac{M_i f_i}{2l} \sin \alpha_i \qquad \text{Eq. 2 b}$$

Relationship between M and N

The no. of ends crossing length 2 l, (M) can be expressed in terms of the no. of ends crossing the circumference (N), the winding angle (α), the length (l) and diameter (d).

Consider the following geometry:

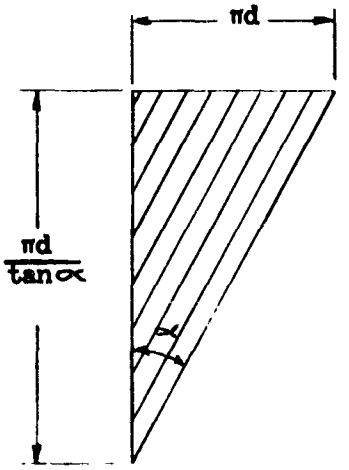

No. of ends crossing circumference πd = N

No. of ends crossing length, $\frac{\pi d}{\tan \alpha}$ = N

No. of ends per inch of length = $\frac{N \tan \alpha}{\pi d}$

No. of ends in total length of 2 l = 2 l $\left(\frac{N \tan \alpha}{\pi d}\right)$

But, M = No. of ends crossing length 2 l

$$\therefore \frac{M}{N} = \frac{2\,l}{\pi d} \tan \alpha \qquad \text{Eq. 3}$$

Note: For winding angles of 0° and 90° (corresponding to pure longitudinal and pure circumferential windings), $\tan\alpha$ has values of 0 and ∞ respectively. This means that either M or N becomes 0 depending on whether the windings are longitudinal or circumferential.

Relationship between Fiber force and Winding Pattern

Noting that:

$N_H = 2 N_L$ { see equations 1 b and 2 b

Then, from Equations 1 b and 2 b, we have:

$$\sum_1^k \frac{Mifi}{2l} \sin\alpha_i = 2 \sum_1^k \frac{Nifi}{\pi d} \cos\alpha_i$$

or $$\sum_1^k Mifi \sin\alpha_i = \frac{4l}{\pi d} \sum_1^k Nifi \cos\alpha_i \qquad \text{Eq. 4 a}$$

Substituting Eq. 3 in Eq. 4a, we have

$$\sum_1^k Nifi \tan\alpha_i \sin\alpha_i = 2 \sum_1^k Nifi \cos\alpha_i \qquad \text{Eq. 4 b}$$

Equations for Cylinder with Two Winding Angles

For the case where k = 2, equations 1 b and 2 b become:

$$N_L = \frac{F_L}{\pi d} = \frac{Pd}{4} = \frac{1}{\pi d} [N_1 f_1 \cos\alpha_1 + N_2 f_2 \cos\alpha_2]$$

$$N_H = \frac{F_H}{2l} = \frac{Pd}{2} = \frac{1}{2l} [M_1 f_1 \sin\alpha_1 + M_2 f_2 \sin\alpha_2]$$

Since the pressure, P, is the same for both types of loading

$$\frac{4}{\pi d^2} [N_1 f_1 \cos\alpha_1 + N_2 f_2 \cos\alpha_2] = \frac{1}{dl} [M_1 f_1 \sin\alpha_1 + M_2 f_2 \sin\alpha_2]$$

$$\therefore \frac{f_1}{f_2} = - \left[\frac{N_2 \cos\alpha_2 - \frac{\pi d}{4l} M_2 \sin\alpha_2}{N_1 \cos\alpha_1 - \frac{\pi d}{4l} M_1 \sin\alpha_1} \right] \qquad \text{Eq. 5 a}$$

For equal force per end in all fibers (i. e. equal fiber stress)

$$f_1 = f_2$$

$$N_1 \cos\alpha_1 - \frac{\pi d}{4l} M_1 \sin\alpha_1 = - \left[N_2 \cos\alpha_2 - \frac{\pi d}{4l} M_2 \sin\alpha_2 \right] \qquad \text{Eq. 5 b}$$

For values of M and N other than 0 (i. e. $0 < \tan \alpha < \infty$ or $0° < \alpha < 90°$)

Since $\frac{\pi d}{2l}$ $M = N \tan \alpha$

$$\frac{N_1}{N_2} = - \frac{2 \cos \alpha_2 - \tan \alpha_2 \sin \alpha_2}{2 \cos \alpha_1 - \tan \alpha_1 \sin \alpha_1} \qquad \text{Eq. 5 c}$$

Appendix VI

Design of Polaris Rocket Motor Case Using 7-1/2 and 90° Winding Angles

Assume stresses in end closure less than stresses in cylindrical portion of container and design on basis of loads acting in the cylinder.

$d = 53.44$ in.

$l = 35.89$ in.

$\alpha_1 = 90°$

$\alpha_2 = 7.5°$

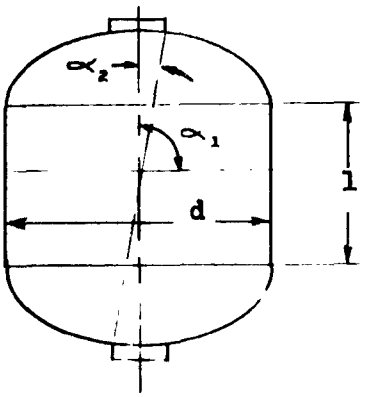

From geometry $N_1 = 0$ (i. e. 90° hoop windings do not contribute to longitudinal strength).

For equal stress in both layers (Eq. 5 b)

$$N_1 \cos\alpha_1 - \frac{\pi d}{4l} M_1 \sin\alpha_1 = -\left[N_2 \cos\alpha_2 - \frac{\pi d}{4l} M_2 \sin\alpha_2\right]$$

but $N_1 = 0$

$\sin\alpha_1 = 1$

$\cos\alpha_1 = 0$

$$\therefore \frac{\pi d}{4l} M_1 = N_2 \cos\alpha_2 - \frac{\pi d}{4l} M_2 \sin\alpha_2$$

But $\frac{\pi d}{2l} M_2 = N_2 \tan\alpha_2$

$$\therefore M_1 = \frac{4l}{\pi d}\left[N_2 \cos\alpha_2 - \frac{N_2}{2} \tan\alpha_2 \sin\alpha_2\right]$$

$$\frac{M_1}{N_2} = \frac{2l}{\pi d}\left[2\cos\alpha_2 - \tan\alpha_2 \sin\alpha_2\right]$$

but $\sin\alpha_2 = .13053$

$\cos\alpha_2 = .99144$

$\tan\alpha_2 = .13165$

$$\therefore \frac{M_1}{N_2} = \frac{(2)(35.89)}{(\pi)(53.44)}\left[2(.99144) - (.13165)(.13053)\right]$$

$$\frac{M_1}{N_2} = 0.84$$

where M_1 = No. of 90° winding ends crossing length 21

N_2 = No. of 7.5° winding ends crossing circumference πd.

Since there are two ends per turn of both the 90 and the 7.5° windings

(No. of 90° turns) = 0.84 (No. of 7.5° turns)

The no. of ends required is as follows:

From equation 1 b for k = 2

$$N_L = \frac{F_L}{\pi d} = \frac{Pd}{4} = \frac{1}{\pi d}\left[N_1 f_1 \cos\alpha_1 + N_2 f_2 \cos\alpha_2\right]$$

but $\cos\alpha_1 = \cos 90° = 0$

$$\therefore \frac{\pi d^2}{4} P = N_2 f_2 \cos\alpha_2$$

Solving for the number of ends, N_2

$$N_2 = \frac{\pi d^2 P}{4 f_2 \cos\alpha_2}$$

For: Proof pressure = 450 psi

$d = 53.44$ in.

$\alpha_2 = 7.5°$

$\cos\alpha_2 = .99144$

$f_2 = (.8)(6) = 4.8$ lbs/end

$$N_2 = \frac{(\pi)(53.44)^2(450)}{(4)(4.8)(.99144)}$$

$N_2 = 212{,}000$ ends crossing circumference, πd

$M_1 = (.84)(212{,}000)$

$M_1 = 178{,}000$ ends crossing length 2 1

The full scale polaris rocket case therefore requires:

106,000 turns at 7.5° winding angle
89,000 turns at 90° winding angle

The 1/4 scale model therefore requires

$\frac{106,000}{16}$ = 6,620 turns at 7.5° winding angle

and

$\frac{89,000}{16}$ = 5,560 turns at 90° winding angle

Note: The no. of turns is proportional to area and therefore varies as the square of the scale factor

Appendix VII

Fiberglass Reinforcement for Circular Holes

Assumptions

1. Fiber tension uniform.
2. Flat bi-directional laminate with fibers at angle from vertical as shown.
3. Fiber loads transmitted directly to reinforcing ring at outer radius of ring r.

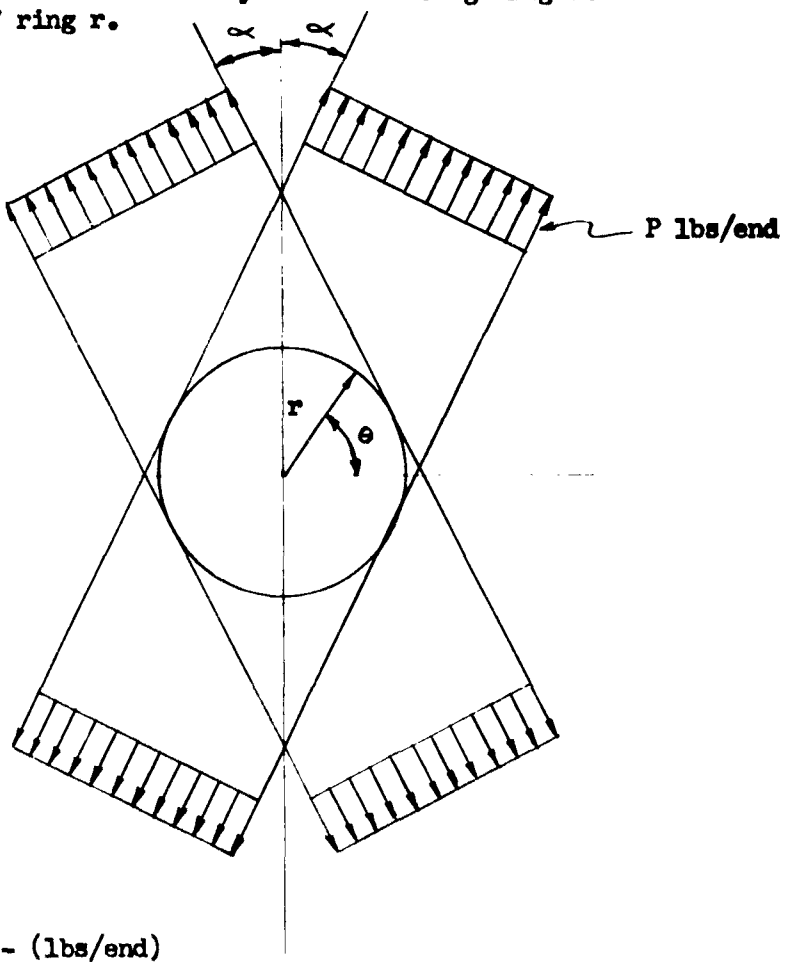

let P = fiber load - (lbs/end)

let M = no. of ends/in. in direction perpendicular to fiber direction

T = PM = load/in. perpendicular to direction of fibers

Radial and Tangential Loads at Outer Circumference of Reinforcing Ring

The radial and tangential loads on the reinforcing ring are found as follows:

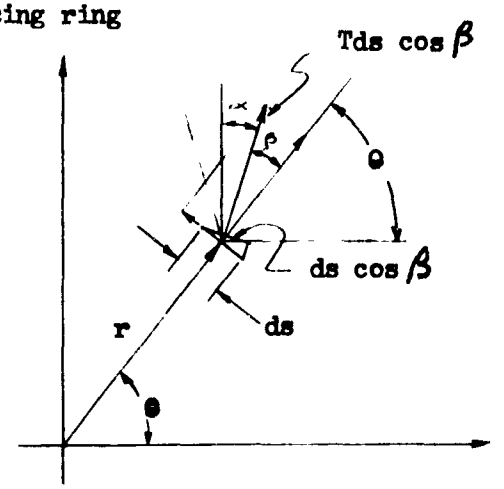

Force due to first layer of fibers

$$F_1 = T\,(ds \cos \beta)$$

Force per unit arc length is

$$\frac{F_1}{ds} = T \cos \beta$$

Radial component, $N_{R_1} = T \cos^2 \beta$

Tangential component, $N_{T_1} = T \sin \beta \cos \beta$

where $\beta = \pi/2 - \alpha - \theta$

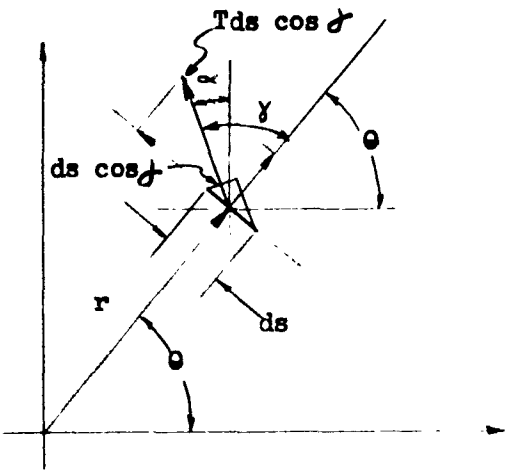

Force due to second layer of fibers

$$F_2 = T\,(ds \cos \gamma)$$

Force per unit arc length is:

$$\frac{F_2}{ds} = T \cos \gamma$$

Radial component:

$$N_{R_2} = T \cos^2 \gamma$$

Tangential component

$$N_{T_2} = T \sin \gamma \cos \gamma$$

where $\gamma = \pi/2 + \alpha - \theta$

Total Radial Load per Unit Length of Circumference

$$N_R = N_{R_1} + N_{R_2} = T \cos^2 \beta + T \cos^2 \gamma$$

$$N_R = T\,[\cos^2 \beta + \cos^2 \gamma\,]$$

{ positive radial load is in outward direction

Total tangential load per unit length of circumference

$$N_T = N_{T_1} + N_{T_2} = T \sin\beta \cos\beta + T \sin\gamma \cos\gamma$$

$$N_T = T[\sin\beta \cos\beta + \sin\gamma \cos\gamma]$$ { positive tangential load is in counterclockwise direction

where $\beta = \pi/2 - \alpha - \theta$

$\gamma = \pi/2 + \alpha - \theta$

The expressions for radial and tangential load per unit length of circumference may be simplified as follows:

$$\frac{N_R}{T} = \cos^2\beta + \cos^2\gamma$$

where $\beta = \pi/2 - (\theta + \alpha)$

$\gamma = \pi/2 - (\theta - \alpha)$

$$\therefore \frac{N_R}{T} = \cos^2[\pi/2 - (\theta + \alpha)] + \cos^2[\pi/2 - (\theta - \alpha)]$$

$$= \sin^2(\theta + \alpha) + \sin^2(\theta - \alpha)$$

$$= [\sin\theta\cos\alpha + \cos\theta\sin\alpha]^2 + [\sin\theta\cos\alpha - \cos\theta\sin\alpha]^2$$

$$= \sin^2\theta\cos^2\alpha + 2\sin\theta\cos\theta\sin\alpha\cos\alpha + \cos^2\theta\sin^2\alpha$$

$$+ \sin^2\theta\cos^2\alpha - 2\sin\theta\cos\theta\sin\alpha\cos\alpha + \cos^2\theta\sin^2\alpha$$

$$= 2[\sin^2\theta\cos^2\alpha + \cos^2\theta\sin^2\alpha]$$

$$= 2\left[\frac{(1 + \cos 2\theta)}{2}\frac{(1 - \cos 2\alpha)}{2} + \frac{(1 - \cos 2\theta)}{2}\frac{(1 + \cos 2\alpha)}{2}\right]$$

$$= \frac{1}{2}\left[1 + \cos 2\theta - \cos 2\alpha - \cos 2\theta\cos 2\alpha + 1 - \cos 2\theta + \cos 2\alpha - \cos 2\theta\cos 2\alpha\right]$$

$$= \frac{1}{2}[2 - 2\cos 2\theta\cos 2\alpha]$$

$$\boxed{\frac{N_R}{T} = 1 - (\cos 2\theta)(\cos 2\alpha)}$$

$$\frac{N_T}{T} = \sin\beta\cos\beta + \sin\gamma\cos\gamma$$

where $\beta = \pi/2 - (\theta + \alpha)$

$\gamma = \pi/2 - (\theta - \alpha)$

$$\frac{N_T}{T} = \sin[\pi/2 - (\theta + \alpha)]\cos[\pi/2 - (\theta + \alpha)]$$

$$+ \sin[\pi/2 - (\theta - \alpha)]\cos[\pi/2 - (\theta - \alpha)]$$

$$= \cos(\theta + \alpha)\sin(\theta + \alpha) + \cos(\theta - \alpha)\sin(\theta - \alpha)$$

$$= [\cos\theta\cos\alpha - \sin\theta\sin\alpha][\sin\theta\cos\alpha + \cos\theta\sin\alpha]$$

$$+ [\cos\theta\cos\alpha + \sin\theta\sin\alpha][\sin\theta\cos\alpha - \cos\theta\sin\alpha]$$

$$= 2[\sin\theta\cos\theta\cos^2\alpha - \sin\theta\cos\theta\sin^2\alpha]$$

$$= 2\sin\theta\cos\theta[\cos^2\alpha - \sin^2\alpha]$$

But: $2\sin\theta\cos\theta = \sin 2\theta$

$\cos^2\alpha - \sin^2\alpha = \cos 2\alpha$

$$\therefore \boxed{\frac{N_T}{T} = (\sin 2\theta)(\cos 2\alpha)}$$

For small winding angles α

$$\cos 2\alpha \approx 1$$

$$\therefore \frac{N_R}{T} = 1 - \cos 2\theta$$

$$\frac{N_T}{T} = \sin 2\theta$$

The approximate variation of $\frac{N_R}{T}$ and $\frac{N_T}{T}$ with θ is therefore given in the following graphs:

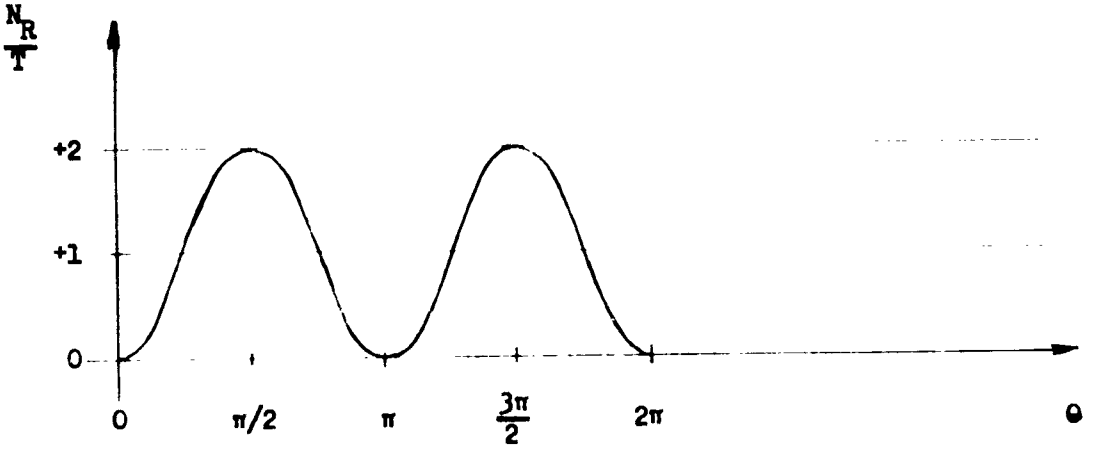

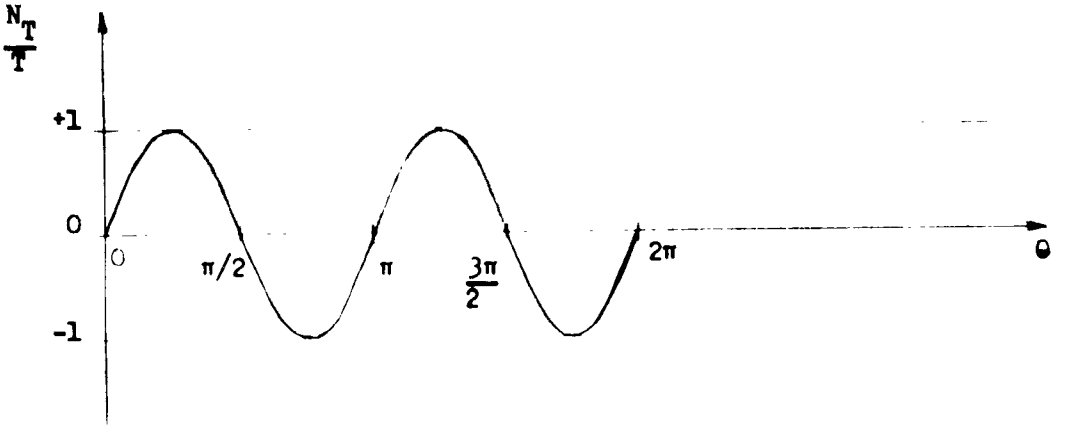

It is interesting to note that when $\alpha = \pi/4$, we have:

$$\frac{N_R}{T} = 1 - (\cos 2\alpha)(\cos 2\theta)$$

$$\frac{N_T}{T} = (\cos 2\alpha)(\sin 2\theta)$$

but $\cos 2\alpha = \cos \pi/2 = 0$

$$\therefore \frac{N_R}{T} = 1$$

$$\frac{N_T}{T} = 0$$

} For all values of θ when $\alpha = \pi/4$

Thus, for a winding angle of 45° the radial load is uniform over the entire circumference of the reinforcing ring, and tangential load is zero. This corresponds to a pure pressure-type loading on the reinforcing ring.

Resultant Load at Reinforcing Ring Outer Circumference

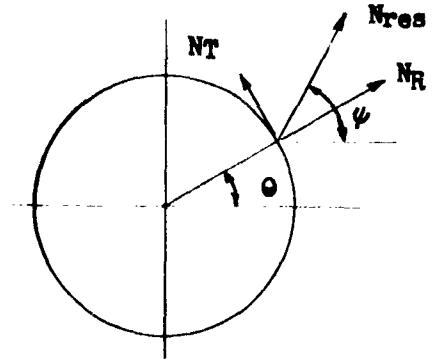

$$N_{res} = \sqrt{N_R^2 + N_T^2}$$

$$N_R = T[1 - (\cos 2\alpha)(\cos 2\theta)]$$

$$N_T = T[(\cos 2\alpha)(\sin 2\theta)]$$

$$N_{res} = \sqrt{T^2\,[1 - (\cos 2\alpha)(\cos 2\theta)]^2 + T^2[(\cos 2\alpha)(\sin 2\theta)]^2}$$

$$\frac{N_{res}}{T} = \sqrt{1 - 2(\cos 2\alpha)(\cos 2\theta) + (\cos^2 2\alpha)(\cos^2 2\theta) + (\cos^2 2\alpha)(\sin^2 2\theta)}$$

$$= \sqrt{1 - 2(\cos 2\alpha)(\cos 2\theta) + (\cos^2 2\alpha)(\cos^2 2\theta + \sin^2 2\theta)}$$

But $\sin^2 2\theta + \cos^2 2\theta = 1$

$$\therefore \boxed{\frac{N_{res}}{T} = \sqrt{1 - 2(\cos 2\alpha)(\cos 2\theta) + \cos^2 2\alpha}}$$

The angle ψ is given by

$$\psi = \theta + \tan^{-1} \frac{N_T}{N_R}$$

$$\boxed{\psi = \theta + \tan^{-1}\left[\frac{(\cos 2\alpha)(\sin 2\theta)}{1 - (\cos 2\alpha)(\cos 2\theta)}\right]}$$

For small winding angle α; $\cos 2\alpha \approx 1$

$$\frac{N_{res}}{T} = \sqrt{2 - 2\cos 2\theta}$$

and

$$\psi = \theta + \tan^{-1}\left[\frac{\sin 2\theta}{1 - \cos 2\theta}\right]$$

The approximate variation of $\frac{N_{Res}}{T}$ with θ is as follows:

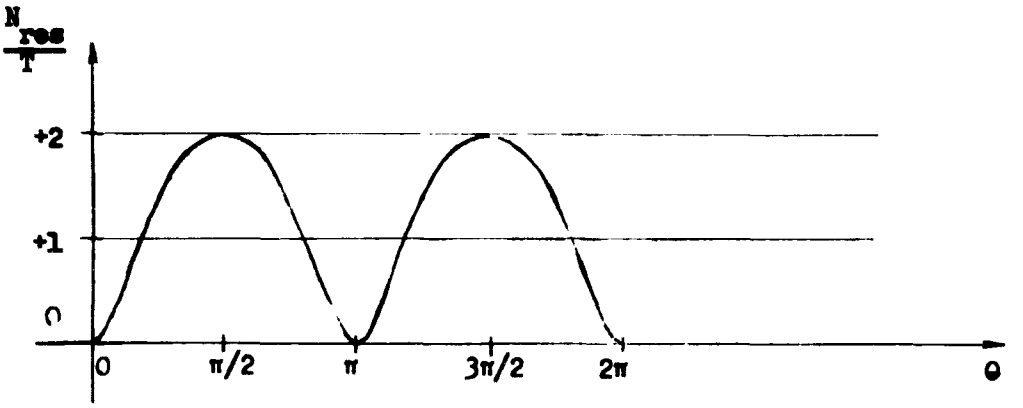

Thus, the resultant load acting on the reinforcing ring is a maximum at $\theta = \pi/2, 3\pi/2$

The direction of the maximum resultant force when $\theta = \pi/2$ for example is:

$$\psi = \pi/2 + \tan^{-1}\left[\frac{0}{1-(-1)}\right]$$

But $\tan^{-1}(0) = 0$

$$\therefore \psi = \pi/2 = \theta$$

The maximum resultant load has a value of:

$$(N_{res})_{max} = 2T$$

and acts in the radial direction.

This occurs at $\theta = \pi/2$ and $\theta = 3\pi/2$.

Hoop Load in Reinforcement Ring

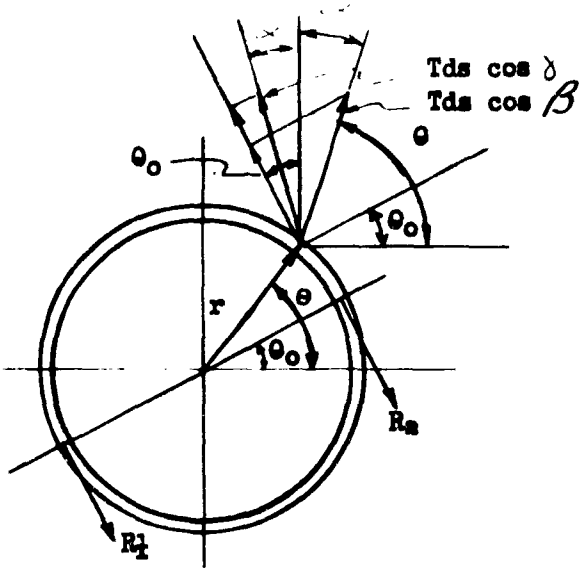

Assume:

1. Fiber tension uniform
2. Flat bi-directional laminate with fibers at angle α from vertical
3. Fiber loads transmitted directly to reinforcing ring at outer edge of ring
4. Thin reinforcing ring

Let $R = R_1 + R_2$ = resultant load acting on ring from θ_o to $(\theta_o + \pi)$

$$R = \int_{\theta_o}^{\theta_o + \pi} [Tds \cos \gamma \cos(\theta_o - \alpha) + Tds \cos\beta \cos(\theta_o + \alpha)]$$

but $ds = r\, d\theta$

$$\cos\gamma = \cos[\pi/2 - (\theta - \alpha)] = \sin(\theta - \alpha)$$

$$\cos\beta = \cos[\pi/2 - (\theta + \alpha)] = \sin(\theta + \alpha)$$

$$R = Tr \int_{\theta_o}^{\theta_o + \pi} [\cos(\theta_o - \alpha)\sin(\theta - \alpha) + \cos(\theta_o + \alpha)\sin(\theta + \alpha)]d\theta$$

$$\frac{R/r}{T} = \int_{\theta_o}^{\theta_o + \pi} \left\{ \begin{array}{l} \cos(\theta_o - \alpha)[\sin\theta \cos\alpha - \cos\theta \sin\alpha] \\ \quad + \cos(\theta_o + \alpha)[\sin\theta \cos\alpha + \cos\theta \sin\alpha] \end{array} \right\} d\theta$$

$$\frac{R/r}{T} = 4(\cos^2\theta_o \cos^2\alpha + \sin^2\theta_o \sin^2\alpha)$$

$$\frac{R/r}{T} = 4\left[\frac{(1 + \cos 2\theta_o)}{2} \frac{(1 + \cos 2\alpha)}{2} + \frac{(1 - \cos 2\theta_o)}{2} \frac{(1 - \cos 2\alpha)}{2} \right]$$

$$\boxed{\frac{R}{2rT} = [1 + (\cos 2\alpha)(\cos 2\theta_o)]}$$

For small winding angles α ,

$$\cos 2\alpha \approx 1$$

$$\therefore \frac{R}{2\pi T} = [1 + \cos 2\theta_o]$$

The variation of $\frac{R}{2\pi T}$ with θ_o is as follows :

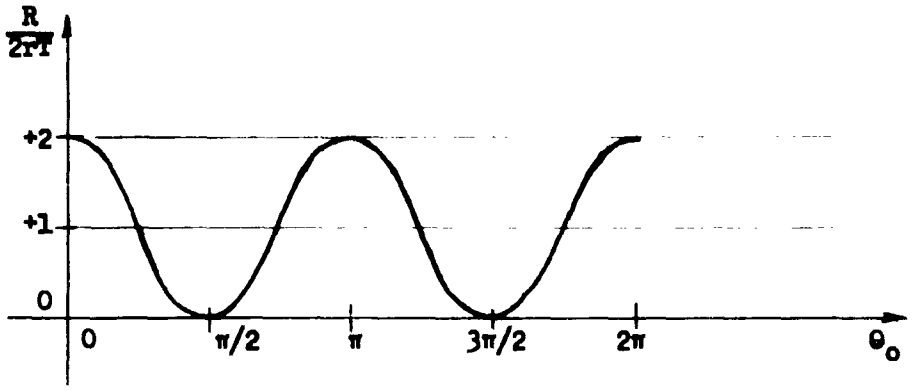

Sizing of Reinforcement Pads

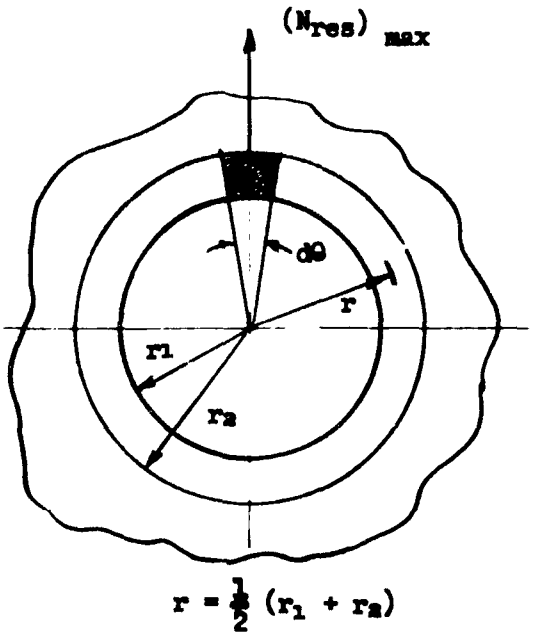

Shear Area based on Maximum Resultant Load

For small α

$$(N_{Res})_{max} = 2T$$

For narrow ring

$$r \approx r_2$$

Therefore,

$$(N_{Res})_{max} (r d\theta) = 2 f_s A_s n$$

where f_s = shear stress (interlaminar)

A_s = shear area

n = number of reinforcement layers

$$\text{But } A_s = \frac{1}{2} r_2^2 \, d\theta - \frac{1}{2} r_1^2 \, d\theta = \frac{r_2^2 - r_1^2}{2} d\theta$$

$$\therefore (N_{Res})_{max} (r d\theta) = 2 n f_s \frac{(r_2^2 - r_1^2)}{2} d\theta$$

$$\text{But } r = \frac{1}{2}(r_1 + r_2)$$

$$(r_2^2 - r_1^2) = (r_2 + r_1)(r_2 - r_1)$$

$$\therefore (N_{Res})_{max} \frac{1}{2} (r_1 + r_2) = 2 n f_s \frac{1}{2} (r_2 + r_1)(r_2 - r_1)$$

$$f_s = \frac{(N_{Res})_{max}}{2n(r_2 - r_1)}$$

or $$\boxed{f_s = \frac{T}{n(r_2 - r_1)}}$$ { for small winding angle α

Sizing of Reinforcement Pads

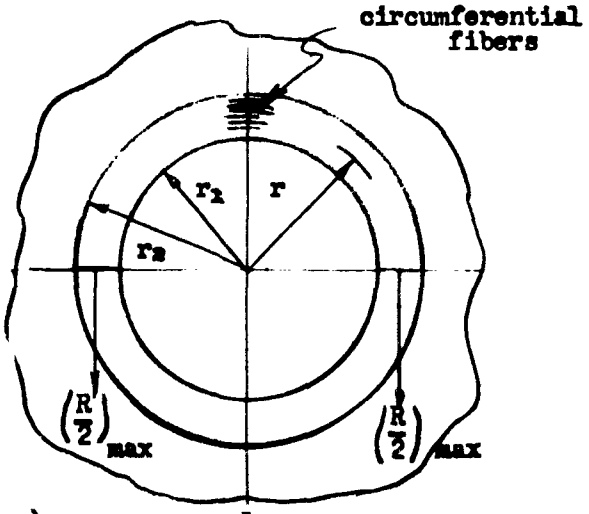

$r = \frac{1}{2}(r_1 + r_2)$

No. of circumferential ends based on maximum reinforcement hoop load.

For small α

$\left(\frac{R}{2}\right)_{max} = 2rT$ { This occurs at $\theta_o = 0, \pi$

Let $\left(\frac{R}{2}\right)_{max} = n\,P's$

where P' = load per end (circumferential fibers)
S = number of circumferential ends per layer
n = number of reinforcement layers

$\therefore 2\,rT = n\,P's$

But $T = P.M$

where P = load per end in unreinforced sheet

M = number of ends per inch $\perp$ to direction of fibers

$\therefore 2\,r\,PM = nP's$

$$S = \frac{2rPM}{nP'} = \frac{2rT}{nP'} = \frac{(r_1 + r_2)T}{nP'}$$

Sizing of Reinforcement Pads

Method of Sizing Pad

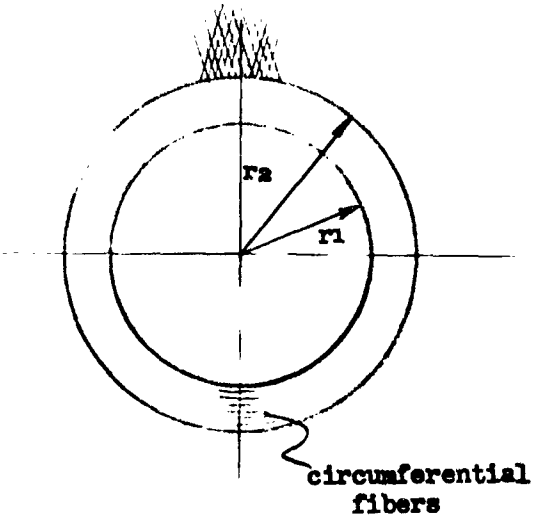

1. Determine values of the following

   P - Load per end of unreinforced sheet

   N - Number of fibers per in.⊥ fiber direction (same for each winding direction)

2. Calculate

   $T = P.N$ = load per in.⊥ fibers

3. For given r_1, calculate r_2 based on allowable shear in reinforcing ring. (Assume a value for n)

   $$r_2 = r_1 + \frac{T}{nf_{sa}}$$

   where f_{sa} = allowable interlaminar shear (psi)

   n = number of reinforcement layers

4. Calculate number of circumferential ends per layer of reinforcement

   $$S = (r_1 + r_2)\ \frac{T}{nP'}$$

   where P' = allowable load per end of circumferential windings in reinforcement pad

5. Calculate packing of circumferential reinforcement fibers

   $$Q = \frac{s}{r_2 - r_1}$$

   where Q = no. of circumferential ends per inch along radius for each reinforcement layer.

DISTRIBUTION LIST FOR FIBERGLASS DEVELOPMENT (REVISION #2)

National Aeronautics and Space Adm.
1512 H. Street, N.W.
Washington 25, D.C.
Attn: Chief, Div. of Research Information
(1 copy)

Commander
Air Force Ballistic Missile Division
Hq. Air Res. and Dev. Command
P.O. Box 262
Inglewood, California (1 copy)

Commanding General
Aberdeen Proving Ground
Maryland (1 copy)

Commanding Officer
Picatinny Arsenal
Dover, N. J. (1 copy)

Commander
Army Ballistic Missile Agency
Redstone Arsenal, Alabama (1 copy)

Dept. of the Navy
Bureau of Naval Weapons
Washington 25, D.C.
Attn: RMMP (2 copies)

Aerojet-General Corporation
P.O. Box 296
Azusa, Calif.
Attn: Librarian (1 copy)

Jet Propulsion Lab
4800 Oak Grove Drive
Pasadena 3, California
Attn: I.E. Newlan Chief,
Reports Group (1 copy)

Commander
Aeronautical Systems Div. ASRCNC-1
AF Systems Command
U.S. Air Force
Wright-Patterson AFB, Ohio (2 copies)

Plastic Evaluation Center
Picatinny Arsenal
Dover, N. J.
Attn: ORD-BB (2 copies)

Commander
U. S. Naval Ordnance Test Station
China Lake, Calif.
Attn: Mr. S. Herzog, Code 5557

Commander
Armed Services Technical
Information Agency
Arlington Hall Station
Arlington 12, Virginia (10 copies)

Department of the Army
Office, Chief of Ordnance
Washington 25, D.C. (1 copy)

Commander
Army Rocket and Guided
Missile Agency
Redstone Arsenal, Alabama (1 copy)

Department of the Navy
Bureau of Naval Weapons
Washington 25, D.C.
Attn: Technical Library (2 copies)

Allegany Ballistics Lab.
Hercules Powder Company
Cumberland, Maryland
Attn: Mr. R. Winer (2 copies)

Solid Propellant Information Agency
Applied Physics Lab.
The Johns Hopkins University
Silver Spring, Maryland
Attn: G. McMurray (3 copies)

Hercules Powder Company
Bacchus Works
Magna, Utah
Attn: Librarian (1 copy)

Director, Special Projects
(SPN) Dept. of Navy
Wash. 25, D.C.
Attn: SP20 (4 copies)
ATTN: SP-27 (2 copies)

Lockheed Missiles and Space Company
A division of Lockheed Aircraft Corp.
1122 Jagels Rd.
Sunnyvale, California
Attn: Mr. H. H. Patton (1 copy)

Lockheed Missiles & Space Co.
A Division of Lockheed Aircraft Corp.
3151 Hanover St.
Palo Alto, Calif.
Attn: Mr. M. Steinberg (1 copy)

Aerojet-General Corp.
P. O. Box 1947
Sacramento, Calif.
Attn: Dr. W. O. Wetmore (5 copies)

Defense Metals Information Center
Battelle Memorial Institute
505 King Ave.
Columbus 1, Ohio (1 copy)

Director
U.S. Naval Research Lab
Washington 25, D.C.
Attn: Code 6210 (1 copy)

Commander
U.S. Naval Ordnance Lab
White Oak, Maryland (1 copy)

John I. Thompson & Co.
1118 22nd Street N.S.
Washington 7, D.C. (1 copy)

The Bendix Corp.
Bendix Products Div.
South Bend 20, Indiana
Attn: Mr. Wade Hardy (1 copy)

Black, Sivalls & Bryson
Oklahoma City, Oklahoma
Attn: Mr. J. Carter (1 copy)

B.F. Goodrich Co.
500 S. Main
Akron, Ohio
Attn: Mr. H. W. Stevenson (1 copy)

Goodyear Aircraft Corp.
Akron 15, Ohio
Attn: Mr. R. Burkley (1 copy)

Bureau of Naval Weapons
Representative
P.O. Box 504
Sunnyvale, California (1 copy)

Bureau of Naval Weapons
Resident Representative
P.O. Box 1947
Sacramento, California (1 copy)

Bureau of Naval Weapons
Branch Representative
Allegany Ballistics Lab.
Cumberland, Maryland Attn: Code 4 (1 copy)
Attn: Mr. R. Woodberry, 1 copy; Attn: Mr. J.G. Armstrong, 1 copy

Bureau of Naval Weapons
Resident Representative
(Special Projects Office)
c/o Hercules Powder Company
Bacchus Works
Magna, Utah (1 copy)

Narmco Industries, Inc.
Research & Development Div.
8125 Aero Drive
San Diego, California
Attn: Mr. W. Otto (1 copy)

Walter Kidde Company
Aerospace Division
Belleville, N.J.
Attn: Mr. T. Siuta (1 copy)

General Electric Company
Schenectady, New York
Attn: Mr. T. Jordan (1 copy)

Hercules Powder Co.
P.O. Box A
Rocky Hill, N.J.
Attn: Mr. R. Carter (1 copy)

Rocketdyne Engineering
Div. of North American Aviation, Inc.
6633 Canoga Ave.
Canoga Park, Calif.
Attn: Mr. E. Hawkinson (1 copy)

University of Vermont
Dept. of Mechanical Engr.
Burlington, Vermont
Attn: Prof. J.O. Outwater (1 copy)

University of Ill.
Dept. of Theoretical & Applied Mechanics
Urbana, Ill.
Attn: Prof. H. T. Corten (1 copy)

Westinghouse Electric Corp.
E. Pittsburgh, Pa.
Attn: Mr. H.R. Sheppard (1 copy)

Mr. C.D. Oughton
Mr. W. Sylvester
Mr. J. McNeilly
Mr. A. Schmidlin
Mr. P. Evans
Mr. H. Joseph
Mr. F. Wolff
3642 File
Inspector of Material
1130 Rt. 22, Mountainside, N.J.